

AN ABSTRACT OF THE THESIS OF

Michael D. Polander for the degree of Master of Science in Mechanical Engineering presented on May 30, 2018.

Title: Investigation of Destratification in Warehouses

Abstract approved: _____

Brian M. Fronk

A significant source of energy consumption comes from maintaining desired indoor environment conditions in warehouses and other industrial facilities. In efforts to combat the raising energy costs, studies into more efficient heating and cooling strategies has been a topic of consideration for a number of years. One of the areas of investigation is the implications of a thermally stratified environment. In heating, removing the stratification phenomena has been linked to savings in the cost of fuel to heat an environment. Whereas in cooling a highly stratified environment is desired.

The primary method of destratification is the utilization of ceiling fans. However, the required parasitic fan power reduces the overall savings of destratification. A solution to offset the reliance on grid power is the use of solar powered ceiling fans. The challenge with utilizing solar power during heating seasons is a reduction in the time the sun is available to charge and store energy to run the fans. While

there are studies into the impact of thermal stratification, with air as a medium in an indoor environment, there is a lack of information on the frequency at which the ceiling fans need to operate to maintain a destratified environment. The determination of a fan operation frequency, to maintain a destratified environment, informs potential designers on the viability of installing solar powered fans as an alternative to grid powered fans. In the event that solar powered fans were not a viable option, it also provides information on the frequency that a grid powered fan would need to run to maintain destratification.

To determine a fan operating frequency, a numerical analysis was performed. This numerical analysis assessed the time required to maintain a destratified environment based on inputs such as flow rate and spatial considerations. In order to establish the quality of the numerical analysis, two experiments were conducted to observe the impact of destratification. One experiment was located at a large distribution center, the other was a small classroom. The data collected from these experiments was compared to the models developed to validate the findings. It was found that a destratification fan could maintain a destratified environment by operating at a 35% fan duty cycle.

©Copyright by Michael D. Polander
May 30, 2018
All Rights Reserved

Investigation of Destratification in Warehouses

by

Michael D. Polander

A THESIS

submitted to

Oregon State University

in partial fulfillment of
the requirements for the
degree of

Master of Science

Presented May 30, 2018
Commencement June 2018

Master of Science thesis of Michael D. Polander presented on May 30, 2018.

APPROVED:

Major Professor, representing Mechanical Engineering

Director of the School of Mechanical, Industrial, and Manufacturing Engineering

Dean of the Graduate School

I understand that my thesis will become part of the permanent collection of Oregon State University libraries. My signature below authorizes release of my thesis to any reader upon request.

Michael D. Polander, Author

ACKNOWLEDGEMENTS

First and foremost I would like to thank my graduate advisor, Dr. Brian Fronk, for providing me with the opportunity to perform this study, for working with me through the many complications that I presented as a student with many external obligations, and for helping me through the challenges of creating a thesis of merit. I would also like to thank my lab mates, Tabeel Jacob, Paul Armatis, Saad Jajja, and Ahmad Bukshaisha for listening to the complaints and the questions, and for offering suggestions and support where it was needed. I would be remiss if I did not acknowledge Elsa Harder and John Tijerina for their work setting up the experiments and collecting data from them. Thank you to Rick Seaver, who helped me through the many hurdles and pitfalls of creating a functional, and useful, model. Lastly, and most importantly, I want to acknowledge and thank my wife, Jennifer Polander, for her support and dedication throughout the entire process of working on this thesis. For taking care of our kids and home through the long nights and weeks. I wouldn't be where I am today without her.

TABLE OF CONTENTS

	<u>Page</u>
1 Introduction	1
1.1 Stratification	1
1.2 Thesis Objective	7
1.3 Thesis Outline	10
2 Literature Review	11
2.1 Heating	11
2.2 Cooling Season	18
2.3 Numerical Model Studies of Indoor Stratification	20
2.4 Need for Present Work	24
3 Experimental Setup	26
3.1 Large Warehouse Experimental Setup	26
3.2 School Room Experimental Setup	36
4 Model Development	40
4.1 Model Setup	40
4.1.1 ANSYS CFX & ICEM CFD	43
4.1.2 Solver	47
4.2 Mesh	51
4.3 Mixing and Cooling Models	56
5 Experiment Results	61
5.1 Warehouse Results	61
5.2 Schoolhouse Results	84
5.3 Discussion	85
6 Model Results	87
6.1 Thermal Mixing Simulations	87
6.1.1 Thermal Mixing: 15k CFM SunCooler 40 ft Ceiling Height 90 ft Fan Spacing	88

TABLE OF CONTENTS (Continued)

	<u>Page</u>
6.1.2 Thermal Mixing: 15k CFM SunCooler 32 ft Ceiling Height 90 ft Fan Spacing	95
6.1.3 Thermal Mixing: 15k CFM SunCooler 32 ft Ceiling Height 90 ft Fan Spacing - Disabled Fans	104
6.1.4 Thermal Mixing: 2.5k CFM SunCooler 20 ft Ceiling Height 50 ft Fan Spacing	107
6.2 Cooling	109
6.3 Model Validation	117
6.3.1 Effect of Thermal Mass	123
6.4 Model Limitations	128
6.5 Discussion	129
7 Study Impact and Limitations	133
7.1 Estimated Simple Payback	133
7.1.1 Cooling Season Energy Costs and Savings Potential	133
7.1.2 Heating Season Energy Costs and Savings Potential	136
7.1.3 Simple Payback	140
7.2 General Impact on Destratification Control	144
7.3 Study Limitations	149
8 Conclusions	154
8.1 Summary	154
8.2 Contribution	156
8.3 Recommended Future Work	157
Bibliography	157

LIST OF FIGURES

<u>Figure</u>		<u>Page</u>
1.1	Vertical temperature distributions in various warehouses (Porras-Amores et al., 2014)	2
1.2	Thermal plume and thermocline visualization (Bouzinaoui et al., 2005)	4
1.3	Characteristic thermal profiles determined by heating and mixing (Aynsley, 2005)	6
1.4	Fan operation modes, (NWREC, 2017)	9
2.1	Thermal profiles before and after destratification (Armstrong et al., 2009)	13
2.2	Thermal profiles over time (Armstrong et al., 2009)	16
2.3	Example thermal profile developed by UFAD (Bauman et al., 2007)	19
2.4	Universal Velocity Profile (ANSYS, 2017)	23
3.1	Covered roof penetration	28
3.2	Roof curb installation	28
3.3	Water proofing and insulation installation	29
3.4	Installed destratification unit	30
3.5	Installed SunCooler housing	31
3.6	Warehouse blueprint with sensor notes	32
3.7	Warehouse sensor layout	33
3.8	Base unit RTR 500 repeater	34
3.9	MAU heater, interior view	35
3.10	Front view of school building	37
3.11	School room sensor setup	38

LIST OF FIGURES (Continued)

<u>Figure</u>	<u>Page</u>
4.1 Generalized warehouse schematic	41
4.2 Example of model geometry	42
4.3 Example of ICEM CFD interface	44
4.4 Example of CFX-Pre interface	46
4.5 Mesh Δy example	53
4.6 y^+ output example	54
4.7 Sample mesh with 13367665 nodes	56
5.1 Control location 3 monthly temperature average vs height	62
5.2 Experimental location 3 monthly temperature average vs height	63
5.3 Control location 1 monthly temperature average vs height	64
5.4 Experimental location 1 monthly temperature average vs height	65
5.5 Control location 5 monthly temperature average vs height	66
5.6 Experimental location 5 monthly temperature average vs height	67
5.7 May 2017 stratification profile	68
5.8 July 2017 stratification profile	69
5.9 August 2017 stratification profile	69
5.10 October 2017 stratification profile	70
5.11 November 2017 stratification profile	70
5.12 May 2017 Δ temperature	71
5.13 July 2017 Δ temperature	72
5.14 August 2017 Δ temperature	72
5.15 October 2017 Δ temperature	73

LIST OF FIGURES (Continued)

<u>Figure</u>	<u>Page</u>
5.16 November 2017 Δ temperature	73
5.17 Average temperature difference - control vs experimental	75
5.18 Average ceiling temperature difference - control vs experimental	77
5.19 Ceiling height temperature - SunCooler 2, December 29th 2016	78
5.20 Ceiling height temperature - SunCooler 2, December 30th 2016	79
5.21 Ceiling height temperature - SunCooler 4, September 17th 2016	80
5.22 CO ₂ levels - SunCooler 3, September 30th 2016	81
5.23 CO ₂ levels - SunCooler 6, September 18th 2016	82
5.24 CO ₂ levels - SunCooler 1, January 2nd 2017	83
5.25 School room temperature at height - control and experimental	85
5.26 School room temperature difference - control and experimental	85
6.1 5k CFM SunCooler 40 ft ceiling height 90 ft fan spacing: temperature, time = 0 seconds	89
6.2 15k CFM SunCooler 40 ft ceiling height 90 ft fan spacing: temperature, time = 4 seconds	90
6.3 15k CFM SunCooler 40 ft ceiling height 90 ft fan spacing: temperature, time = 36 seconds	91
6.4 15k CFM SunCooler 40 ft ceiling height 90 ft fan spacing: temperature, time = 84 seconds	92
6.5 15k CFM SunCooler 40 ft ceiling height 90 ft fan spacing: temperature, time = 124 seconds	93
6.6 15k CFM SunCooler 40 ft ceiling height 90 ft fan spacing: temperature, time = 162 seconds	94
6.7 Temperature monitors for geometry with 40 ft ceiling height	95

LIST OF FIGURES (Continued)

<u>Figure</u>	<u>Page</u>
6.8 15k CFM SunCooler 32 ft ceiling height 90 ft fan spacing: temperature, time = 0 seconds	96
6.9 15k CFM SunCooler 32 ft ceiling height 90 ft fan spacing: temperature, time = 4 seconds	97
6.10 15k CFM SunCooler 32 ft ceiling height 90 ft fan spacing: temperature, time = 36 seconds	98
6.11 15k CFM SunCooler 32 ft ceiling height 90 ft fan spacing: temperature, time = 72 seconds	99
6.12 15k CFM SunCooler 32 ft ceiling height 90 ft fan spacing: temperature, time = 108 seconds	100
6.13 15k CFM SunCooler 32 ft ceiling height 90 ft fan spacing: temperature, time = 144 seconds	101
6.14 15k CFM SunCooler 32 ft ceiling height 90 ft fan spacing: streamlines	102
6.15 15k CFM SunCooler 32 ft ceiling height 90 ft fan spacing: top view streamlines	103
6.16 15k CFM SunCooler 32 ft ceiling height 90 ft fan spacing: velocity .	104
6.17 15k CFM SunCooler 32 ft ceiling height 90 ft fan spacing: disabled fans	106
6.18 15k CFM SunCooler 32 ft ceiling height 90 ft fan spacing: disabled fans - 90° rotation.	106
6.19 15k CFM SunCooler 32 ft ceiling height 90 ft fan spacing: disabled fans - top view streamlines	107
6.20 2.5k CFM SunCooler 20 ft ceiling height 50 ft fan spacing: temperature monitors	108
6.21 2.5k CFM SunCooler 20 ft ceiling height 50 ft fan spacing: streamlines	109
6.22 20 ft ceiling height cooling: all time steps	110
6.23 20 ft ceiling height cooling: 0 - 600 seconds	111

LIST OF FIGURES (Continued)

<u>Figure</u>	<u>Page</u>
6.24 Cooling model, time = 0 seconds	112
6.25 Cooling model, time = 96 seconds	112
6.26 Cooling model, time = 132 seconds	113
6.27 Cooling model, time = 200 seconds	114
6.28 Cooling model, time = 380 seconds	115
6.29 Cooling model, time = 968 seconds	115
6.30 Cooling model, time = 1304 seconds	116
6.31 Top view of validation model	118
6.32 Side view of validation model	119
6.33 Model vs actual experimental temperature data points	120
6.34 Model vs modified experimental temperature data points	121
6.35 Comparison of model data, with and without a heated floor	122
6.36 Control volume for thermal mass analysis	123
6.37 Results of thermal analysis	127
6.38 Ceiling height temperature - SunCooler 2, December 30th 2016	132
7.1 Combined run time for exhaust/intake fans	134
7.2 Estimated simple payback for varying hours of operation and power cost	143
7.3 Time for air replacement at variable fan spacing	145
7.4 Trendline developed from model results	146
7.5 Variable fan spacing for constant flow rate and heights	147
7.6 Variable flow rates for constant mixing volume	148

LIST OF TABLES

<u>Table</u>	<u>Page</u>
2.1 Turbulence Ratings (Zhang et al., 2007)	21
3.1 Experimental equipment utilized	39
5.1 SunCooler run times for warehouse experiment	61
6.1 Mixing model results summary	87
6.2 Cooling model results	116
6.3 Material Properties	125
7.1 Average temperature data - Albany, Oregon	138
7.2 Heat lost through ceiling at various temperatures.	139
7.3 Fuel savings (dekatherms)	139
7.4 Fuel savings (dollars)	139
7.5 Estimated simple payback (years)	142

Chapter 1: Introduction

Energy efficiency in is a topic of increasing importance for engineers. A large percentage of energy in buildings is consumed to for heating, cooling, and ventilation to maintain the indoor environments preferred for human comfort, and the storage of goods. One way to reduce energy costs for indoor enclosures is through the manipulation of thermal stratification. To better understand how manipulating a stratification profile can result in cost reduction, it is necessary to first understand stratification and when it occurs. It is also beneficial to summarize when destratification should be performed and with what equipment. Once these topics are covered, the purpose of this study will be discussed. The final section of the introduction will provide an outline of subsequent chapters.

1.1 Stratification

Thermal stratification exists when there is a temperature gradient within a medium of interest. This phenomena is of interest as it can affect indoor environments. A paper by Porras-Amores et al. (2014) provides useful examples of stratification within warehouses and storage facilities. In this paper, the vertical distributions of air temperature within warehouses were studied. Experiments were run at five locations in Spain, with the intent of collecting temperature pro-

file data in different seasons. The warehouse locations included: two above ground warehouses, with and without air conditioning, one basement warehouse, an earth-sheltered warehouse, and an underground warehouse. None of these sites were heated, and only the air conditioned site was cooled (Porrás-Amores et al., 2014). Figure 1.1 shows the results of the temperature data collected from each experimental site. Each data set is the temperature difference observed with respect to height. The data is averaged for each month.

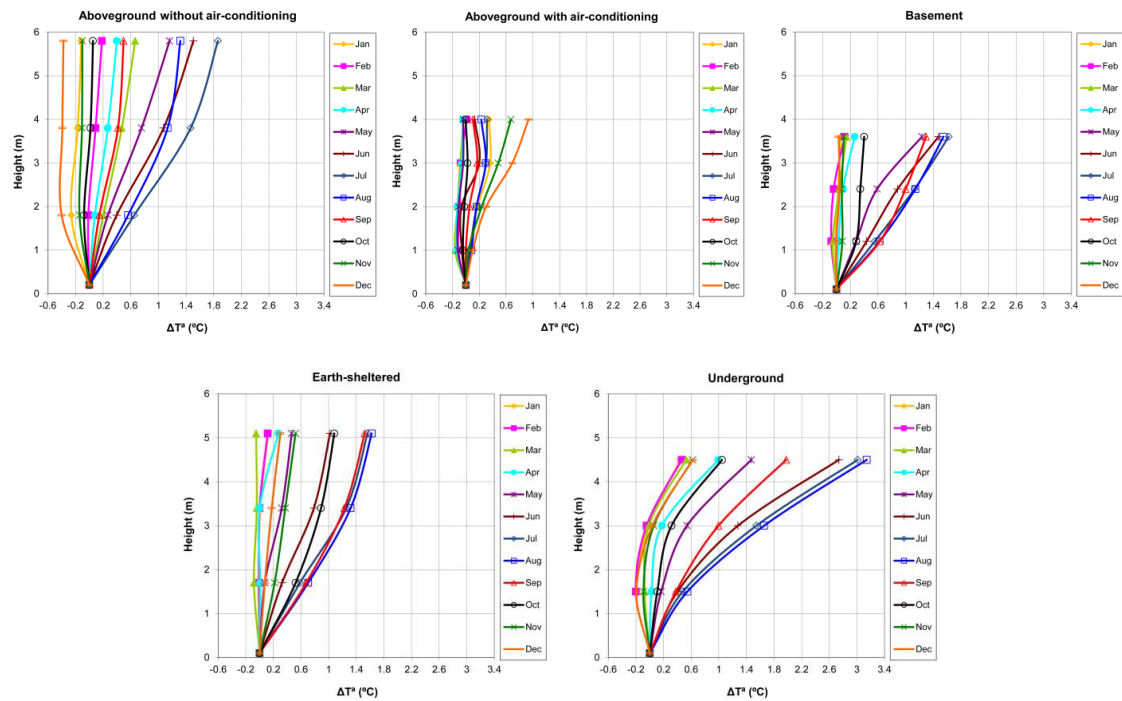


Figure 1.1: Vertical temperature distributions in various warehouses (Porrás-Amores et al., 2014)

While the specific results from each site vary, generally these results indicate that the time of greatest stratification occurs in the warmer months and the least

stratification occurs in the colder months, for unheated warehouses. This is attributed to the heat exchange caused by external temperatures. A colder external temperature creates a temperature difference which will cause heat to flow out to the environment. Without active heating of the building, this will continue to occur until the room is at a more uniform temperature. The exchange occurs primarily through the roof, due to its increased exposure to the external temperature and lower quality insulation. (Porrás-Amores et al., 2014).

When heating is introduced during a cold season, thermal stratification will begin to develop. As the air is heated, warmer air will be displaced upward by the cooler, denser, air. The nature of the stratification profile will vary depending on the way in which the building is heated. In a study by Bouzinaoui et al. (2005), the thermal stratification for ventilated enclosed spaces is studied through experimentation. This study uses the thermocline to define the stratification profile which results from placing a heating source in the lower region of the room. Thermocline is defined as the location characterized by a steep temperature gradient which divides the lower cooler air and higher warmer air. Bouzinaoui et al. (2005) shows that by heating in this fashion, a thermal plume is formed which is subsequently displaced upward to form a warmer upper region (Bouzinaoui et al., 2005). This is shown in Figure 1.2:

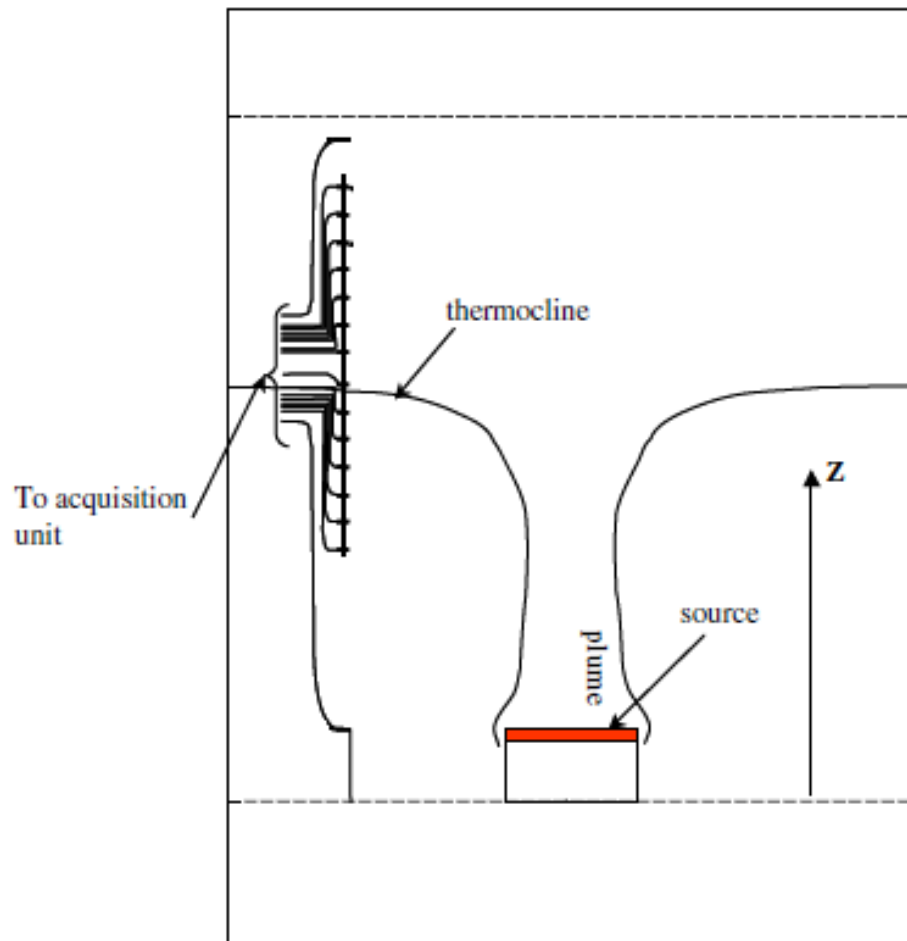


Figure 1.2: Thermal plume and thermocline visualization (Bouzinaoui et al., 2005)

The study concluded that the elevation of the thermocline is determined to be a function of the flow rate of the ventilation, and that the temperature of the heat source only impacts the temperature difference within the thermocline (Bouzinaoui et al., 2005). The result of which is a higher upper region above the thermocline, while the region below the thermocline remains at a lower temperature.

The heating methods seen in this studies experiments did not reflect the heating profile mapped by Bouzinaoui et al. (2005). Therefore, more thermal profiles were found in a paper by Aynsley (2005). The profiles without mixing follow trends similar to the thermal profile described by Bouzinaoui et al. (2005), but have profiles that match the expected heating scenarios for this study. The additional profiles can be seen in Figure 1.3:

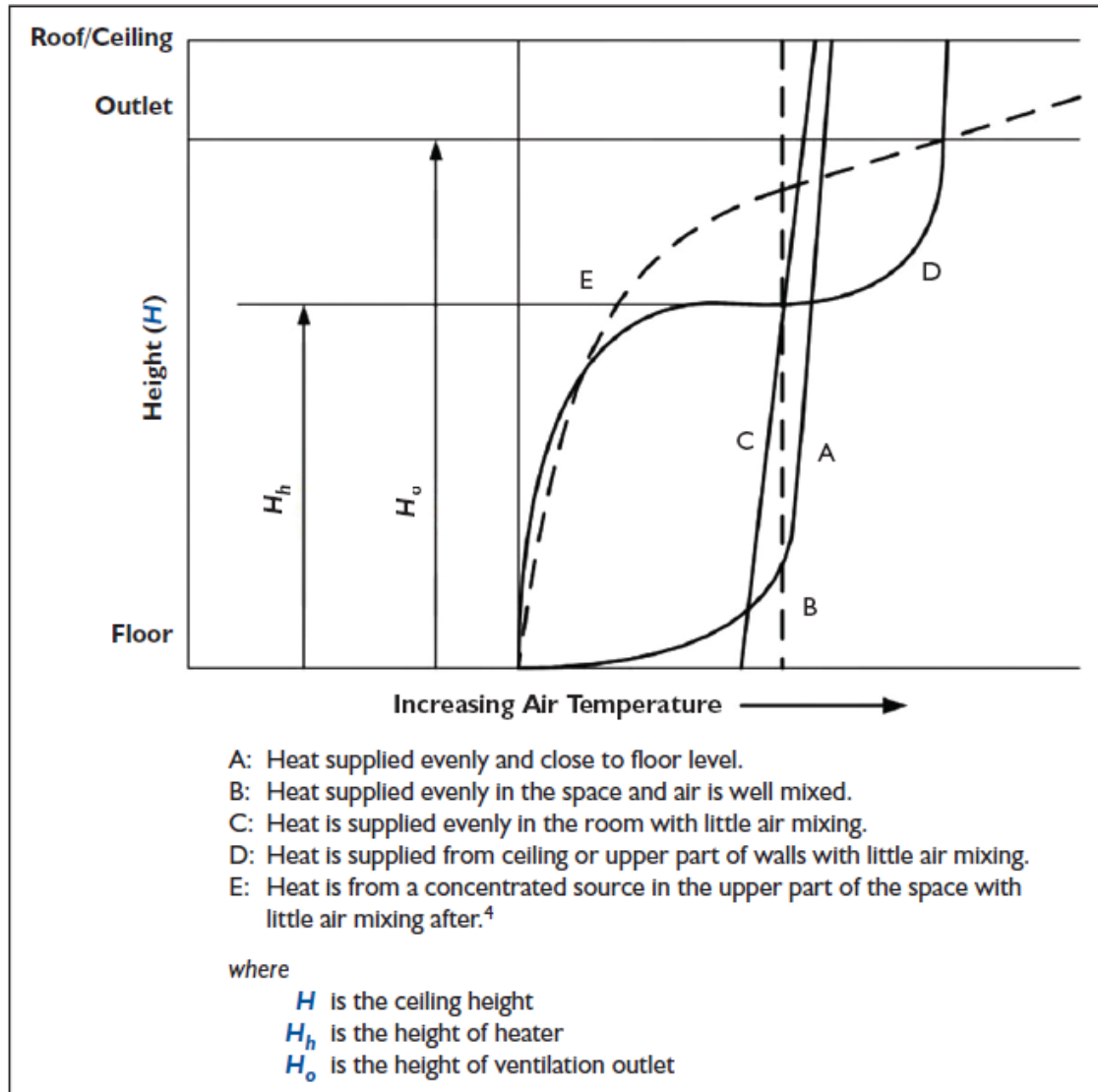


Figure 1.3: Characteristic thermal profiles determined by heating and mixing (Aynsley, 2005)

For this paper, profile E, from Figure 1.3, will be adopted when referencing thermal stratification, as both of the experimental locations utilize heating from upper regions of the enclosures. When heating from the upper portion of an

enclosure, without mixing, there are consequences to energy usage. The heat of the upper region must be increased such that the lower leg of the profile will be increased enough to satisfy the rooms thermostat settings. This is coupled with an increase of heat lost through the roof by the higher ceiling temperature and larger indoor-to-outdoor driving temperature difference. Both of these factors tend to increase the heating demand, and by extension fuel costs.

1.2 Thesis Objective

While there are several stratification profiles which can form within a building, destratification is the method used to adjust a temperature profile. More specifically, destratification is the process of introducing mixing to a heated environment. Mixing causes the thermal profiles to approach profile B, from Figure 1.3. The benefit of mixing the stratified air is creating a uniform temperature throughout the enclosure. This brings the lower temperature to the desired thermostat temperature more rapidly. It also reduces the interface temperature at the ceiling, lowering the heat lost through the ceiling. Reduction in heat lost through the ceiling results in a net reduction of fuel usage to maintain a given temperature.

To create the mixing effect, ceiling fans are typically utilized. However, fans introduce an additional source of energy consumption which must be balanced with the reduction in heating energy. In general, fans are run continuously when destratification is desired. To remove dependence on grid power, solar powered fans can be adopted. This removes the negative impact of fan power on net sav-

ings. Solar powered ventilation devices developed by Northwest Renewable Energy Corp., a small Oregon-based business, are evaluated in this study. Experiments are conducted in a large warehouse environment, and a more easily controlled single school room environment. The solar powered fans utilized in this study provide additional features that can help to alter indoor air conditions for all seasons. Listed are the fans advertised capabilities (NWREC, 2017):

- Night operation via battery.
- Day operation powered by integrated solar photovoltaic array.
- Ventilates and charges battery simultaneously.
- Induction, Exhaust, and Destratification modes.

The induction mode can be described as when the fan unit is open to external air and the fan pulls the air in for air replacement or cooling. Cooling would be done during the night on battery power, when the outdoor ambient temperature is lower than the indoor temperature. It also provides air replacement which can have an impact on CO₂ levels.

The exhaust mode is when the fan unit is open to external air, but the fan direction is reversed, pulling air from the indoor environment. This can aid with cooling in daytime operation by removing the heated air that collects at ceiling level via stratification in warmer seasons (Porrás-Amores et al., 2014).

The final mode, destratification, occurs when dampers are closed to the external air and internal baffles are opened to gain access to ceiling height air for mixing.

The three modes can be seen in Figure 1.4:

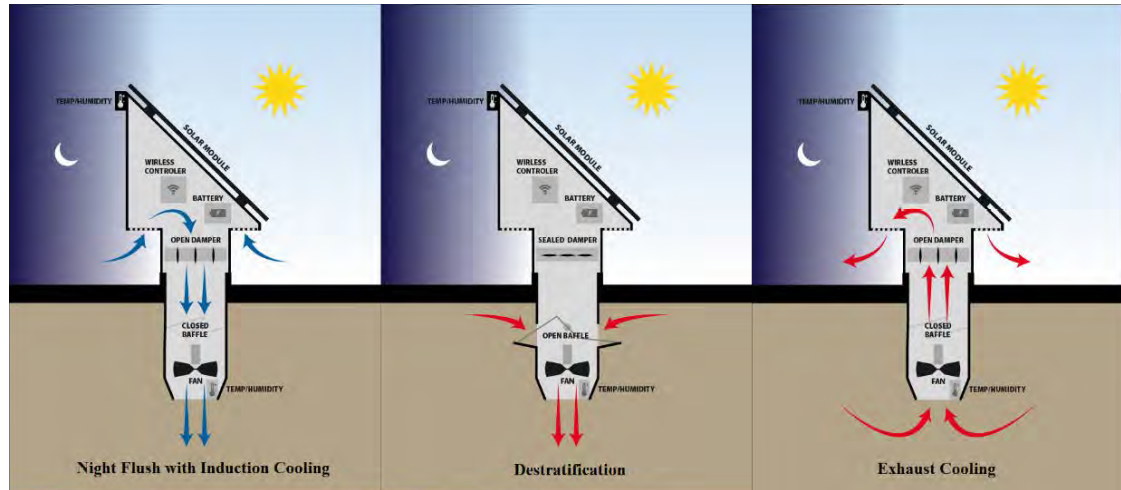


Figure 1.4: Fan operation modes, (NWREC, 2017)

An important component of the fan unit capabilities is its ability to perform destratification in the heating season, i.e. when solar power is least available. The minimum operating time to maintain a destratified environment is the central focus of this study. The operating time is determined through modeling the mixing of a stratified environment, and heat loss by a completely mixed environment. The results of modeling are compared to the collected experimental data. The simulations cover multiple geometries to observe how mixing changes with changes in parameters such as building height, fan spacing, and inlet strength. The primary output of this study is a fan duty cycle which predicts the relative time required to maintain destratification in an enclosed space.

1.3 Thesis Outline

The remaining chapters of the thesis will cover the following topics:

- Chapter 2: Reviews literature on stratification, existing energy savings models, and previous modeling of indoor environments for purposes of heating and cooling.
- Chapter 3: Introduces the experimental setups at the large warehouse and school room.
- Chapter 4: Discusses the model development, software package utilized to perform modeling, property assumptions, and schemes employed.
- Chapter 5: Presents results of data collected from both the large warehouse and school room experiments.
- Chapter 6: Presents modeling results for stratification and destratification. Introduces resulting computational formula.
- Chapter 7: Discusses the impacts of the study, such as the payback estimates of installing SunCooler units for the purpose of destratification, and/or exhaust and intake purposes, the requirements to maintain destratification, and potential improvements for future studies.
- Chapter 8: Conclusions drawn from experimental and computational results. Includes recommendations for use of model and future work that could be done to improve upon existing results.

Chapter 2: Literature Review

In general, studies on destratification in the open literature are relatively limited. Of the existing studies, prior experimental and computational work on indoor thermal stratification has focused on two areas which are relevant to this study: destratification during a heating season, and implications of destratification during a cooling season. Studies in both modes have focused on identifying the most cost effective way to maintain an indoor environment ideal for the building's purpose (e.g., warehouse, school, office building, etc.). There also exists literature discussing the modeling of indoor environments, with the goal of better understanding available numerical practices. This chapter will explore relevant studies in all three areas and then identify the gaps in the open literature that the present work will fill.

2.1 Heating

Investigation on destratification during the heating season is primarily focused on quantifying the potential energy and economic savings attained by the destratification of an indoor environment. Warehouses are the structure most analyzed for savings due to their large physical envelope, high ceiling height, and high cost of heating. Typically, destratification during heating season is believed to save

energy primarily through a reduced ceiling temperature (Aynsley, 2005). Aynsley (2005) provides a set of equations which estimate the heat loss difference between a stratified and destratified environment. At a given ambient temperature, heat loss through the roof will increase with an increase in temperature at the ceiling height. With destratification, the temperature at the ceiling will decrease as the air is mixed to a more uniform temperature (Aynsley, 2005). This can be seen within the data provided in a study by Armstrong et al. (2009). Figure 2.1 shows a temperature profile created using 6 temperature sensors from ground level to ceiling height. The independent axis is temperature and the dependent axis is physical distance from the floor.

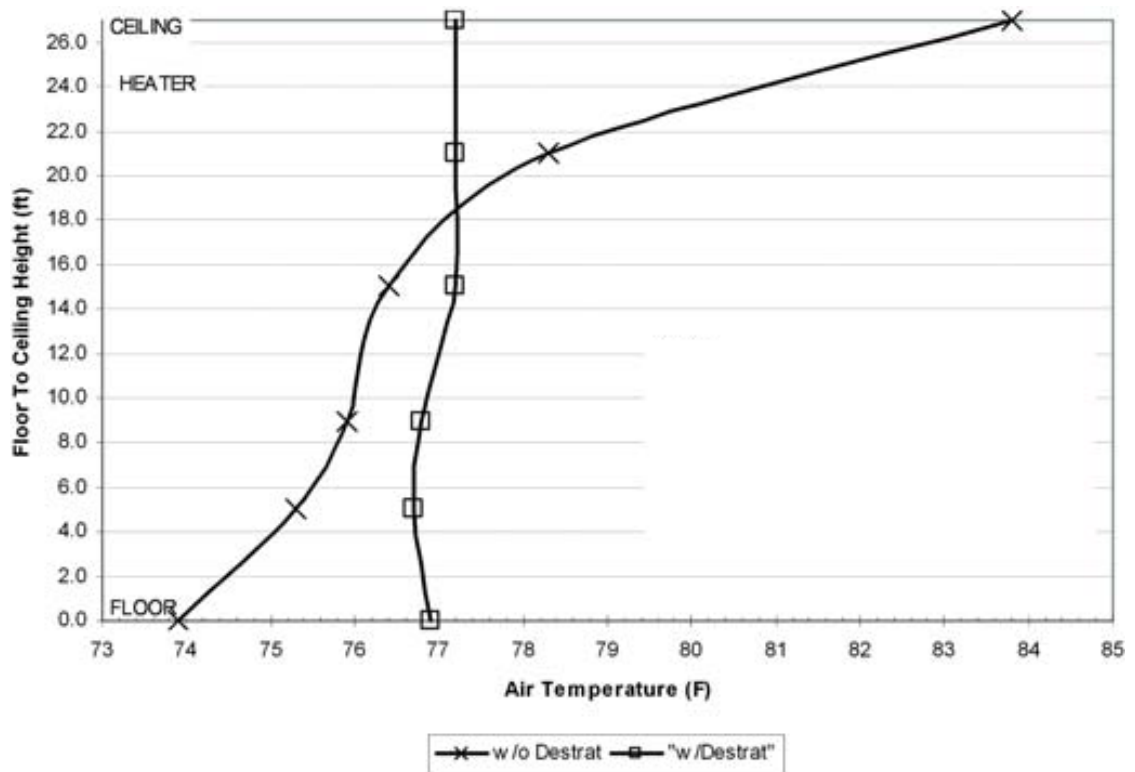


Figure 2.1: Thermal profiles before and after destratification (Armstrong et al., 2009)

The figure shows that without destratification the ceiling temperature is approximately $84^{\circ}F$ and after destratification the ceiling temperature is approximately $77^{\circ}F$, suggesting much higher heat loss through the ceiling for the stratified condition. This is consistent with claims made by Aynsley (2005). The heat lost through the side walls is considered to remain relatively constant before and after stratification. This is because the driving temperature difference for transport through the wall is governed by the average temperature of the room, which does not change between the two conditions (Aynsley, 2005). Therefore, while heat lost

through the wall is significant when considering total heat lost, it is not a key factor when evaluating savings due to destratification.

The equations used by Aynsley to estimate cost savings can be simplified to equation 2.1.

$$\dot{Q}_{ad} = \dot{Q}_{bd} \left(\frac{T_{ibd} - T_{ad}}{T_{ibd} - T_o} \right) \quad (2.1)$$

This equation predicts the expected heat lost with a destratified environment, \dot{Q}_{ad} . The value \dot{Q}_{bd} includes all of the heating energy utilized for a heating season and expected heat produced by sources such as a lighting and personnel. T_{ibd} is the temperature at the ceiling height prior to destratification, T_o is the average outdoor temperature during the heating season, and T_{iad} is the expected average temperature of the room based on the initial temperature profile from Figure 1.3. With \dot{Q}_{ad} solved for, the percentage of energy savings can be calculated using equation 2.2 (Aynsley, 2005).

$$Fuel\ Savings = 100 \left(\frac{\dot{Q}_{bd} - \dot{Q}_{ad}}{\dot{Q}_{bd}} \right) \quad (2.2)$$

If desired, this can be converted to a monetary savings using the fuels caloric value, LHV, the heater efficiency, η , and the cost of fuel, FC , as shown in equation 2.3 (Aynsley, 2005).

$$Fuel\ Value = \left(\frac{\dot{Q}_{bd} - \dot{Q}_{ad}}{LHV\eta} \right) FC \quad (2.3)$$

Aynsley (2005) demonstrates the effectiveness of this method by comparing

the estimated percentage savings with the actual savings of a warehouse located in Middletown, New York. Working with the facility owners, Aynsley (2005) collected energy consumption and temperature data for heating in February, March, and April of 2003. This data was used to create a savings estimate with the provided equations. The destratification fans were then installed and operated over the same months the following year. The results were an estimated savings of 28%, which calculated the expected average indoor temperature with profile D from Figure 1.3. The actual savings were a 26.4% reduction in gas usage. The prediction methods utilized by Aynsley (2005) predicted 28% fuel usage savings, which is 6.1% greater than the actual savings. Putting the prediction within a 10% margin of error (Aynsley, 2005).

The study shows the potential for energy savings by destratification during the heating season. It also provides basic tools which can be used to estimate savings that would be provided by utilizing the solar powered fan units provided by Northwest Renewable Energy Corp in the present study. Aynsley (2005) does not include the cost of fan operation in the savings calculation, but does estimate that at the time of the paper, for a 89 day period, the fans would use \$64.08 of electricity. It is worth noting that Aynsley is the director of research and development for the Big Ass Fan Company, which could impact the fan estimates (Aynsley, 2005). The paper by Aynsley (2005) also lacked experimental data, favoring showing the method used to estimate savings rather than the experimental data validating the savings estimate. This prompted an interest in locating additional studies that provided more experimental data to confirm the conclusions from the Aynsley (2005) paper.

The experimental study by Armstrong et al. (2009), which was mentioned when introducing Figure 2.1, investigated stratification in a single warehouse. Their setup included five data collection locations throughout the warehouse, each with 6 temperature sensors to characterize temperature profile. The fans in this facility were installed prior to the experimental setup. Rather than collecting data one year without destratification and one year with destratification they opted to collect data for one week periods. Alternating between having the fans enabled and disabled. The effect of the fans can be seen in Figure 2.2 (Armstrong et al., 2009).

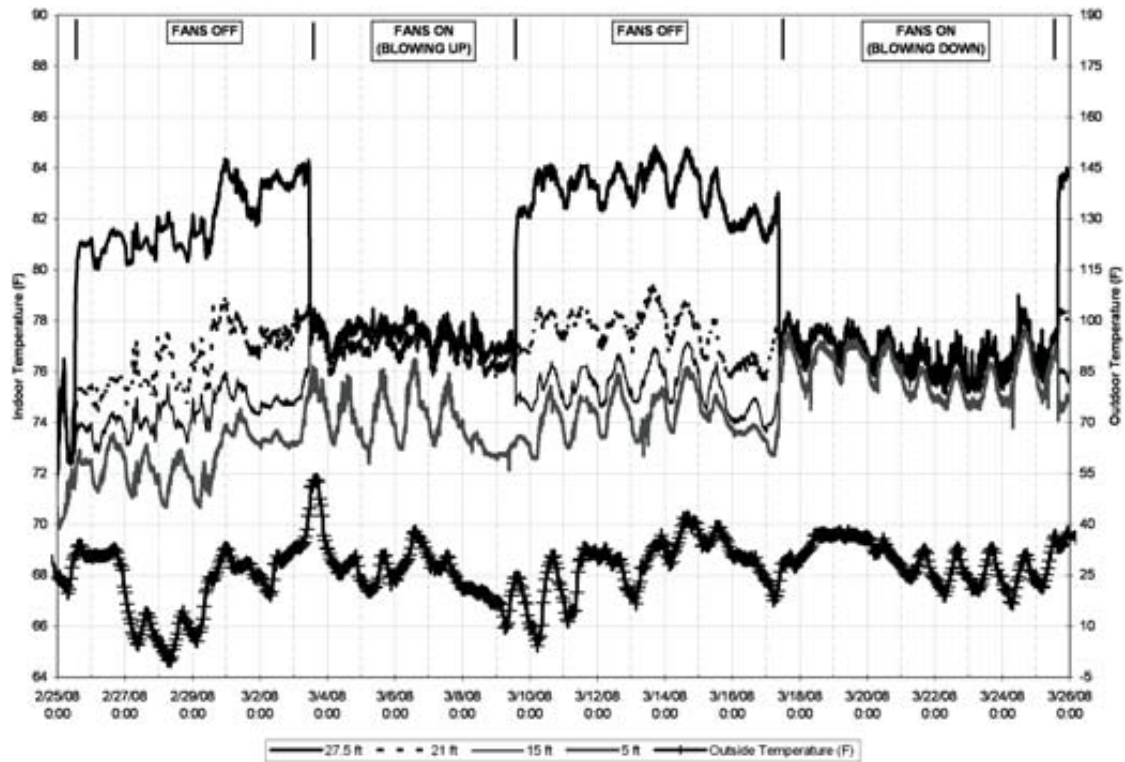


Figure 2.2: Thermal profiles over time (Armstrong et al., 2009)

The fans are run in forward and reverse for the Armstrong et al. (2009) experi-

ment. The reverse mode, blowing upward, is less effective at removing the stratified profile and is deemed ineffective for destratification. Blowing downward shows a much more effective removal of the stratification, lowering the ceiling temperature by $7.2\text{ }^{\circ}F$ and increasing the floor temperature by $2.7\text{ }^{\circ}F$, as shown in Figure 2.1. The study found, through experimentation, that a fuel savings of 19.8% is achieved with destratification. This accounts for a 5% parasitic reduction due to fan operation (Armstrong et al., 2009). While the fuel savings are similar to those estimated by Aynsley (2005), the cost of fan operation is much greater.

A conference paper by Hughes (2006) also documents an experimental study of the savings provided by destratification. The study is performed by the Naval Facilities Engineering Service Center for the purposes of determining if destratification fans should be installed at existing Naval warehouses. The study is performed at three locations, but only data from two sites is provided in the paper. The findings are similar to those of the other two papers, with destratification lowering the energy lost from the building. However, in one of their cases it was found that the cost of operating the fans exceeded the savings attained through destratification. This is significant as the other papers discussed have presented fan costs which are much less than the savings attained by destratification. Also of interest, both of the Hughes (2006) sites, Maryland and Indiana, are further south than the Armstrong et al. (2009), Ontario, Canada, and Aynsley (2005), New York, locations. The location disparity could have an impact on the average ambient temperature, which would affect the savings possible by destratification. Sites at more northern locations would have longer heating seasons, as well as

larger average ambient-to-indoor temperature differences. The Hughes (2006) paper concludes that destratification of their warehouses is desirable, but only after an investigation of the facility to determine its suitability (Hughes, 2006).

2.2 Cooling Season

Compared to the heating season, there is notably more literature on stratification during the cooling season. There are two methods by which cooling is typically executed. The first, and older method, of cooling is mixing ventilation (MV). This method vents cooled air into a room at an elevated position, mixing the room's air and attempting to achieve a uniform temperature (Lin et al., 2005). The second method is displacement ventilation (DV). DV supplies cool, low velocity, air at the floor level, displacing warmer air upwards, which is then exhausted out of the room (Lin et al., 2005). With the MV method, a flat temperature profile is created, where as with DV, a stratified temperature profile will be developed.

When studying cooling, the goal is to determine the best method by which people are kept "comfortable." Thermal comfort is a complicated subject and includes several factors such as: metabolic rate, clothing, air velocity, air temperature, thermal stratification, radiant temperature asymmetry, relative humidity, and turbulence intensity (Lin et al., 2005). Lin et al. (2005) performs a comparison between MV and DV cooling methods, with the goal of determining if DV is a suitable cooling option when compared to the traditional MV method. It is concluded that DV is able to create a comfortable environment with a user dissatisfaction less than

10%, whereas with MV dissatisfaction tends to be above 20% (Lin et al., 2005).

When looking at more recent publications, DV cooling is the most studied and seems to be replacing the simpler MV cooling method. A similar method to DV is under-floor air distribution (UFAD). Both UFAD and DV methods take advantage of the thermal plume effect and fall under the category of stratified air-distribution systems. The UFAD method has been increasing in popularity in North America for cooling (Lee et al., 2012). An example of a temperature profile attained by UFAD can be seen in Figure 2.3.

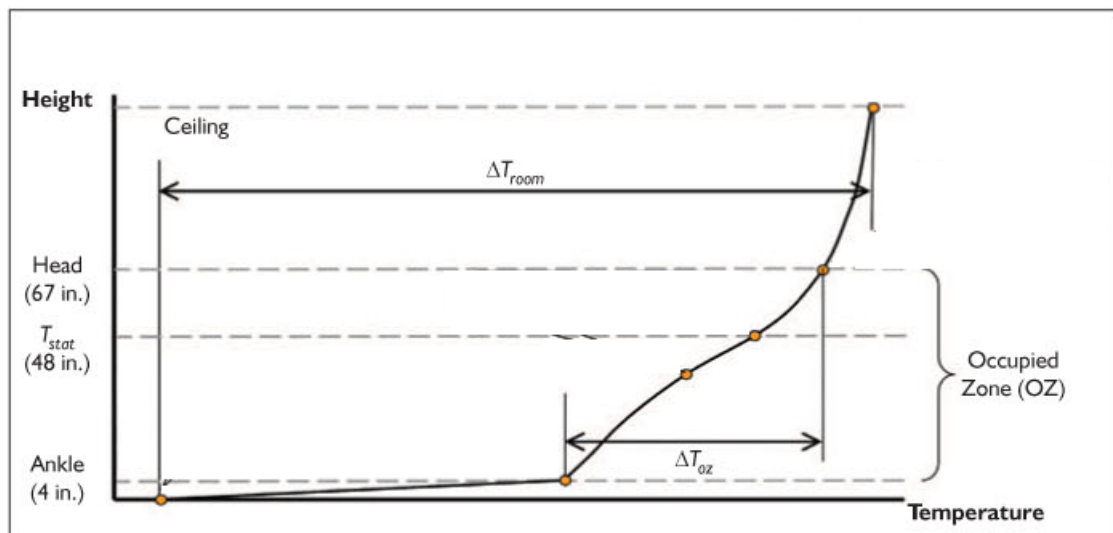


Figure 2.3: Example thermal profile developed by UFAD (Bauman et al., 2007)

In UFAD, cool air enters at ground level and is kept in place by the thermal plume effect. Warmer air is displaced upward where it can be exhausted from the room. The region of interest in UFAD is the occupied zone, shown in Figure 2.3. In UFAD design, the goal is to minimize the ΔT within this occupied zone.

Different diffusers can be utilized to push the cooler air up to mix the occupied zone, without impacting the exhaust region above (Lee et al., 2012). Swirl diffusers have been concluded to be best for this function, but the velocity of the inlet air is a critical factor in establishing the stratified profile (Bauman et al., 2007).

Based on this review, it is apparent that stratification is actually desired during the cooling season. In the warehouse under consideration, there is no mechanical cooling, and no way for the cooling stratification profile to be modified using the solar powered and existing ventilation. Thus, the present investigation will focus on stratification effects during the heating season.

2.3 Numerical Model Studies of Indoor Stratification

Numerical model studies tend to investigate cooling strategies such as mixing or displacement ventilation. Despite the focus on cooling strategies, these studies are still of interest as they investigate turbulence models and other computational techniques for predicting transport in large indoor environments (Rohdin and Moshfegh, 2011) (Zhang et al., 2007). Mixing studies are also of interest as destratification is simply a mixing process.

Zhang et al. (2007) performed an investigation of several turbulence models utilizing ANSYS FLUENT. Turbulence models were compared using 4 different modeling and experimental cases: natural convection, forced convection, mixed convection, and strong buoyancy flow. Each turbulence model was then rated based on its comparison to available experimental data. The experimental cases

included: natural convection in a tall cavity, forced convection in a room with partitions, mixed convection in a square cavity, and strong natural convection in a model fire room.

To compare the turbulence models, a letter rating system was imposed. The ratings were: A = within 10% of experimental data, B = within 10-20%, C = 20-50%, D = greater than 50% of experimental data. If the model could not solve for a specific case, an n/a was listed for not applicable. If the model was unable to converge, an n/c rating was given (Zhang et al., 2007). The results can be seen in Table 2.1:

Table 2.1 Turbulence Ratings (Zhang et al., 2007)

Cases	Compared Items	Turbulence Models							
		0-eq.	RNG $k - \epsilon$	SST $k - \omega$	LRN-LS	V2f-dav	RSM-IP	DES	LES
Natural convection	Mean temperature	B	A	A	C	A	A	C	A
	Mean velocity	D	B	A	B	A	B	D	B
	Turbulence	n/a	C	C	C	A	C	C	A
Forced convection	Mean velocity	C	A	C	A	A	B	C	A
	Turbulence	n/a	B	C	B	B	B	C	B
Mixed convection	Mean temperature	A	A	A	C	A	B	B	A
	Mean velocity	A	B	B	B	A	A	B	B
	Turbulence	n/a	A	D	B	A	A	B	B
Strong Buoyancy Flow	Mean temperature	A	A	A	A	A	n/c	n/a	B
	Mean velocity	B	A	A	A	A	n/c	n/a	A
	Turbulence	n/a	C	A	B	B	n/c	n/a	B

The models that were successful most often in matching real world data utilized RNG $k - \epsilon$ and V2f-dav turbulence solvers (Zhang et al., 2007). Rohdin and Moshfeqh (2011) also found the RNG $k - \epsilon$ model to more accurately fit with their studies

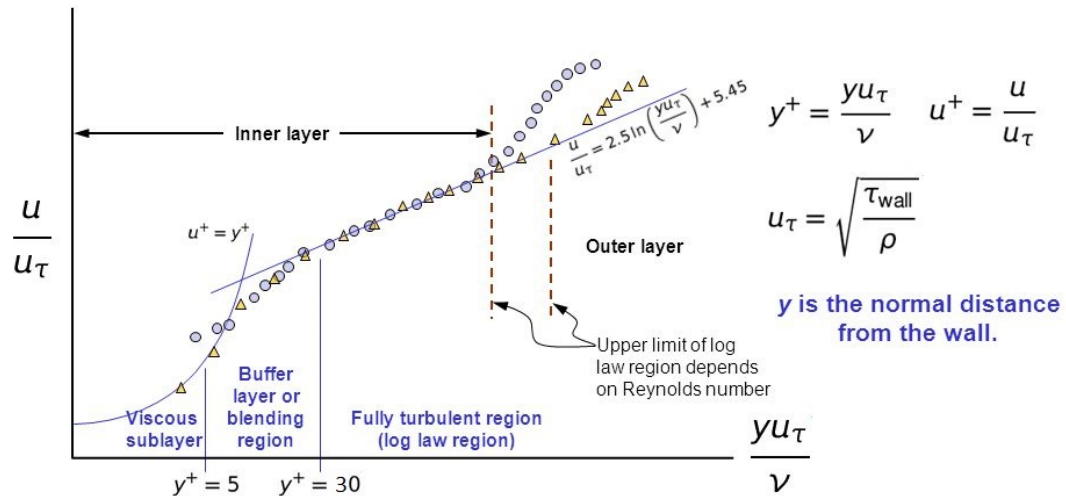
experimental data (Rohdin and Moshfegh, 2011). This is partially related to the computation time. With models which had results closest to experimental data, there was a general increase in computational time required to converge (Zhang et al., 2007). This is related to the number of new equations introduced to solve for turbulence (Versteeg and Malalasekera, 1995). The other contributor to accuracy is if the additional equations are designed for the geometry and flow which they are solving, such as the different experimental cases presented by Zhang et al. (2007) (Versteeg and Malalasekera, 1995).

Prior to running simulations, it is important to establish the quality of the selected mesh. In Zhang et al. (2007), the mesh coarseness was determined using y^+ values, a dimensionless value used as a guideline to inform the size of the cells at the model boundaries. y^+ values are utilized to create the Universal Law of the Wall, or the universal velocity profile, seen in Figure 2.4. This velocity profile applies to all turbulent boundary layers. The y^+ values are a function of distance from the wall, and the shear stress seen at that wall.

Turbulence Modeling

The Universal Law of The Wall





- Dimensionless velocity profiles plotted in the near-wall coordinates
- The linear section in the semi-log plot is called the universal law of the wall layer, or log law layer, for equilibrium turbulent boundary layers (TBL)

Figure 2.4: Universal Velocity Profile (ANSYS, 2017)

Each model has different target values for y^+ , depending on what assumptions were made when developing the model. For example, the $k-\epsilon$ model expects y^+ values to be in the fully turbulent region of the universal velocity profile, Figure 2.4. This is because the model has been designed to treat the first cell as the sub-viscous later and an assumed value is assigned for the first cell. In the case of Zhang et al. (2007) the meshes had y^+ values of 0.3 and less than 0.1. Due to these low values, the RNG and RSM-IP models required an enhanced wall treatment setting available in FLUENT to compensate for y^+ values which are not ideal for

those turbulence models (Zhang et al., 2007). Another method of evaluating mesh quality is a mesh independence study. This is the method of reducing cell size incrementally and performing repeated simulations. The size at which the results of the mesh cease to have a notable difference is considered the minimum mesh size (Ho et al., 2010).

2.4 Need for Present Work

The limited prior studies of destratification during heating season have focused on predicting the cost savings due to reducing the stratification profile. There is little attention given to the performance of the destratifying fans, other than as a parasitic loss on savings. However, fans are shown in multiple studies to have parasitic losses on savings attained by destratification, in at least one case to the point that the fans cost more than the savings attained by destratification were negated (Aynsley, 2005; Armstrong et al., 2009; Hughes, 2006). The potential for losses suggests that it is important to understand fan size, power, control strategy and locations within an environment.

In the present study, the solar powered ventilation devices under investigation can provide destratification without grid power, effectively eliminating the parasitic losses. However, there is a concern that the solar powered fans are most needed when the least solar power is available during the short winter days. Thus, the objective of this study is to use experiments and simulation to quantify the estimate the required run time percentage for destratification fans to provide an

energy savings effect. Any reduction in run time will increase the overall savings of maintaining destratification. To determine a fan duty time, two models were developed. One model shows mixing behavior, calculating the time required to achieve destratification. The other model calculates the time for the building to cool sufficiently that heaters need to be activated. The combination of these two models can be used to optimize control strategies of either solar or grid powered fans, and help designers size battery backup for solar powered fans so that minimum run times can be achieved.

Chapter 3: Experimental Setup

Two separate experimental setups were utilized by this study. One located in a large warehouse with a single row of SunCooler destratification fan units installed, and the other in a school room with a single SunCooler unit installed. Within the large warehouse the experiment is designed to collect temperature data at discrete heights throughout the warehouse, CO₂ concentration, and relative humidity data. This is executed over a large range of the warehouse, both for areas serviced by SunCooler units, and areas well away from the SunCooler units. The school room experiment was designed to collect temperature data at discrete heights to characterize the induction cooling which the SunCooler unit was designed to perform at that site. This chapter will cover the specific setup of each location, the sensors used, and justification for the setup. Table 3.1, located at the end of this chapter, lists all sensors that were used for the experiments, where they were utilized, and their capabilities.

3.1 Large Warehouse Experimental Setup

The first experimental site is a 1.5 million square foot warehouse. This warehouse serves as a distribution center and has considerable traffic in and out of the building as packages are unloaded, stored, and reloaded. Approximately 0.5 mil-

lion square feet of the warehouse were utilized for this experiment. The warehouse operates in two modes, summer and winter. Exhaust fans are enabled during summer mode, and heaters are enabled during winter mode. Within this space there are 4 zones which contain 10 HP wall and roof exhaust fans which can either exhaust or induct air. In total there are 8 wall exhaust fans, and 2 roof exhaust fans. These fans are utilized to cool the building via night flush, inducting external air during the night. The heaters utilized are Direct Gas-Fired Make-Up Air (MAU) units. These heaters pull air from the outside and passes it through a gas burner to heat the air prior to venting it into the building. There are 7 heater units, which are rated for 12,045 CFM and utilize 1.3 million BTU/hour, heater locations can be seen in Figure 3.7. During winter mode, these heaters are set to activate when thermostats at a height of 6 feet read 63 °F at the Northern wall, or 62 °F at the Southern wall.

Seven SC15000 model SunCooler units were installed at the warehouse in a North-South oriented column at a 90 ft spacing. The units were installed evenly between North to South running girder trusses. Holes were drilled from the interior at the four corners of the installation site to be located externally. The roof membrane and insulation were removed in preparation for cutting a hole for the installation of the SunCooler unit. Plywood was then placed on the underside of the installation site to provide a temporary barrier while the unit is being installed and ensure no personnel can fall through the hole being cut, shown in Figure 3.1.



Figure 3.1: Covered roof penetration



Figure 3.2: Roof curb installation

With the plywood in place, the metal decking is secured with chain links and then cut out and removed. With the metal decking removed, the roof curb, shown in Figure 3.2, was oriented using the previously drilled holes. Insulation can be re-installed around the edge of the curb and waterproofing can be installed on top of that, shown in Figure 3.3.



Figure 3.3: Water proofing and insulation installation



Figure 3.4: Installed destratification unit

With the water proofing installed, the plywood is removed, and the SunCooler destratification unit, shown in Figure 3.4, is lowered into place. Once the destratification unit is installed, all that remained was the placement of the housing unit, which is where the photovoltaic modules are located. The completed installation can be seen in Figure 3.5.



Figure 3.5: Installed SunCooler housing

The SC15000 model SunCooler units are designed to output air at 15000 CFM and are capable of all three modes of operation shown in Figure 1.4. The units also come equipped with internal sensors for: indoor temperature °F, indoor relative humidity %, indoor CO₂ ppm, outdoor temperature °F, and outdoor relative humidity %.

Inside the warehouse, wireless sensors were installed as shown in Figure 3.7. The network consisted of remote sensor units, repeaters, and a single base unit. The units communicated with one another through short range radio communication FCC Part15 Section 247/IC RSS-210 (Frequency Range 902 to 928 MHz, RF Power: 7 mW). Data was sent from remote units to the closest repeater, and then

relayed to the base unit. The base unit was AC powered, while all other units were battery powered.

When setting up the temperature and humidity sensor network it was first necessary to find an area of low wireless interference (from radio communication, facility wi-fi, etc.) and low physical obstruction to maximize the distance that the sensors could communicate. As the warehouse is a distribution center with large storage racks with high turnover, it was difficult to find a location that would be consistently unobstructed, but an area that had less activity for certain times of the day was located. Figure 3.6 shows the blueprint of the warehouse provided by the facility and is notated with sensor, repeater, and data collection locations.

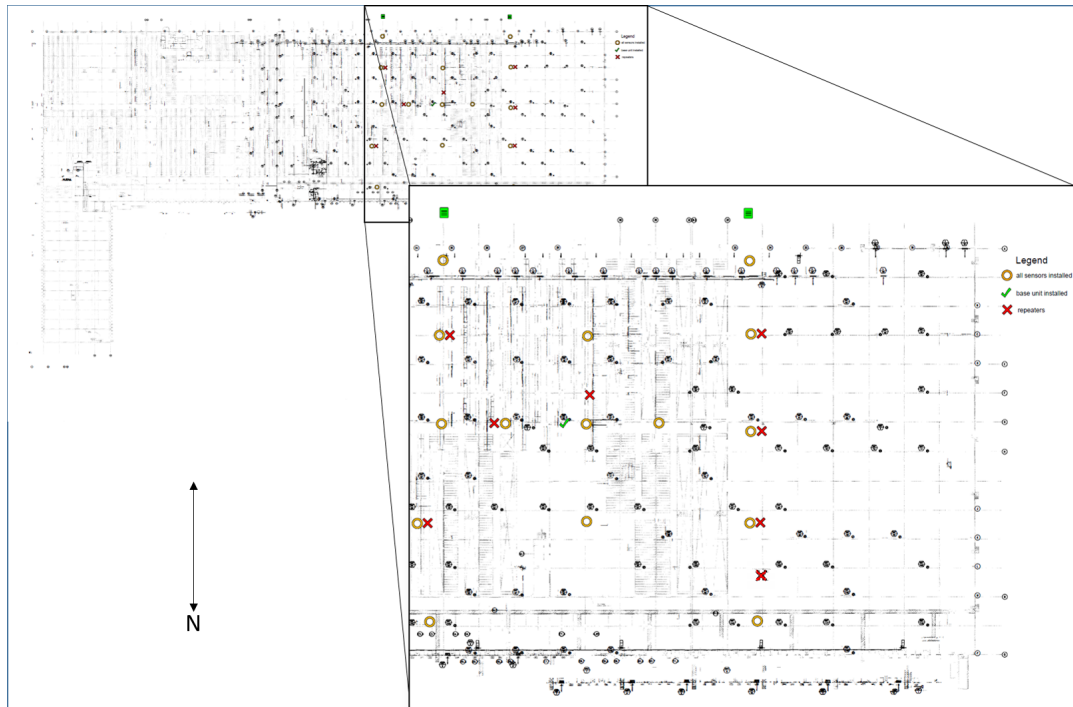


Figure 3.6: Warehouse blueprint with sensor notes

The L-shape in Figure 3.6 represents the warehouse, with the magnified portion showing where the sensor network was setup. The sensor setup was divided into three sections: an experimental section where the SunCooler units are located, a control section approximately 500 ft away from the experimental section, and a buffer section in between. Figure 3.7 provides a more detailed view of sensor, heater, and SunCooler locations.

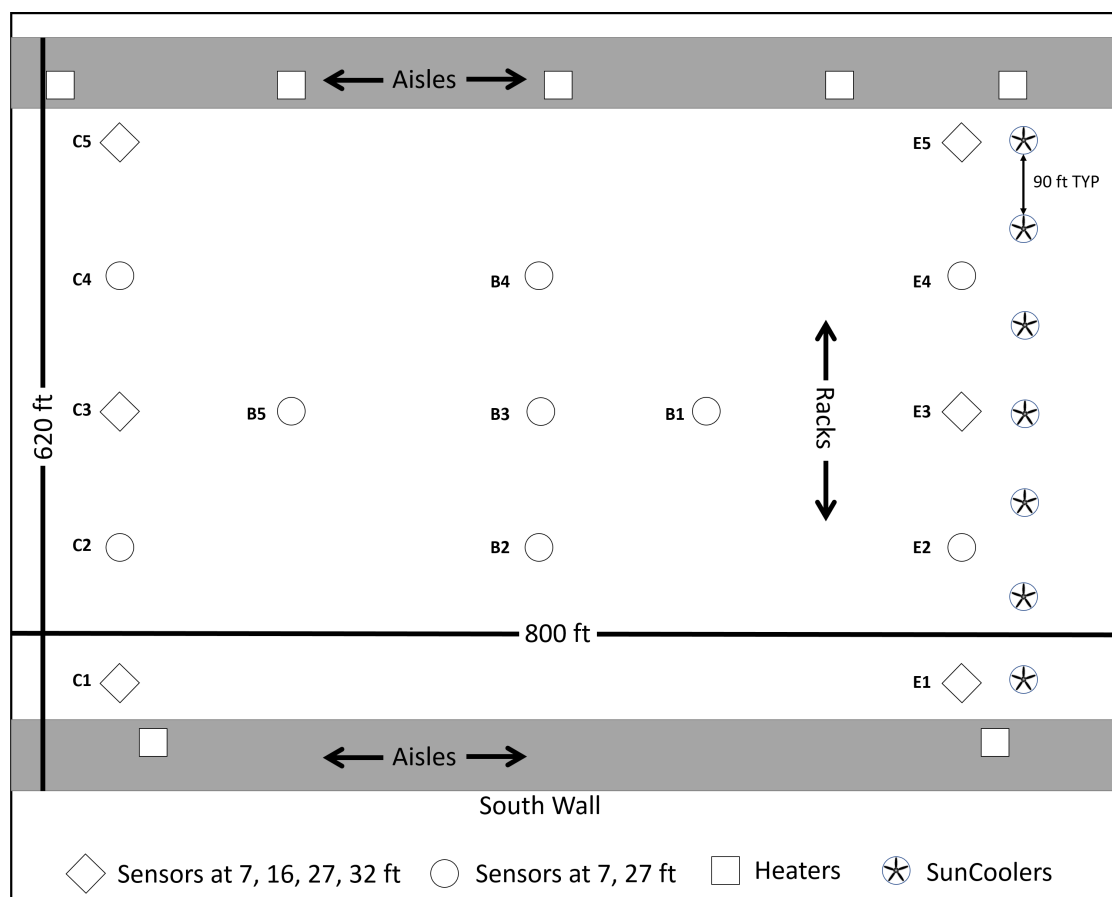


Figure 3.7: Warehouse sensor layout

Two different types of sensors were used to setup each column. RTR 501L sen-

sors which collected only temperature data and RTR 503L sensors which collected temperature and relative humidity data. The sensors have a reported accuracy of ± 1 °F and operate over a range of -40 °F to 176 °F. To compensate for weaker signals due to installation locations and obstructions, RTR 500 Repeaters were installed to boost the signal between the sensors and the base unit. Additionally, the base unit was installed in a location that was known to have lower noise during night hours and the sensors were setup to only send the collected data at these times. The laptop that acted as the base unit also utilized an RTR 500 Repeater to receive the data from the sensors, as seen in Figure 3.8.



Figure 3.8: Base unit RTR 500 repeater

Initially all sensor columns contained three sensors at 7 ft, 16 ft, and 27 ft. It

was later decided that more detail was required at the deck height of 32 ft, which prompted the install of additional RTR 501L sensors at the E-1, E-3, E-5, C-1, C-3, and C-5 locations, this was done in March of 2017. The sensors were all set to collect data at 5 minute intervals and send data to the base unit after midnight. The data was then downloaded manually from the base unit on a weekly basis.

The warehouse utilizes makeup air units (MAU) for heating, which are installed at the ceiling, shown in Figure 3.9. To determine when these units were utilized, RTR 501L temperature sensors were installed on the MAU units to detect when the temperature would increase dramatically, indicating that the MAU unit was on. These units collected data every 5 minutes and reported to the base unit at preset times.



Figure 3.9: MAU heater, interior view

To monitor the warehouses exhaust fans, HOBO Motor On/Off Data Loggers

(UX90-004) were installed inside fan control areas. Assistance was needed from the warehouses Engineering and Facilities personnel to access these sensors. Only four sensors were installed, one for each of the four exhaust fan zones which overlapped with the experimental setup. The sensors were attached to a single fan in each zone. When one fan activates in a zone, it indicates that all other zone fans are also running. A HOBO U-Shuttle was used to offload data from these sensors as they were not allowed to communicate through the local wireless network and were not a part of the RTR 500 series data loggers. Due to the difficulty of accessing data it was collected on a monthly basis.

Throughout the experiment the SunCooler units were set to perform night flushes, destratification, and exhaust at preset periods. Data was collected for this experiment from September 2016 to January 2018.

3.2 School Room Experimental Setup

While collecting data from the warehouse experimental setup, there was some concern regarding the region of influence for seven SunCooler units in such a large volume. This prompted an investigation into an alternative experiment setup where more control over the environment could be exercised. Prior to this study, the 1k SunCooler unit model had been installed in classrooms to perform induction cooling in Corvallis, Oregon. The classroom is 567 square feet with a ceiling height varying between 9 and 12 ft. The SunCooler installed at this location did not come with sensors, but was equipped with wireless access to schedule cooling periods.

Fortunately, the school faculty were willing to allow the experimental setup at their location. Figure 3.10 shows the classrooms with SunCooler units installed on the ceiling. There are three classrooms in this building, with only the left most one being used for experiments.



Figure 3.10: Front view of school building

The classroom was occupied during the day, so a permanent experimental setup was not possible. To work around this limitation, wireless HOBO ZW-006 and HOBO ZW-007 temperature sensors were setup along the walls where they would not be in the way of regular classroom activity. Additionally, sensors were installed

on posts that could be moved around the classroom for quick setup and breakdown of the experiment. The classroom setup is shown in Figure 3.11.

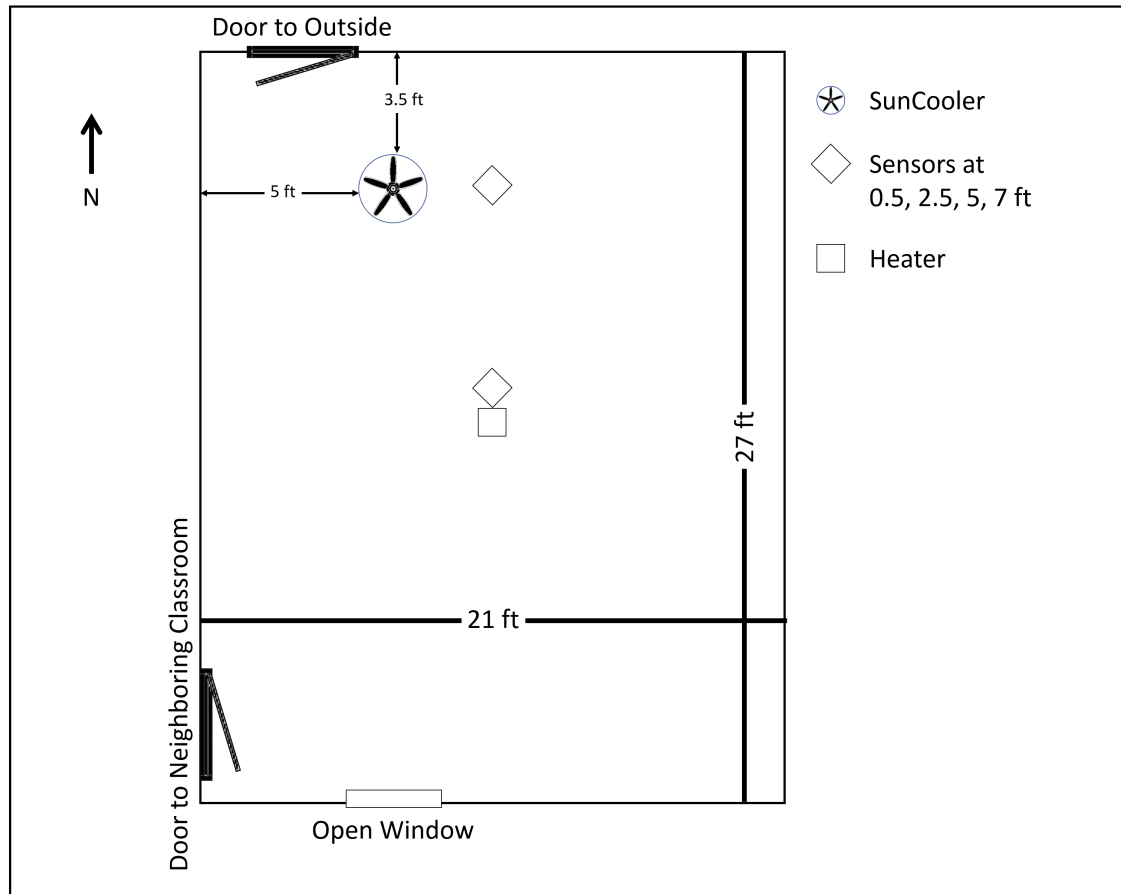


Figure 3.11: School room sensor setup

Each sensor post supported 4 sensors at heights of 0.5, 2.5, 5, and 7 ft. These sensors reported to a HOBO Data Receiver (ZW-RCVR) which was plugged into a laptop which remained on site. Experiments would be setup on evenings after the last day of class for a given week and broken down the morning prior to class starting again. Data from the prior weekend was collected at this time.

Experiments consisted of activating the SunCoolers after the room had reached a steady state temperature profile to determine the impact of induction cooling on the stratified profile by the SunCooler units. Experiments were run at this site from November 2017 to January 2018.

Table 3.1 Experimental equipment utilized

Item	Location	Purpose	Data Collected	Uncertainty
RTR 501L	Warehouse	Profile Data	Temperature	± 1 °F
RTR 502L	Warehouse	MAU On/Off Tracking	Temperature	± 0.6 °F
RTR 503L	Warehouse	Profile Data	Temperature and Relative Humidity	± 0.6 °F
RTR 500 Repeater	Warehouse	Sensor Range Extension and Base Station	None	N/A
HOBO Motor On/Off Data Logger (UX90-004)	Warehouse	On/Off Data for Exhaust Fans	On/Off Data	N/A
HOBO U-Shuttle	Warehouse	Data Collection from HOBO Motor On/Off Data Logger	None	± 1 minute/month
HOBO Data Receiver (ZW-RCVR)	School Room	Base Station	None	N/A
HOBO ZW-007	School Room	Profile Data	Temperature	± 0.38 °F
HOBO ZW-006	School Room	Profile Data	Temperature	± 0.38 °F
TMC1/6/20	School Room	Profile Data	Temperature	± 0.38 °F

Chapter 4: Model Development

This chapter discusses the modeling approach to perform simulations, the boundary conditions employed, the solvers utilized, and the outputs of the simulations.

4.1 Model Setup

The goal of the modeling portion of this study is to model the mixing and cooling behavior of air in a large scale warehouse. The model will produce qualitative predictions of required time for destratification for a given initial stratification profile and fan flow rate. It will also provide an estimate for how long the destratified profile will remain once fans have been turned off. Combined, this information will enable estimates of required destratification fan run time.

The model has been designed to predict performance over a range of possible geometric parameters representative of warehouses. This expands the studies investigation to warehouses of different heights and for different destratification capabilities, making the results of the study applicable for more than just the experimental case. The model will contain nine inlets representing fans. Inlets were selected to represent fans as the modeling package used did not have the capability to model a fan directly. Each inlet supplies air at specified flow rate (representing different fans) at the ceiling temperature. The inlets were arranged so that inter-

actions between fans with fans and fans with walls could both be observed. As the model is designed with inlets, pressurization of the model needs to be accounted for. With destratification no pressure build up should occur as it would operate in a closed system, assuming doors and windows remain closed. Therefore, outlets representing building exfiltration need to be included in the model to ensure that a pressure buildup does not occur. A generalized schematic of a warehouse is shown in Figure 4.1:

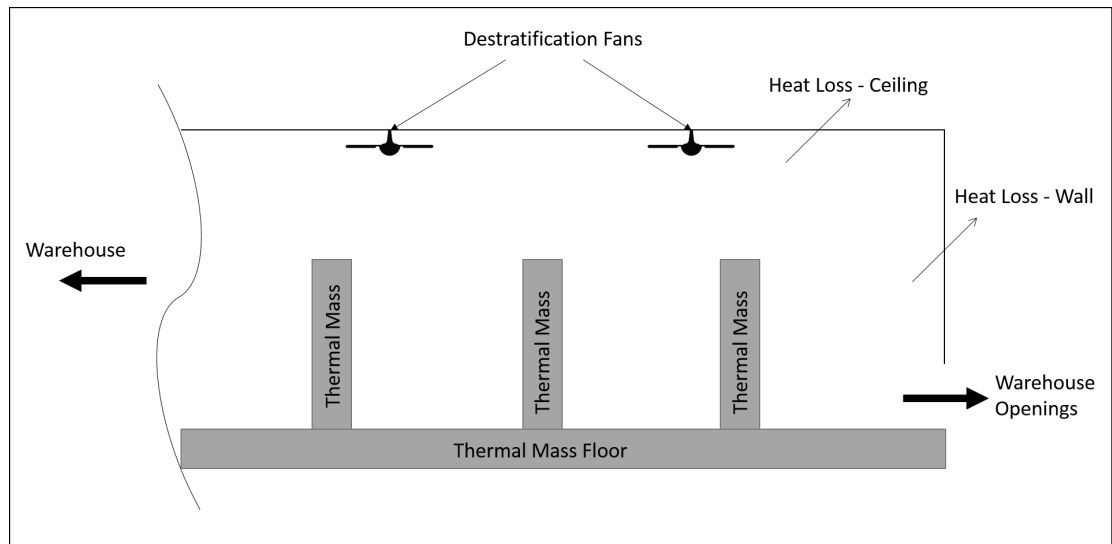


Figure 4.1: Generalized warehouse schematic

The primary components in the schematic are: the fans which perform destratification, heat lost through the ceiling and walls, and the thermal mass present in the warehouse. The thermal mass represents objects such as stored items, machinery, lighting, and personnel, and it affects mixing and cooling separately. For the cooling of the warehouse, the thermal mass could slow the cooling process as the

energy generated or stored by the mass would continue to warm the air, offsetting the cooling from heat lost at the boundaries. For mixing, the thermal mass acts as impediment to the velocity profile development, which drives the mixing, and would therefore slow mixing time. An analysis of the thermal mass is deemed to be beyond the scope of this investigation, due to time constraints. If mass were included, the mixing times would be expected to take longer, as discussed in the conclusions of this thesis.

When deciding upon a geometry, the model needed to be small enough to run in a reasonable time frame, while also being large enough to capture the fans interactions with each other and the walls. It was decided that a geometry with nine fans in a 3x3 grid would best satisfy this requirement.

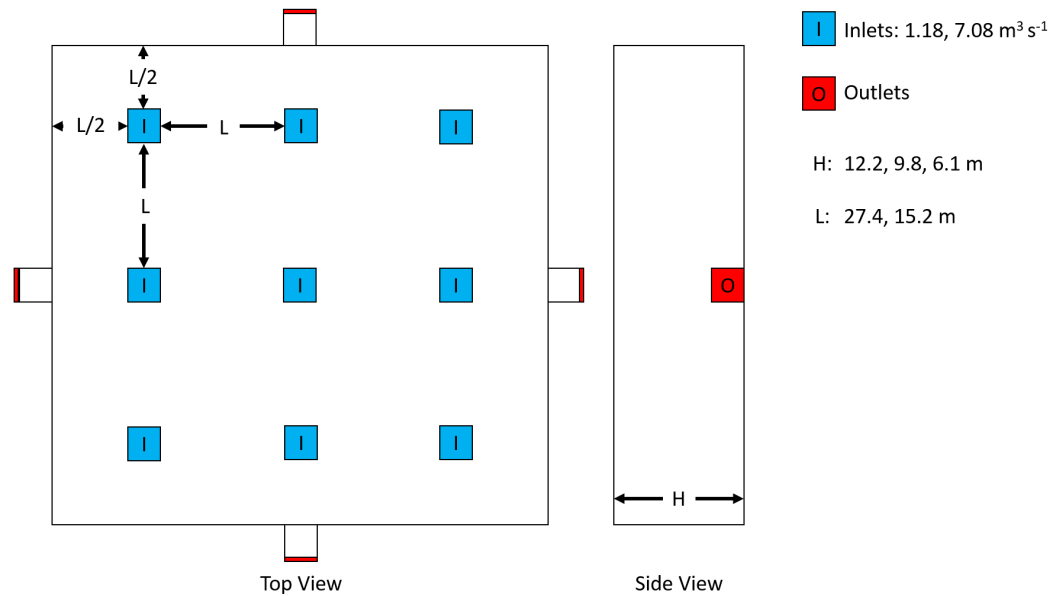


Figure 4.2: Example of model geometry

Figure 4.2 shows an example of the model geometry. The nine blue spots on the top of the box, labeled with an I, are inlets which represent fans. The fans represented will be the 15000 CFM and 2500 CFM SunCooler units. The inlet geometry is determined by which flow rate will be set at the boundary. The protrusions on the side of the box are outlets provided to ensure that the model roughly maintains the expected atmospheric pressure. The box size is determined by the spacing of the inlets and the expected height of a given warehouse. In a discussion with Jason Wright, CEO of NWREC, it was determined that for a 15000 CFM unit the expected coverage was 90 ft². Based on this, the fan spacing was set for 90, 75, 50, and 35 ft for the 15000 CFM unit and 50, 35, 25, and 15 ft for the 2500 CFM unit. It was also determined from this conversation that the typical warehouse heights are 20, 32, and 40 ft (Wright, 2017). Modeling of this geometry is executed with ANSYS CFX and ICEM CFD as a solver and mesh developer respectively.

4.1.1 ANSYS CFX & ICEM CFD

ANSYS CFX and ANSYS ICEM CFD are commercially available computational fluid dynamics (CFD) solver packages. ICEM CFD is a meshing tool which defines geometries by using points and curves. Once the geometry has been outlined with points and curves, surfaces are created to define geometry boundaries, which can be separated into parts. Blocks are then created within the geometry which are used to define the mesh. The ICEM CFD interface and a sample

geometry can be seen in Figure 4.3:

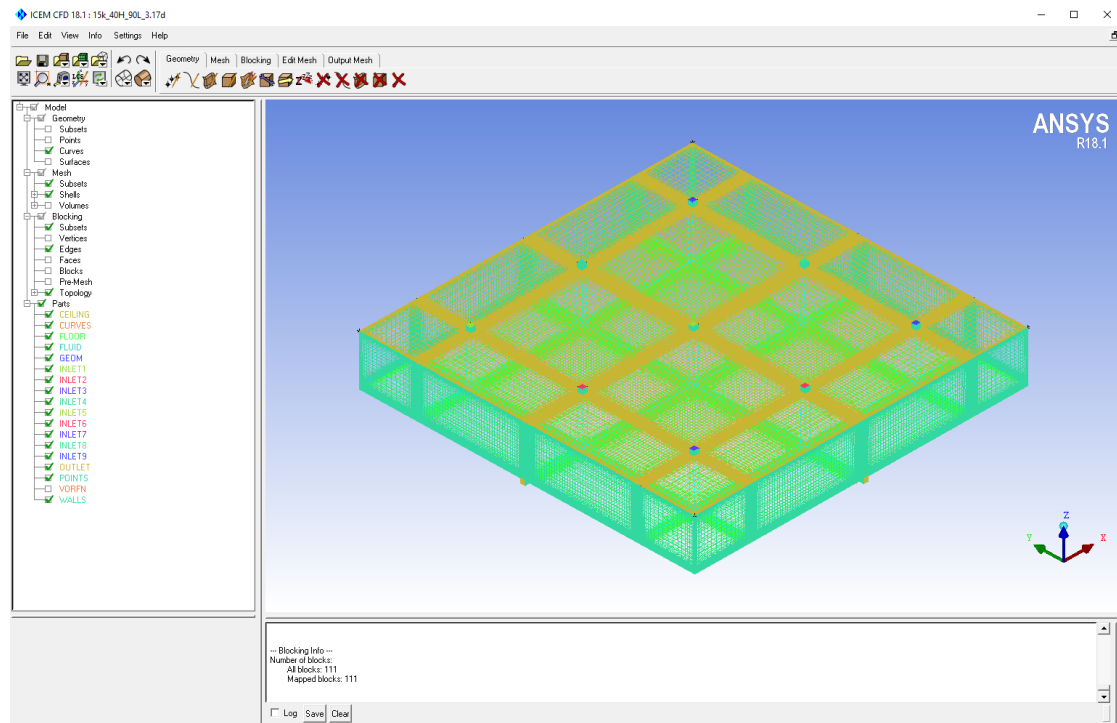


Figure 4.3: Example of ICEM CFD interface

Once meshing is complete, an output file is created which will be imported by CFX tools. ICEM CFD can generate mesh files for a range of CFD tools, and is not limited to CFX.

ANSYS CFX has three tools. CFX-Pre, CFX-Solver Manager, and CFX-Post. CFX-Pre handles all of the setup for a simulation. This is where meshes are imported. When imported, each of the parts defined in ICEM CFD need to be assigned a boundary condition such as a wall or an inlet. Each boundary condition has multiple options that need to be defined. For example, an inlet can be defined by a velocity, a mass flow rate, or a pressure.

There are also options for turbulence intensity, defined in section 4.3.1, and inlet temperature. Once all of the boundaries have been set, an analysis type needs to be selected. This can be steady state or transient. If transient flow is selected, there are options for how many time steps to take and how to define those time steps. The frequency at which these will be saved and where to save them is found under Output Control/Trn Results. The default domain contains options for fluid definition and fluid models for heat transfer and turbulence. Solver Control is selected to determine the residual target for the model to target, as well as the number of coefficient loops the solver has available to achieve this target. The residual is the measure of the models convergence. A residual is defined as the imbalance of input values to output values for a control volume. Convergence is considered to be acceptable when the residual is equal to or less than $1e-4$ (ANSYS, 2017). There is also an option to create custom variables, expressions, within CFX-Pre. These variables can be designed to change as the model changes or with location in the geometry. Expressions are needed to define parameters such as a temperature that changes with height. Figure 4.4 shows the CFX-Pre interface.

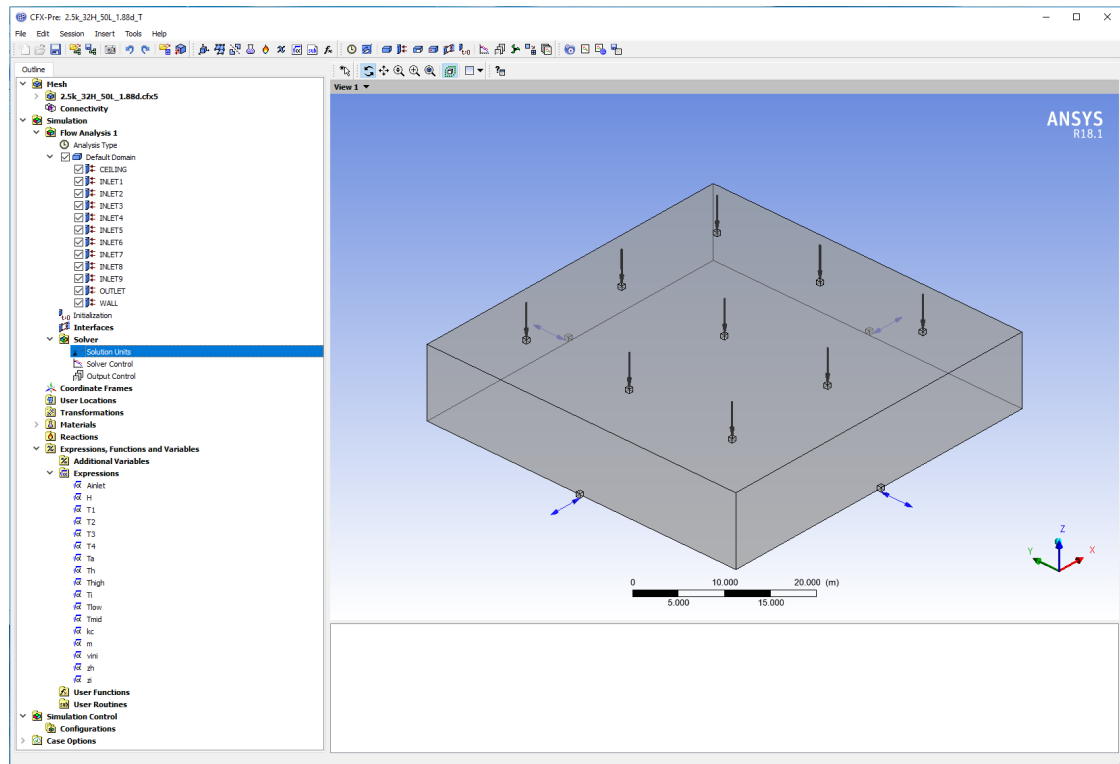


Figure 4.4: Example of CFX-Pre interface

Once all of the parameters have been set in CFX-Pre, a definition file is written out to be submitted to the CFX-Solver Manager. The solver manager defines the run using the definition file and can also choose to import initial values from a previous run.

CFX-Solver Manager outputs a results file which can be uploaded to CFX-Post. CFX-Post has a number of options for post processing results attained from a run. For this study it is used to create planes which are colored by temperature and velocity. It is also used to inspect y^+ values on each of the wall boundaries and generate streamlines.

4.1.2 Solver

When solving a turbulent flow there are 5 equations which govern the solver (Versteeg and Malalasekera, 1995):

Continuity:

$$\frac{\partial \rho}{\partial t} + \text{div}(\rho \mathbf{U}) = 0 \quad (4.1)$$

Where:

- $\frac{\partial \rho}{\partial t}$ is mass storage
- $\text{div}(\rho \mathbf{U})$ is momentum

Reynolds Averaged Navier-Stokes equations:

$$\frac{\partial(\rho U)}{\partial t} + \text{div}(\rho U \mathbf{U}) = -\frac{\partial P}{\partial x} + \text{div}(\mu \nabla U) + \left[-\frac{\partial(\overline{\rho u'^2})}{\partial x} - \frac{\partial(\overline{\rho u'v'})}{\partial y} - \frac{\partial(\overline{\rho u'w'})}{\partial z} \right] + S_{Mx} \quad (4.2)$$

$$\frac{\partial(\rho V)}{\partial t} + \text{div}(\rho V \mathbf{U}) = -\frac{\partial P}{\partial y} + \text{div}(\mu \nabla V) + \left[-\frac{\partial(\overline{\rho u'v'})}{\partial x} - \frac{\partial(\overline{\rho v'^2})}{\partial y} - \frac{\partial(\overline{\rho v'w'})}{\partial z} \right] + S_{My} \quad (4.3)$$

$$\frac{\partial(\rho W)}{\partial t} + \text{div}(\rho W \mathbf{U}) = -\frac{\partial P}{\partial z} + \text{div}(\mu \nabla W) + \left[-\frac{\partial(\overline{\rho u'w'})}{\partial x} - \frac{\partial(\overline{\rho v'w'})}{\partial y} - \frac{\partial(\overline{\rho w'^2})}{\partial z} \right] + S_{Mz} \quad (4.4)$$

Where:

- $\frac{\partial(\rho U)}{\partial t} + \text{div}(\rho U \mathbf{U})$ are the inertial forces
- $\frac{\partial P}{\partial x}$ is the pressure forces
- $\text{div}(\mu \nabla U)$ is the viscous forces
- $\left[-\frac{\partial(\overline{\rho u'^2})}{\partial x} - \frac{\partial(\overline{\rho u'v'})}{\partial y} - \frac{\partial(\overline{\rho u'w'})}{\partial z} \right]$ are the Reynolds Stresses
- S_{M_x} is external forces

Scalar transport equation:

$$\frac{\partial(\rho \Phi)}{\partial t} + \text{div}(\rho \Phi \mathbf{U}) = \text{div}(\Gamma_\Phi \nabla \Phi) + \left[-\frac{\partial(\overline{\rho u' \Phi'})}{\partial x} - \frac{\partial(\overline{\rho v' \Phi'})}{\partial y} - \frac{\partial(\overline{\rho w' \Phi'})}{\partial z} \right] + S_\Phi \quad (4.5)$$

Where:

- $\frac{\partial(\rho \Phi)}{\partial t}$ is the unsteady term
- $\text{div}(\rho \Phi \mathbf{U})$ is the convection term
- $\text{div}(\Gamma_\Phi \nabla \Phi)$ is the diffusion term
- $\left[-\frac{\partial(\overline{\rho u' \Phi'})}{\partial x} - \frac{\partial(\overline{\rho v' \Phi'})}{\partial y} - \frac{\partial(\overline{\rho w' \Phi'})}{\partial z} \right]$ are the Reynolds Stresses
- S_{M_x} is the sources term

In equations 4.2-4.5 the Reynolds stresses are present. These terms constitute turbulent stresses. The terms cannot be solved directly and are what turbulence

models are designed to solve for. When studying literature, the RNG $k-\epsilon$ model was stated to be one of the most robust of the turbulence models tested for internal convective flows in large buildings similar to those under investigation here (Zhang et al., 2007). When investigating the difference between the standard $k-\epsilon$ and the RNG model, it was found that the only change is the alteration of the $C_{\epsilon 1}$ term from a constant to an additional coupling term between the k and ϵ equations. This alteration to the standard $k-\epsilon$ primarily yields improved results for modeling rotating cavities, which this study is not concerned with (ANSYS, 2017). Another model that could be utilized for this study is the Reynolds Stress Model. Where the $k-\epsilon$ model introduced two additional equations, the Reynolds Stress Model introduces an additional seven. While the Reynolds Stress Model does offer potential improvement with buoyant flows, it suffers from the same shortcomings of the $k-\epsilon$ model in that it over predicts the spreading rate of axis-symmetric jets in stagnant surroundings. Without improvement on the relevant $k-\epsilon$ shortcomings, the increased cost of the Reynolds Stress Model was considered to be a poor trade-off to the relatively inexpensive $k-\epsilon$ model. Additionally, the $k-\epsilon$ model is reported to perform well for confined flows where Reynolds stresses are highly important (Versteeg and Malalasekera, 1995). Due to the enclosed nature of the model, and the need for several different simulations, the standard $k-\epsilon$ equation provided a good fit in terms of accuracy and computational cost.

The standard $k-\epsilon$ model adds two additional equations which are used to solve the bracketed terms in Eq 4.2-4.5 (Versteeg and Malalasekera, 1995):

$$\frac{\partial(\rho k)}{\partial t} + \text{div}(\rho k \mathbf{U}) = \text{div} \left[\frac{\mu_t}{\sigma_k} \nabla k \right] + 2\mu_t E_{ij} \cdot E_{ij} - \rho \epsilon \quad (4.6)$$

$$\frac{\partial(\rho \epsilon)}{\partial t} + \text{div}(\rho \epsilon \mathbf{U}) = \text{div} \left[\frac{\mu_t}{\sigma_\epsilon} \nabla \epsilon \right] + C_{1\epsilon} \frac{\epsilon}{k} 2\mu_t E_{ij} \cdot E_{ij} - 2C_{2\epsilon} \rho \frac{\epsilon^2}{k} \quad (4.7)$$

where:

$$\mu_t = \rho C_\mu \frac{k^2}{\epsilon} \quad (4.8)$$

and:

- $\frac{\partial(\rho k)}{\partial t}$ is the rate of change of k or ϵ
- $\text{div}(\rho k \mathbf{U})$ is the transport of k or ϵ by convection
- $\text{div} \left[\frac{\mu_t}{\sigma_k} \nabla k \right]$ is the transport of k or ϵ by diffusion
- $2\mu_t E_{ij} \cdot E_{ij}$ and $C_{1\epsilon} \frac{\epsilon}{k} 2\mu_t E_{ij} \cdot E_{ij}$ are the rate of production of k or ϵ
- $\rho \epsilon$ and $2C_{2\epsilon} \rho \frac{\epsilon^2}{k}$ are the rate of destruction of k or ϵ

Within these equations C_μ , σ_k , σ_ϵ , $C_{1\epsilon}$, and $C_{2\epsilon}$ are all adjustable constants which were determined by data fitting turbulent flows. To ensure proper model behavior at the boundaries, the standard k- ϵ model expects y^+ values to be between 30 and 500 (Versteeg and Malalasekera, 1995). This corresponds to the fully turbulent (log law) region of boundary layer development, seen in Figure 2.4, which the standard k- ϵ is designed for. Attaining the appropriate y^+ values will be discussed in the mesh section of this chapter.

In addition to the turbulence model, a wall function needs to be selected for solving near wall turbulent behavior. The traditional wall function has the problem of inconsistent results dependent on how fine the near wall mesh is. To offset this, ANSYS CFX has developed a Scalable Wall Function which applies a lower limit for the y^+ value used in the equations which determine shear stress at the wall. By imposing this limit, the mesh points are all forced to be outside of the viscous sublayer, shown in Figure 4.5, and mesh inconsistencies are avoided (ANSYS, 2017). The scalable wall function is the only wall function available when using the standard $k-\epsilon$ turbulence model.

4.2 Mesh

The geometry being used for modeling has 9 inlets and 4 outlets positioned in line with each other. While this is in part due to how the fans themselves would be installed, there is also a meshing consideration for the alignment. After the geometry is completed and fluid blocks have been defined, the mesh needs to be created. To create the mesh, each fluid block edge is assigned a number of node points, which will inform how many cells are present in the fluid block. Additionally, you can select how close to block corner the second node is located, which will be the Δy of the first cell. Each subsequent node spacing is defined by a multiple which gradually increases cell size.

In the geometry used for this study, there are 102 blocks, which means 816 different edges that need to be defined for the mesh. ICEM CFD has the option

to copy an edge parameter to all neighboring edges. When the blocks are designed so that they are in line, this reduces the number of edges that need to be defined to 21. Additionally, when defining the mesh for the inlets and outlets, the mesh needs to be much finer in order to properly model the near wall effects. This means that all cells projecting out from the inlet edge will also need to have the same grid spacing. If the points that require finer meshes are not lined up, the number of cells required to properly define the mesh increases dramatically. By lining the inlets and outlets up, the regions that require a finer mesh bisect each other, reducing the total number of cells.

Mesh size is something that is decided by the results of the simulation. There are two primary ways in which the mesh size is determined: investigation of the y^+ value, which is only done in the case of turbulent simulations as there is no y^+ in laminar flows, and a grid independence study. When investigating the y^+ this is an investigation of how large the Δy of the first cell should be, or the distance between the first and second mesh points. An example of this can be seen in Figure 4.6.

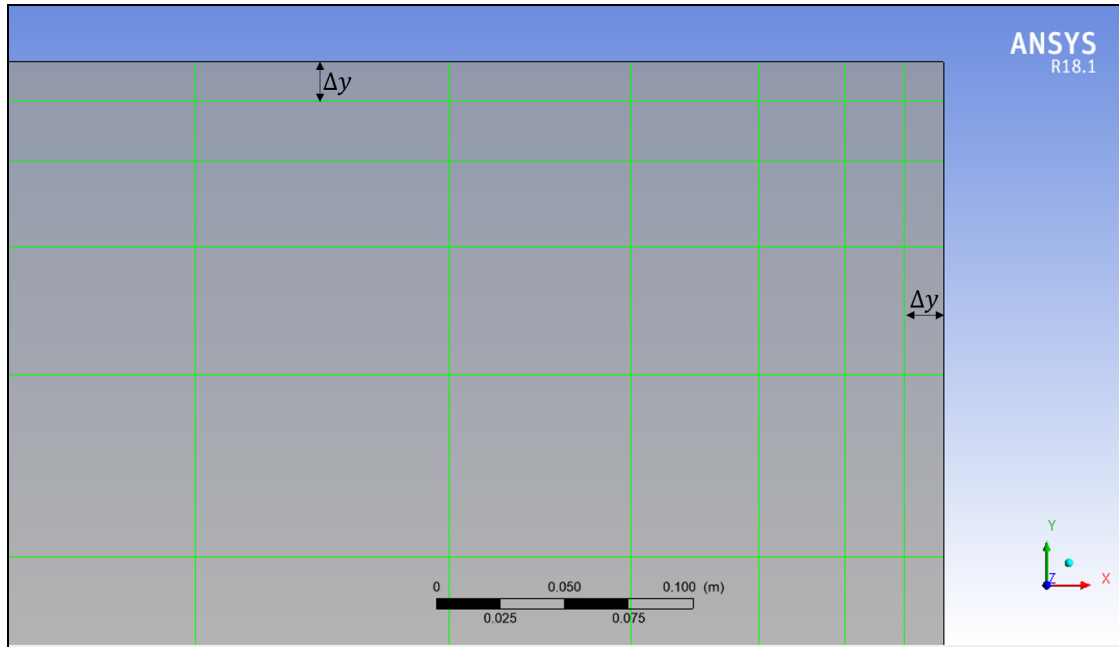


Figure 4.5: Mesh Δy example

The y^+ value is a function of the user set Δy and the calculated shear stress. As the shear stress is not known, initially the first cell size must be guessed. Generally choosing a small value, such as 0.01, for the second node and scaling each subsequent node to be between 1 and 2 times further away is a safe starting point, as we know that we will need a finer mesh at the walls and can have a coarser mesh at midpoints. Once the mesh is defined it can be uploaded to CFX-Pre. The settings which are used for the mixing models will be discussed in the mixing section of this chapter. For the purpose of finding y^+ values, the simulation is set to solve for steady state and solving the transport equation is disabled as the y^+ value is not dependent on energy.

Once the run has completed, the results are uploaded to CFX-Post. In post,

the external walls can be colored according by the y^+ value. The color gradient which represents y^+ can be given custom values. As our target value is between 30 and 500, these values are set initially. From this if there is blue, the lowest range, the color gradient can be reset for 0 to 30. If all the entire box is red, the color representing the highest values, then all of the y^+ values are at least 30 at the walls and the mesh satisfies the turbulence solvers requirements. If values at the wall are below 30 then the Δy value for the first cell should be increased to increase the y^+ value. The reverse is true if the y^+ values are found to be greater than 500. Figure 4.6 shows an example of a mesh which resulted in y^+ values which were too low.

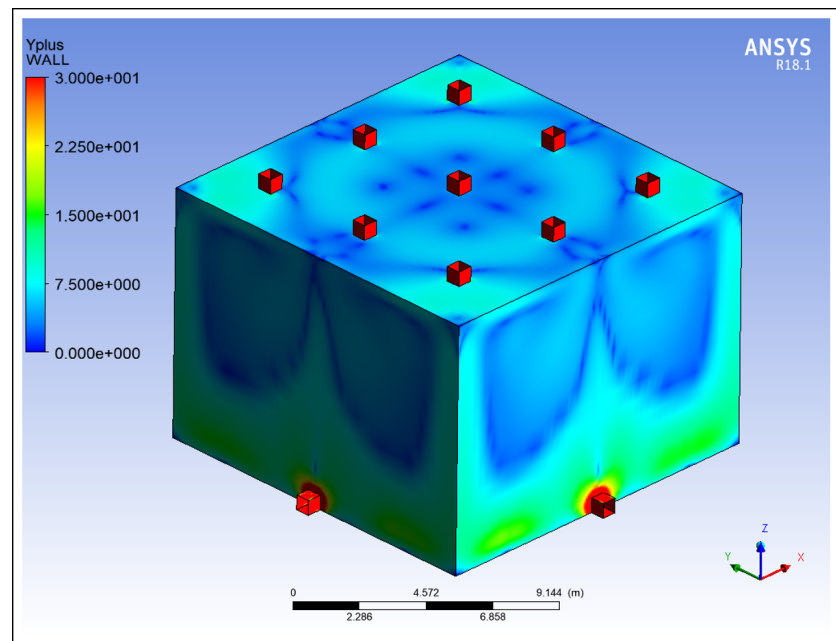


Figure 4.6: y^+ output example

In this case it was found that the entire surface was blue when inspecting for

values between 30 and 500, therefore the values were adjusted to 0-30. From that we can see that the ceiling and walls have y^+ values that are too low while the inlet and outlets have appropriate values. This means that the wall and ceiling Δy values need to be changed, but the inlet and outlet values can remain the same. The process is repeated until all y^+ values are between 30 and 500.

Performing a grid independence study is relatively straight forward by comparison. This is performed by first doing an initial run, then increasing the number of cells per fluid block and performing another run. The results of each run are then compared and if the difference is small the previous grid size is appropriately fine for the evaluated geometry. If the difference is large, the process is repeated until there is no longer a significant difference in the results. In this study, the time required for temperature to converge to within 0.5 °F was compared. As all of the geometries being evaluated were similar, only differing in scale, a single grid independence study was performed and the ratio of approximately 1 cell for 1 foot of physical distance was found to be an acceptable guideline for meshing each geometry. For example, if a block was approximately 10 feet across 10 cells would be assigned to the block. Conversely, the y^+ inspection must be performed on each mesh to ensure that the near wall effects are being properly evaluated by the turbulence model. Figure 4.7 shows a characteristic mesh with 13367665 nodes. The number of nodes for each model ranged from 5583991 for the smallest geometry to 13367665 for the largest.

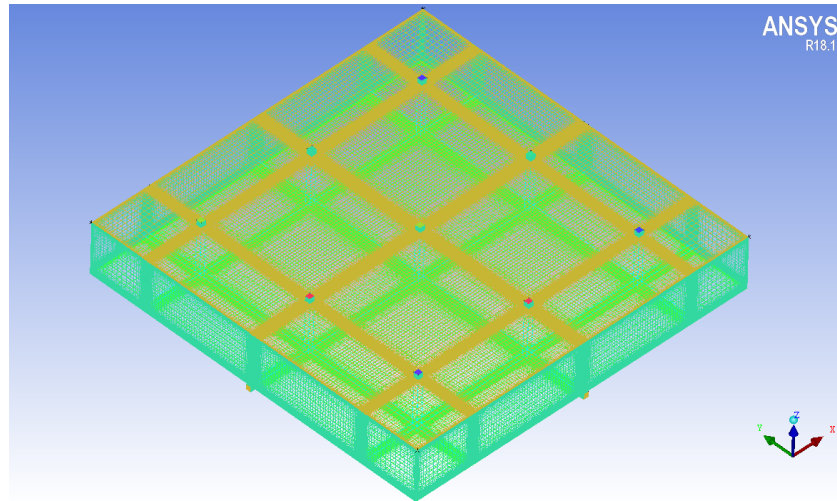


Figure 4.7: Sample mesh with 13367665 nodes

4.3 Mixing and Cooling Models

The cooling and mixing models mostly operate using the same inputs and settings, with some differences. This section will discuss the settings selected for the mixing model, then will note where the cooling model deviates from these settings.

For the ceiling and walls of the simulated warehouse, the boundaries were set with an external heat transfer coefficient of $0.3 \frac{W}{m^2K}$ and an external temperature of 5°F . These values were selected based on data available in the ASHRAE Fundamentals Handbook (ASHRAE, 2017). The floors were set to be adiabatic, no slip, walls. The inlets are set to be subsonic flow, as the fans are rated for relatively low speeds. For mass and momentum, the inlets are assigned a velocity which is calculated from a volumetric flow rate (Q) and the inlet area (A), Eq 4.9, provided by the SunCooler specification sheets.

$$v = \frac{Q}{A} \quad (4.9)$$

The 15000 CFM fan was calculated to output a velocity of approximately 5.5 $\frac{m}{s}$ while the 2500 CFM fan outputs a velocity of approximately 3.6 $\frac{m}{s}$.

When defining an inlet for a turbulent fluid, the expected turbulence intensity (I) needs to be selected. Equation 4.10 is provided to estimate the turbulence intensity as a function of Reynolds number (ANSYS, 2017).

$$I = \frac{0.16}{Re^{-\frac{1}{8}}} \quad (4.10)$$

Re is calculated at the inlet using Eq 4.11, with fluid properties evaluated at room temperature:

$$Re = \frac{vD}{\nu} \quad (4.11)$$

Calculating for turbulence intensity resulted in values of 3.2% and 3.6%. The 5% medium intensity setting was the best fit for these values. The temperature of the inlet was set to 70 °F. This matches the temperature of the warmest point in the initial temperature profile. The inlet temperature remains at this temperature as a crude substitute for heaters which would be expected to continue running while mixing occurs. Each inlet was defined separately with expressions to ensure uniform behavior.

Outlets were defined as pressure openings. This is to allow flow at the outlet to vary as needed. Allowing it the ability to exit or enter through the outlets, as

the pressure of the room dictates. This allows the room to maintain a relatively balanced pressure profile. The relative pressure of the inlet was set to 30 Pa. The turbulence intensity was set at the same value as the inlets. The opening temperature was set to 5 °F. This is representative of the temperature one might expect during a warming season (ASHRAE, 2017). The impact of this temperature on mixing was negligible as flow consistently moves out of the model through the outlets rather than into it.

Fluid properties were defined from the CFX library as air at 25 °C and a reference pressure of 1 atmosphere. For initial conditions, all velocity directions are assumed to be at rest with a static pressure of 30 Pa relative to atmospheric pressure. For the temperature, a profile was created using a linear approximation of profile D from Figure 1.3. The profile is divided into three pieces: a small temperature gradient from floor level to heater level, a large temperature gradient from the heater level to a point halfway between the heater and the ceiling, and a small temperature gradient from the ceiling-heater midpoint to the ceiling. This mimics the pocket of warm air that would be trapped at ceiling level by heating without mixing. Each section is represented by Equation 4.12.

$$T(z) = \frac{(T_i - T_{i-1})}{z_i - z_{i-1}}(z - z_i) + T_i \quad (4.12)$$

Where T is the temperature for the elevation, z is the current height, and i = 2,3,4.

To capture the buoyant effects of the temperature gradient, buoyancy is enabled with gravity set to be $9.81 \frac{m}{s^2}$ in the vertical direction (z). The buoyancy reference

temperature is set to as 20 °C.

For the solver, a Second Order Backward Euler (BE) scheme is employed. The second order BE is a second order accurate implicit time stepping scheme. This is not applicable for turbulence equations however, so the high resolution setting is enabled. This setting switches to a First Order BE scheme when first order accuracy is required. Using the two schemes together allows for the needed accuracy while minimizing run time (ANSYS, 2017). For transient runs, each time step is evaluated 3 times for convergence with a residual target of 1e-4 and a maximum time step of 0.5 seconds. For the initial time steps, a gradual increase in time step is employed starting at 1e-5 seconds and increasing to the maximum step size of 0.5 seconds. The chosen time steps were the result of a time independence study performed on the model. This study determined what the largest time step could be while maintaining the stability of the model. The settings used maintained residuals of 1e-4 or better and maximized the time step to reduce run time.

Models were run for a set number of time steps, then checked periodically to determine if mixing had completed. After a sufficient number of time steps, the maximum temperature difference within the warehouse will be less than 0.5 °F. When this is observed, mixing is considered to be completed. To match literature, the mixed temperature should be roughly 3 °F above the initial low temperature, and 7 °F below the initial high temperature (Armstrong et al., 2009).

For the cooling model, all of the solver settings and mesh validation are identical to that of the mixing model. The inlets and outlets are removed, which leaves only buoyant effects to drive any flow within the geometry. The cooling model does

not have as clear of a stopping point as the minimum allowable temperature is dependent on preference. Instead, it will be determined how long is required until the lowest elevation in the room begins to see a temperature decrease. With the results from mixing and cooling models, a duty cycle can be recommended for fans installed for the purpose of destratification.

Chapter 5: Experiment Results

This chapter presents and discusses the results collected from the warehouse and school room experimental sites.

5.1 Warehouse Results

Experiments were conducted at the warehouse location for a period of 16 months from September 2016 to December 2017. During this time, the SunCooler devices were run in either destratification or induction cooling mode, depending on the season. The time of operation also varied by month. A summary of SunCooler operation parameters is shown in Table 5.1.

Table 5.1 SunCooler run times for warehouse experiment

Date	Run time	Mode
2016 September	Automated	Destratification activated when ceiling temp is equal to 69 °F
2016 October	Automated	
2016 November	Automated	
2016 December	Automated	
2017 January	Automated	
2017 February	Automated	
2017 March	Automated	
2017 April	12pm - 10pm	Destratification
2017 May	12pm - 10pm	
2017 June	12pm - 10pm	
2017 July	12pm - 10pm	
2017 August	9pm - 9am	Induction Cooling (Night Flush)
2017 September	9pm - 9am	
2017 October	9pm - 9am	
2017 November	3pm - 9pm	Destratification
2017 December	3pm - 9pm	

As discussed in Chapter 4, temperature data was collected at various locations throughout the warehouse. Figure 5.1 and Figure 5.2 show monthly average temperatures for each sensor height for location 3 in the control zone and location 3 in the experimental zone, respectively. As shown in Figure 3.7, these locations are at a central point between the North and South walls. For each month, the average temperature at each height is divided by the temperature at the 7 ft height, which is the lowest elevation at which data was collected.

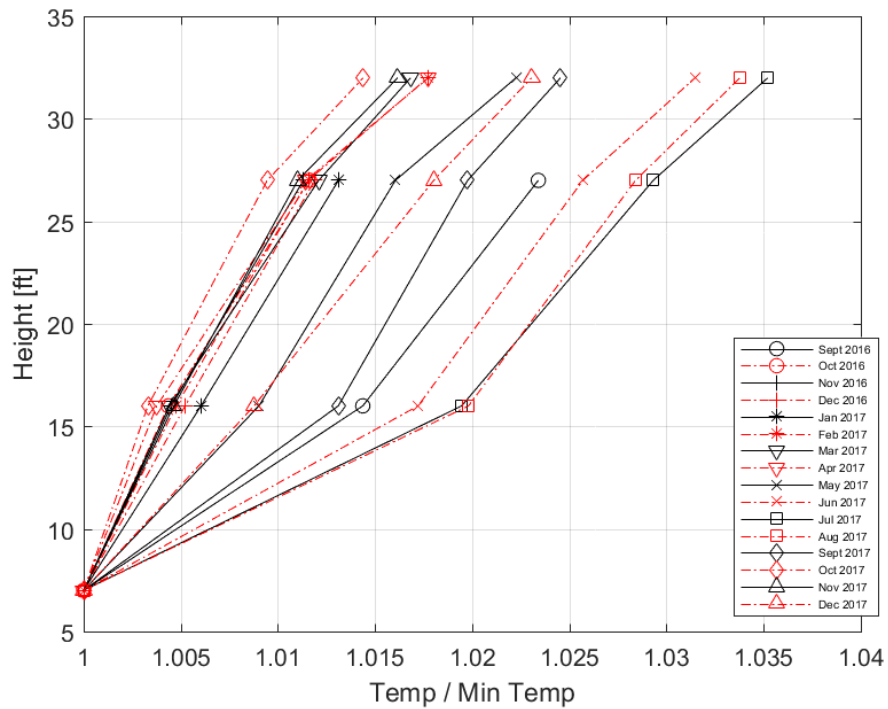


Figure 5.1: Control location 3 monthly temperature average vs height

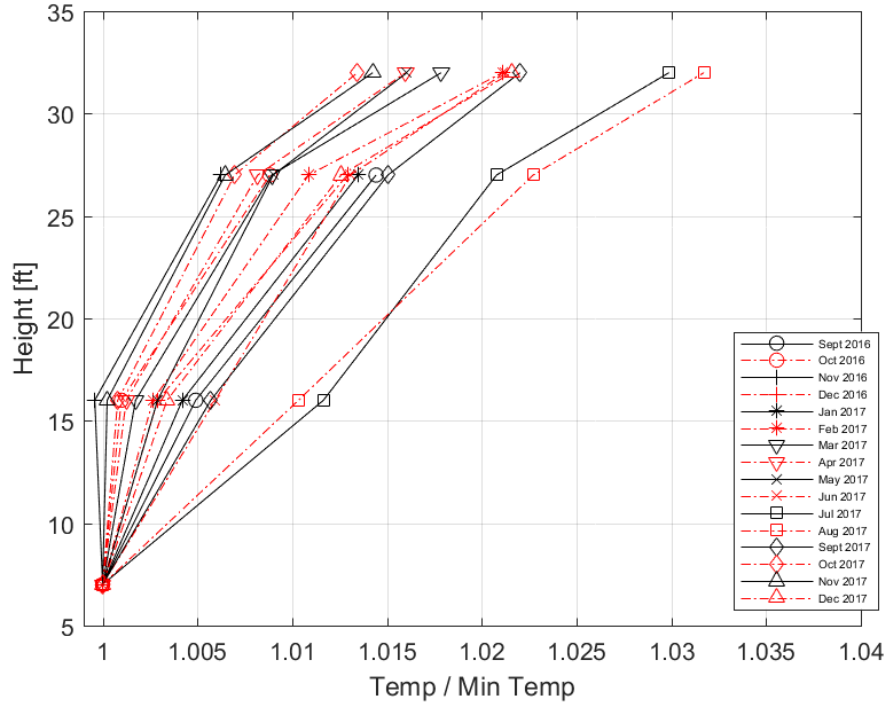


Figure 5.2: Experimental location 3 monthly temperature average vs height

Figure 5.1 shows that the months of greatest stratification occur in cooling months such as July 2017 and August 2017. While the least stratified months are heating months such as October 2017 and December 2017. When compared to Figure 1.1, we can see that the trend of stratification qualitatively matches the data provided by Porras-Amores et al. (2014) for an unheated warehouse. Thus, the data here suggests that the warehouse under investigation is under-heated. This is consistent with the observed warehouse heater runtime. Once the heating season started, the makeup air unit heaters were observed to operate almost continuously, implying that the thermostat was never satisfied and the

warehouse is under heated. Unfortunately, an under/unheated warehouse does not benefit significantly from destratification during the heating season. Figure 5.2 shows the temperature profiles for the experimental zone. These profiles are marginally less stratified compared to the control profiles, with the control peak ratio equaling roughly 1.036 and the experimental peak ratio being approximately 1.032. Profiles at other locations with deck height sensors were all processed and are shown in Figures 5.3, 5.4, 5.5, and 5.6.

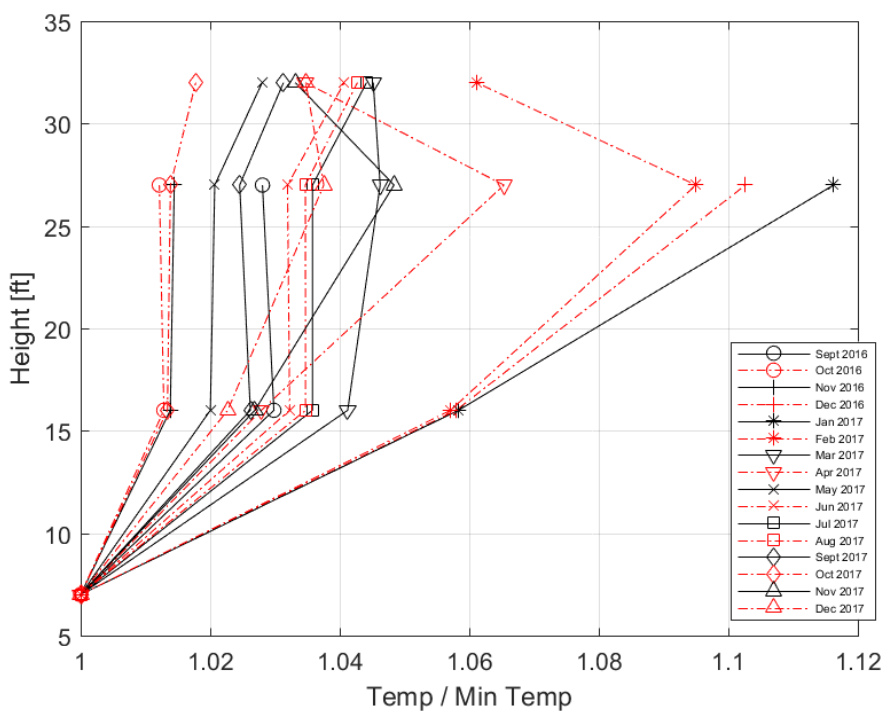


Figure 5.3: Control location 1 monthly temperature average vs height

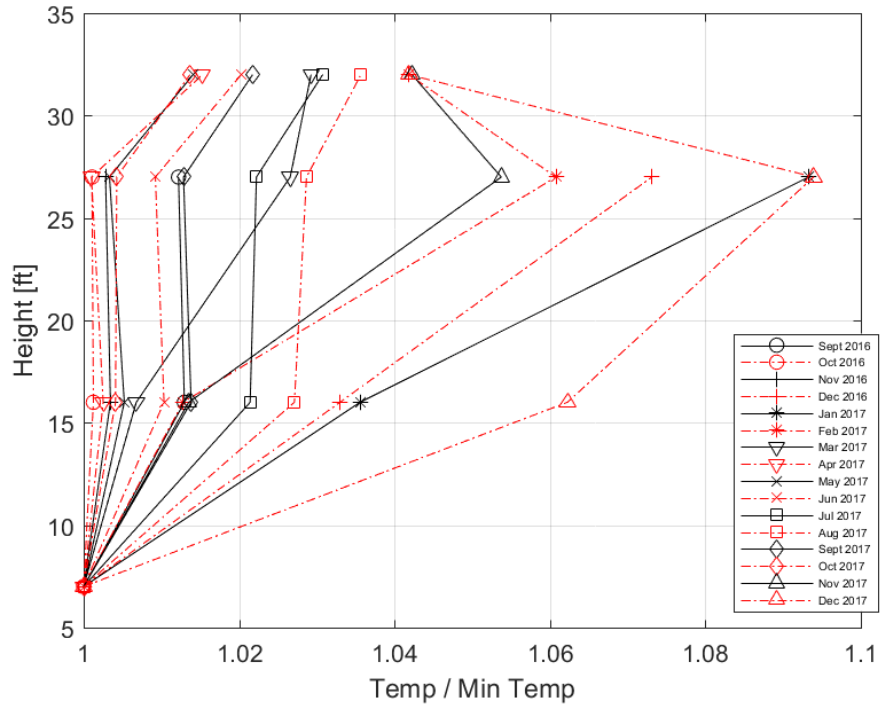


Figure 5.4: Experimental location 1 monthly temperature average vs height

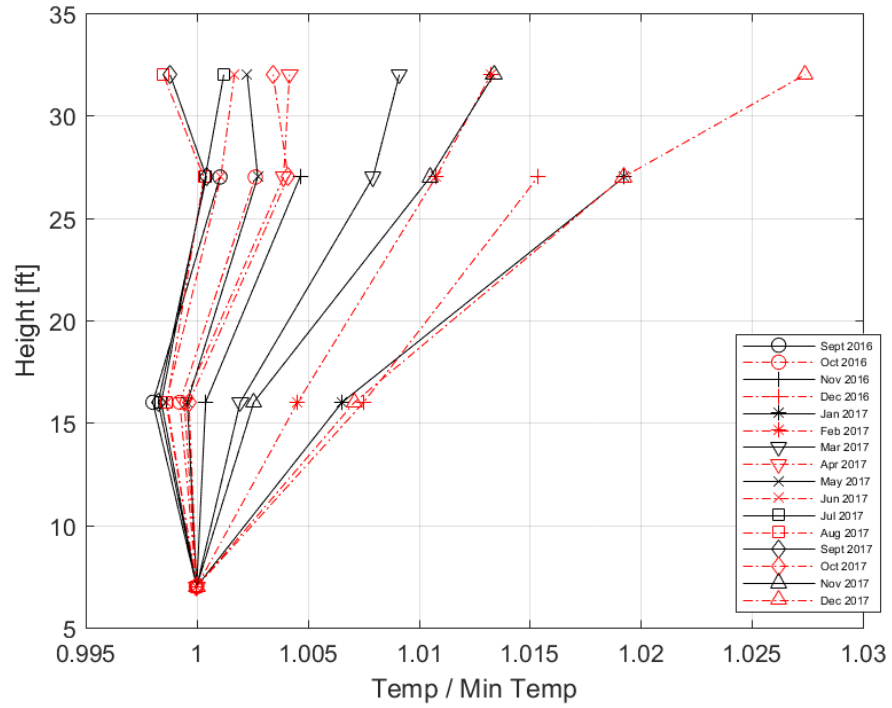


Figure 5.5: Control location 5 monthly temperature average vs height

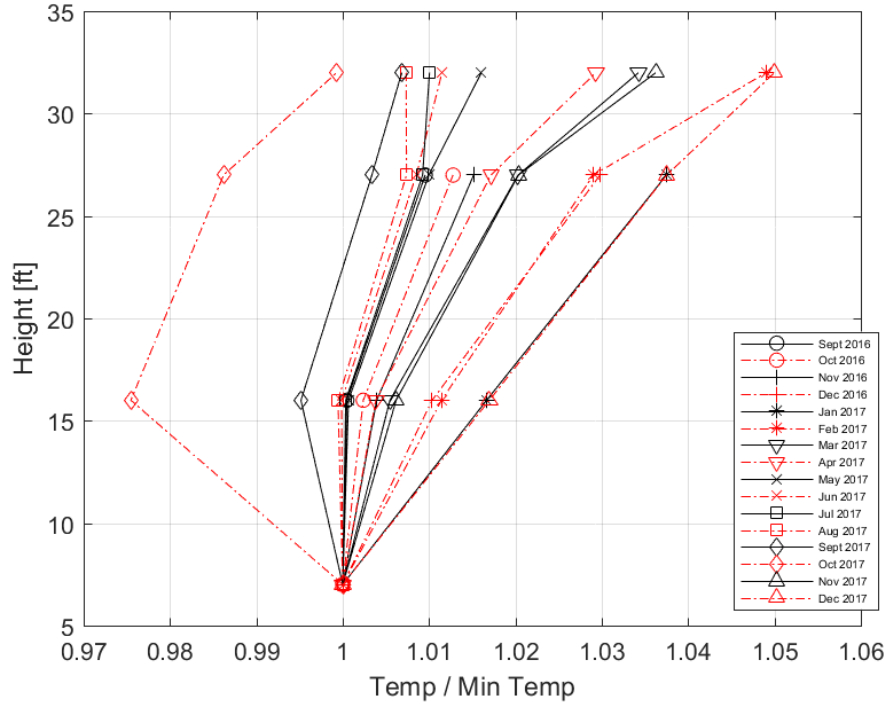


Figure 5.6: Experimental location 5 monthly temperature average vs height

Data from these locations is more erratic, with temperatures often decreasing with height, and is less representative of expected stratification profiles. The sensors collecting data at these locations are located closer to traffic aisles which run perpendicular to the columns of sensors setup along storage racks. These aisles are more subject to drafts from external doors being opened and forklifts traveling the aisles. It is believed that these factors contribute considerable noise to the data collected, and render the results less reliable than data available at the more centralized data collection locations. Due to this addition of noise, all additional plots have been created using data collected from the central experimental, E-3,

and control, C-3, locations.

Figures 5.7 through 5.11 show temperature stratification over a 24 hour period. These profiles are averaged over a given month. Areas shaded in grey indicate that a SunCooler unit was scheduled to operate during that time. Control and experimental locations are listed side by side, with control plots on the left and experimental plots on the right.

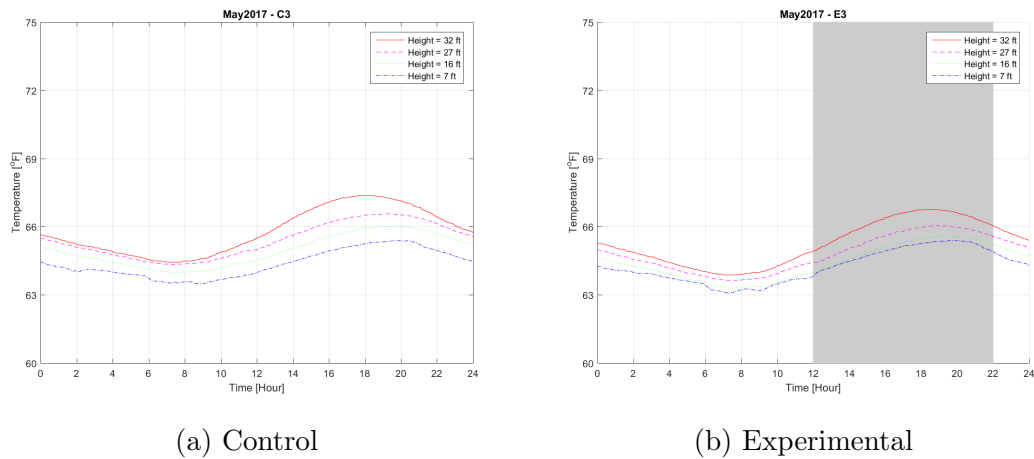
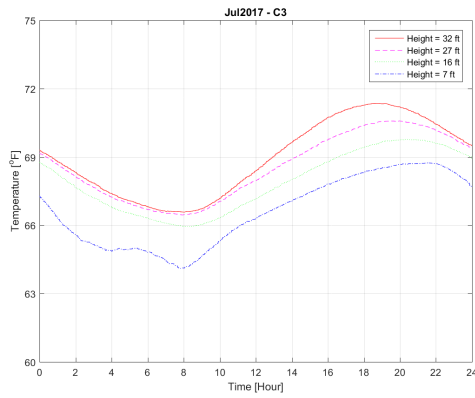
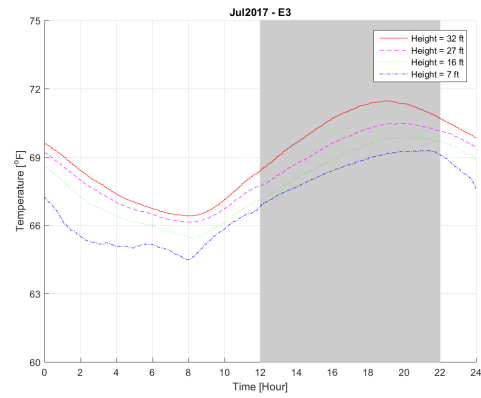


Figure 5.7: May 2017 stratification profile

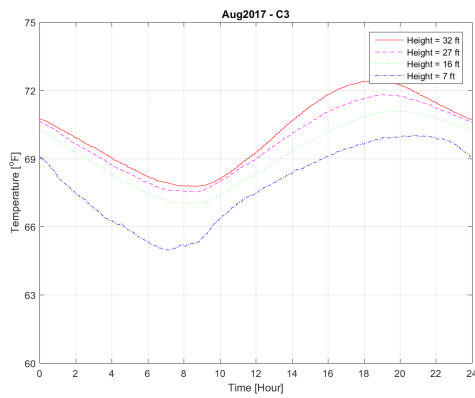


(a) Control

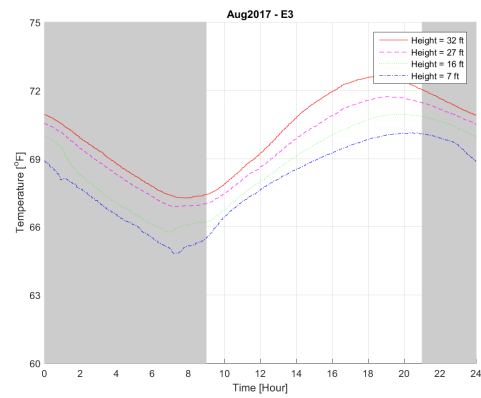


(b) Experimental

Figure 5.8: July 2017 stratification profile



(a) Control



(b) Experimental

Figure 5.9: August 2017 stratification profile

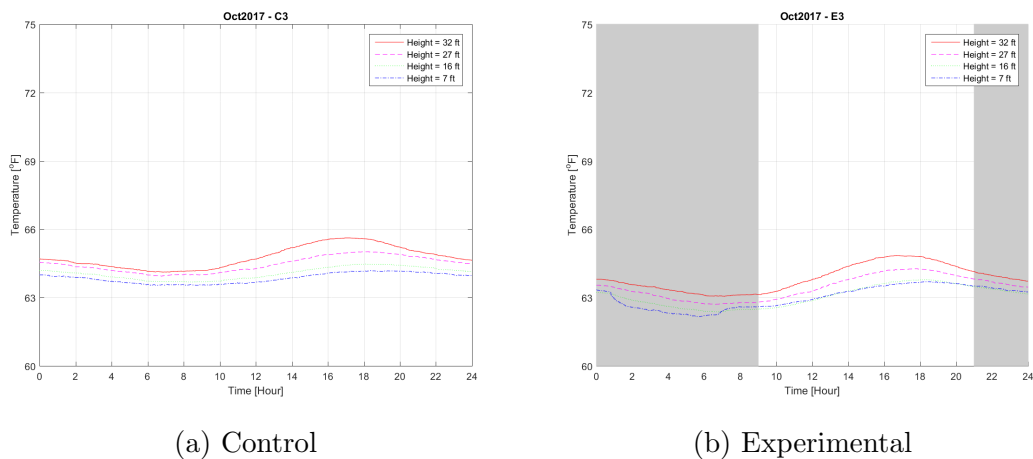


Figure 5.10: October 2017 stratification profile

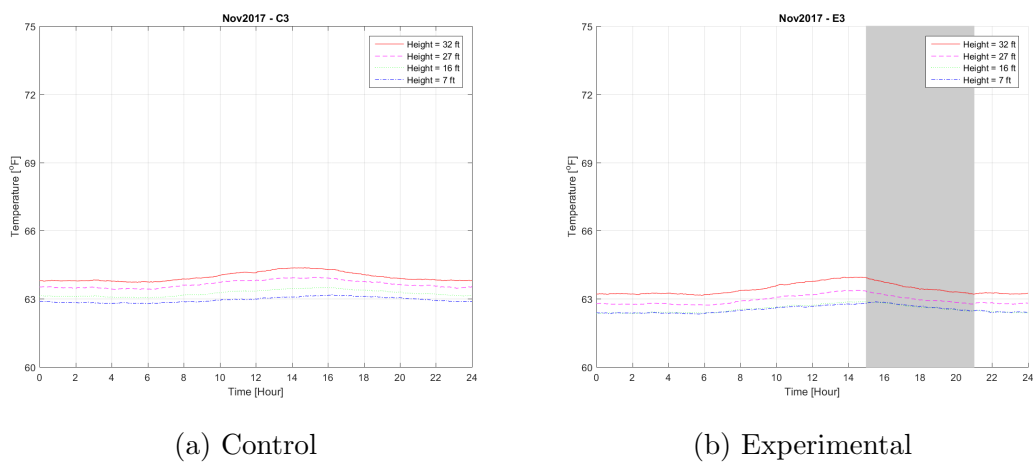
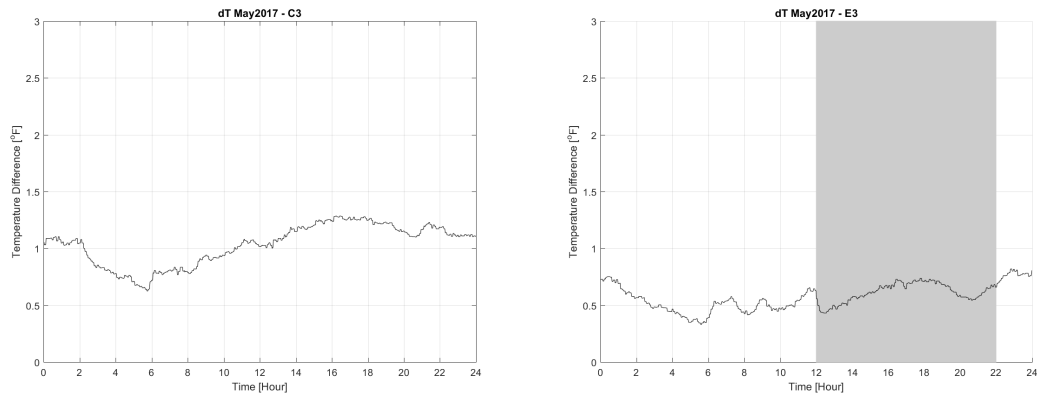


Figure 5.11: November 2017 stratification profile

Figures 5.7 through 5.11 show profiles that are characteristic of data collected in other heating and cooling months. The large temperature gradients during cooling months, and relatively small gradients during heating months provide a more detailed look at the results seen in Figure 5.1 and 5.2. In the heating months the

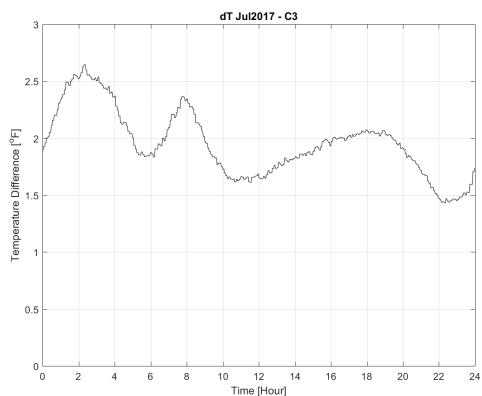
lowest temperatures of the year occur with very little variation in a 24 hour period, further supporting the speculation that the warehouse is under heated. From the above figures, it is difficult to observe a difference in the stratification profile between the control and experimental locations. To better observe impacts on stratification, the following plots were created to show the temperature difference between the deck height sensors and the lowest sensor position. The area shaded in gray represents an operating SunCooler unit.



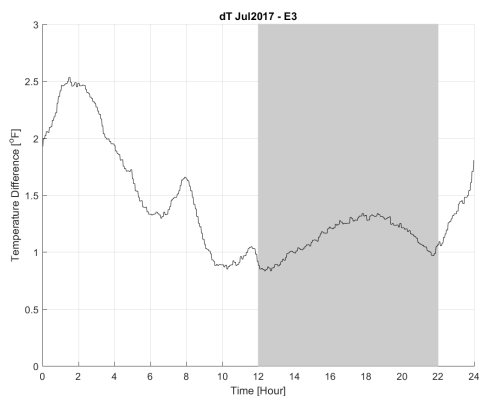
(a) Control

(b) Experimental

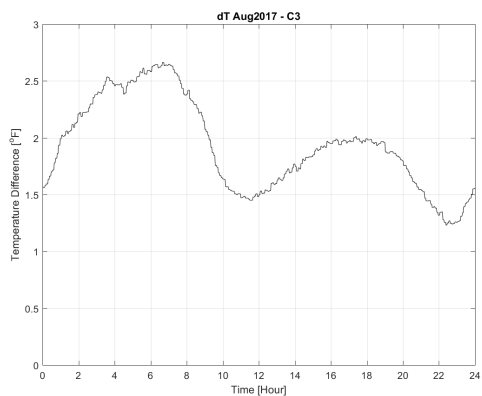
Figure 5.12: May 2017 Δ temperature



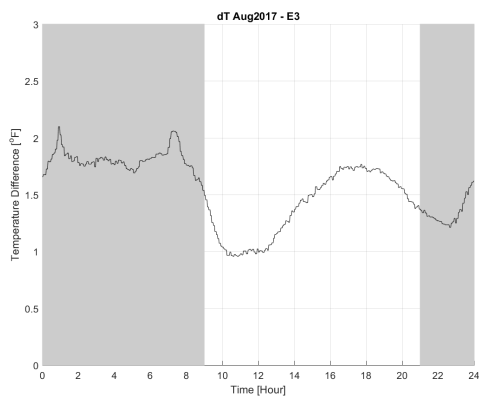
(a) Control



(b) Experimental

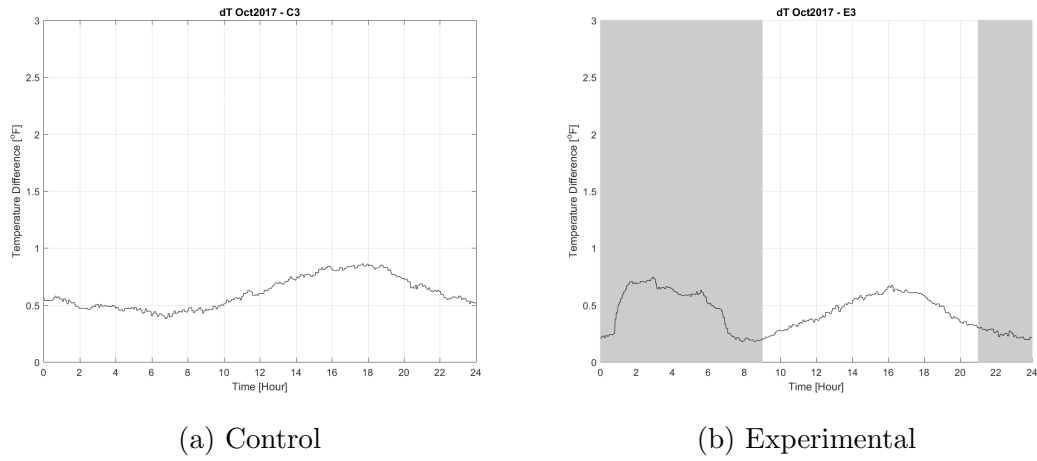
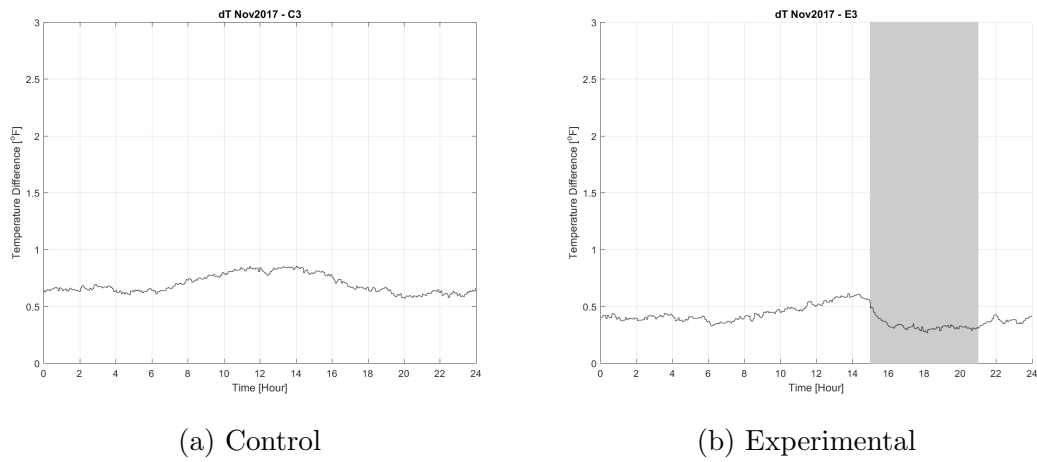
Figure 5.13: July 2017 Δ temperature

(a) Control



(b) Experimental

Figure 5.14: August 2017 Δ temperature

Figure 5.15: October 2017 Δ temperatureFigure 5.16: November 2017 Δ temperature

The data from May 2017, Figure 5.12, shows a small stratification profile throughout a 24 period on average, not exceeding a temperature difference, (ΔT), of 1.5 °F for the control or experimental data. When the SunCooler activates at 12pm a small dip can be seen in the experimental ΔT , though it is hard to deter-

mine if this is coincident or not. It is worth noting that on average the experimental stratification is roughly 0.5 °F lower than the control. May is a transition month showing less stratification than other cooling months, but more stratification than heating months such as November. This makes it difficult to draw conclusions from the comparison of the two zones as the SunCooler appears to be having a positive impact on stratification, but without a more distinct difference between the two it cannot be said for certain.

July's ΔT results, Figure 5.13, similarly do not show significant impact by the SunCooler's destratification mode. This is likely related to the warehouse switching to operating in cooling mode in July, which disables their MAU heaters. This is supported by Figure 5.8b which shows an increase in the temperature at the lowest elevation while the SunCooler is operating. On average, the experimental ΔT appears to remain lower than the average control ΔT .

August, Figure 5.14, has a more interesting comparison between the control and experimental ΔT plots. At this time SunCooler's were operating in induction cooling, and a decrease can be seen on the experimental plot which lines up with the controls peak time of stratification. The unexpected result can be seen in Figure 5.9. Though the temperature difference is seen to be lower, the average room temperature increases. When looking at past ambient temperature data, August 2017 was shown to have temperature lows ranging from 50 °F to 80 °F. This could explain the unexpected temperature increase as the induction cooling seems likely to have been introducing warmer air to the warehouse.

October, Figure 5.15, shows the reverse trend of August, with an increase in

stratification while the SunCooler is operating in induction mode. This result is in line with expectations as cooler air is introduced into the warehouse, and warmer air is displaced upwards, with an overall cooling of environment, as seen in Figure 5.10. November, 5.16 shows results similar to that of May with a general decrease of ΔT in the experimental over its control counterpart. It is worth noting that stratification never exceeds 3 °F for any month, which is much lower than data found in literature, where a temperature difference of 10 °F is more commonly reported (Aynsley, 2005; Armstrong et al., 2009; Hughes, 2006).

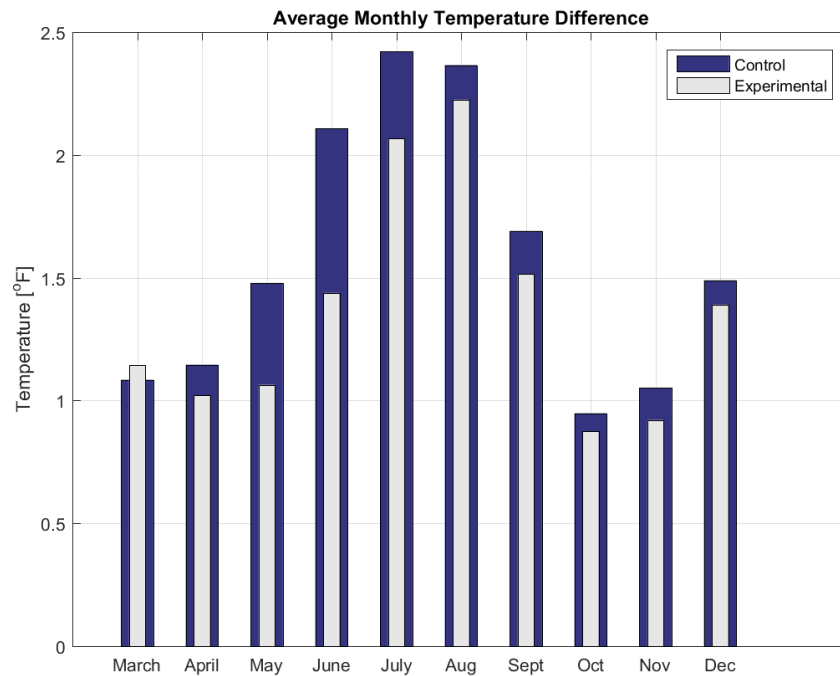


Figure 5.17: Average temperature difference - control vs experimental

Figure 5.17 shows the averaged temperature difference for March 2017 through

December 2017. Early months were not included as they did not have a deck height sensor at those times. This plot allows for a quick inspection of the ΔT values for each month. We can see that for all reported months, except March, the ΔT of the experimental is lower than that of the control. However, the temperature difference is generally small, close to the uncertainty of the measurement device, making meaningful conclusions difficult.

While stratification data is informative, the value that is most indicative of potential energy savings is the temperature at ceiling height (Aynsley, 2005). Figure 5.18 shows the maximum temperatures for the control and experimental zones for March 2017 through December 2017. Again, September 2016 through February 2017 are not reported as ceiling height sensors had not yet been installed during these months.

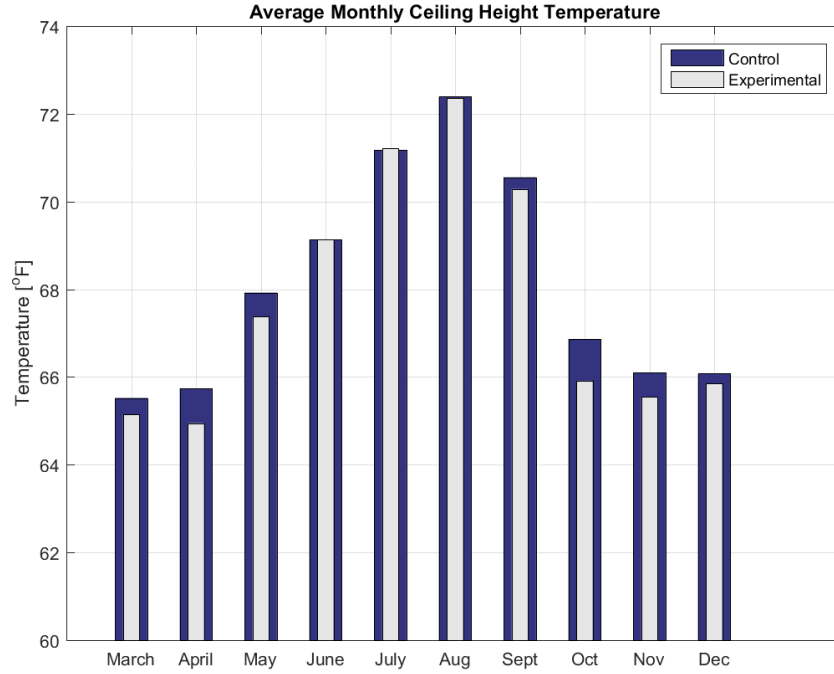


Figure 5.18: Average ceiling temperature difference - control vs experimental

The ceiling temperature differences between control and experimental zones are small with all differences being less than 1 °F. This can be quantified into energy savings by comparing the expected rate of heat lost through the ceiling for both conditions, shown with Eq 5.1 and 5.2.

$$q'' = U(T_{ceiling} - T_{exterior}) \quad (5.1)$$

$$q'' = q''_{Control} - q''_{Experimental} \quad (5.2)$$

The following figures represent data collected by the SC units, they are representative of trends seen from September 2016 through February 2017. Each plot represents real-time data at 30 minute collection intervals. The ability to remotely collect SC data after March 2017 was removed due to security concerns expressed by the warehouse. SunCooler operation is marked by a gray background and labeled with the mode of operation.

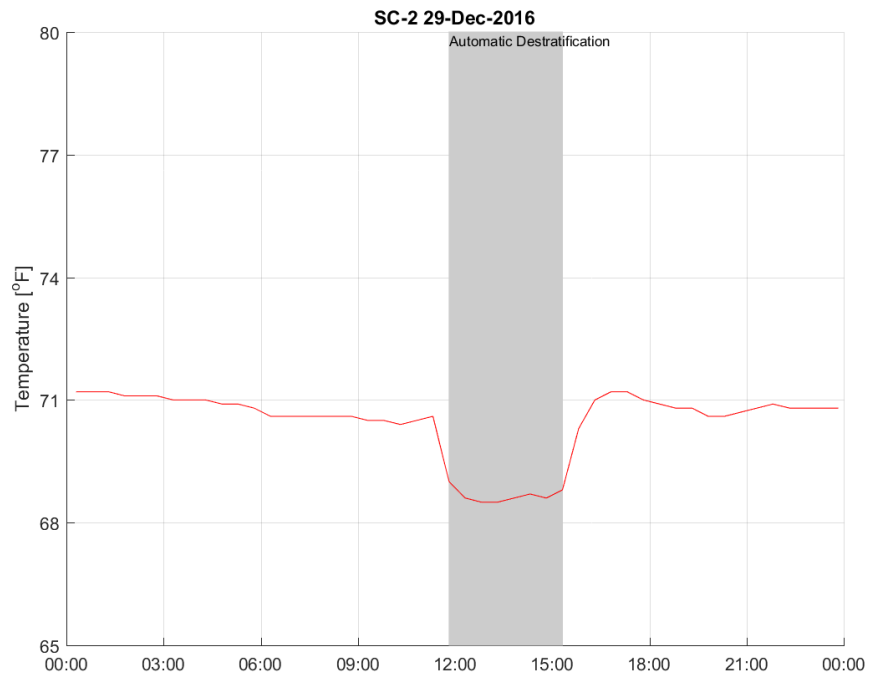


Figure 5.19: Ceiling height temperature - SunCooler 2, December 29th 2016

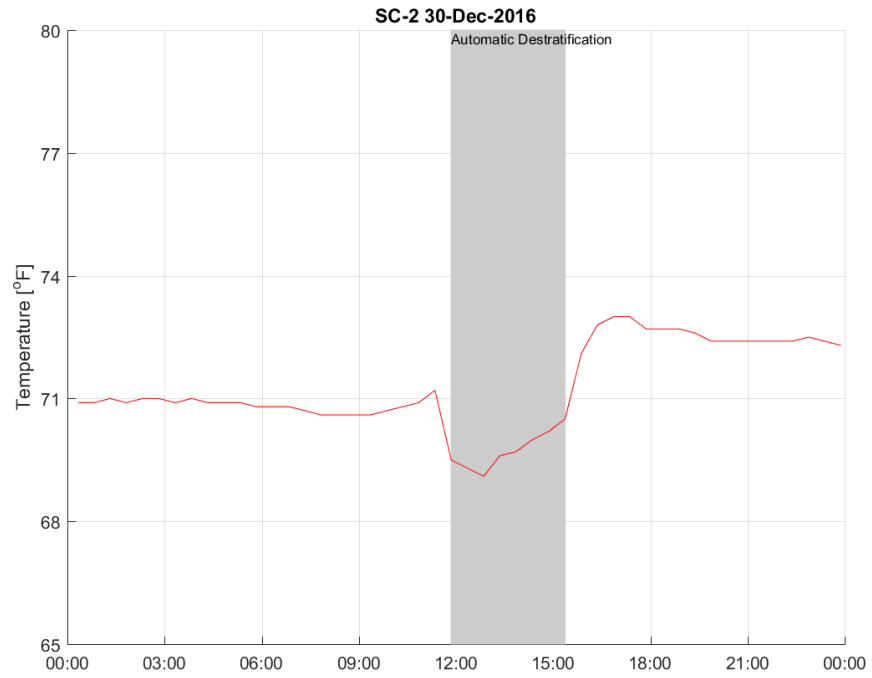


Figure 5.20: Ceiling height temperature - SunCooler 2, December 30th 2016

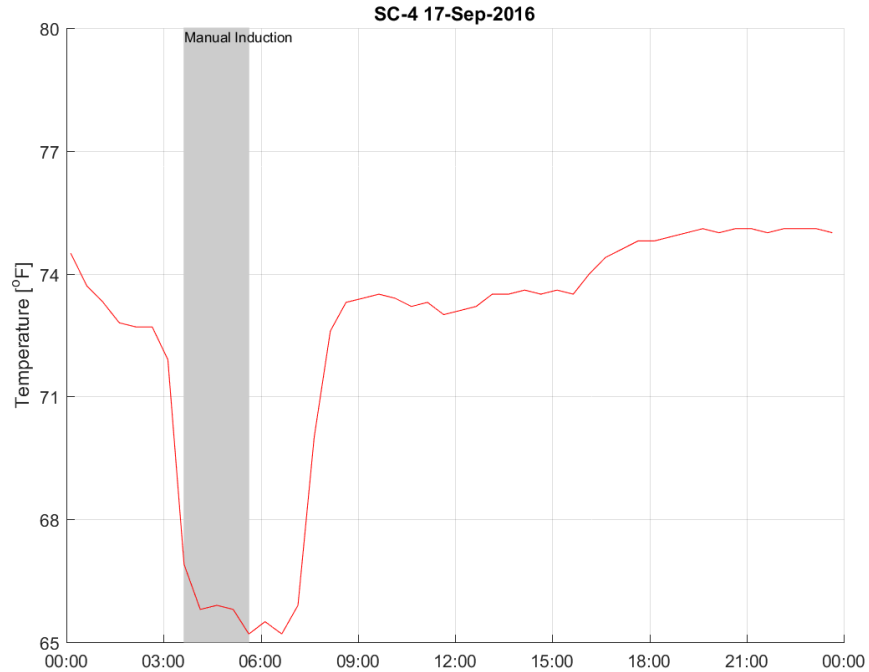


Figure 5.21: Ceiling height temperature - SunCooler 4, September 17th 2016

Figure 5.19 and 5.20 both show the local impact of destratification. When the SunCooler activates, a 1-2 °F temperature drop is observable. Once the SunCooler deactivates the temperature immediately returns to the original temperature in the case of Figure 5.19 or to a higher temperature in the case of Figure 5.20. The same trend is observable at a larger scale in Figure 5.21 when induction cooling is employed. In this mode, temperature decreases by nearly 10 °F. Once the SunCooler unit deactivates the temperature can be seen to increase back to the starting temperature. The operation time marked by the grey area has some uncertainty to it due to the large time difference between reports to the SunCooler

units. In either case, the bulk of the temperature change occurs within the 30 minute window between reports near a SunCooler activation. This information may be more true to the impacts of destratification and induction cooling by the SunCooler than the values provided by Figure 5.18. This because of the limited reach of the SunCooler's within the warehouse.

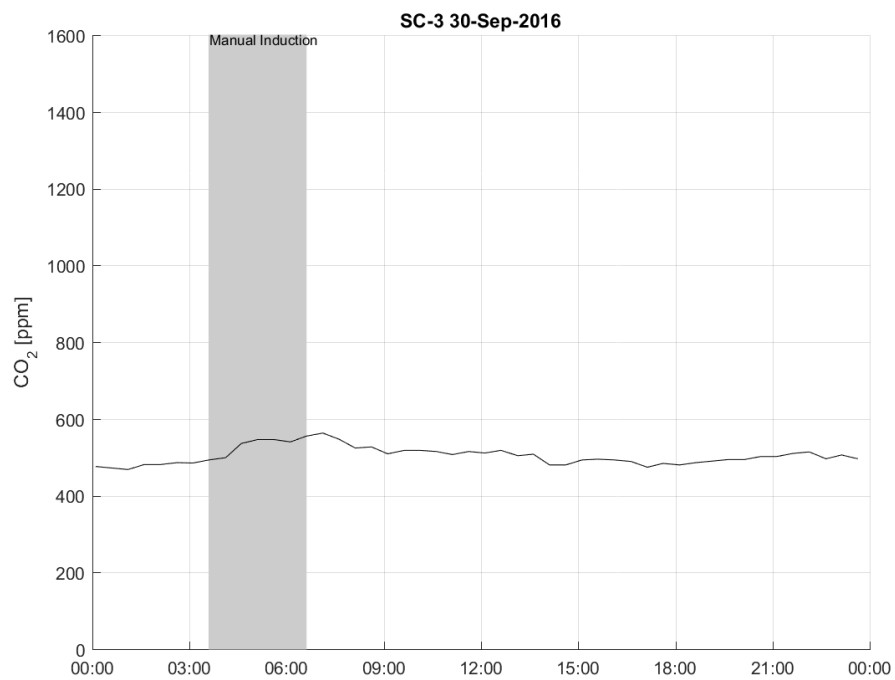


Figure 5.22: CO₂ levels - SunCooler 3, September 30th 2016

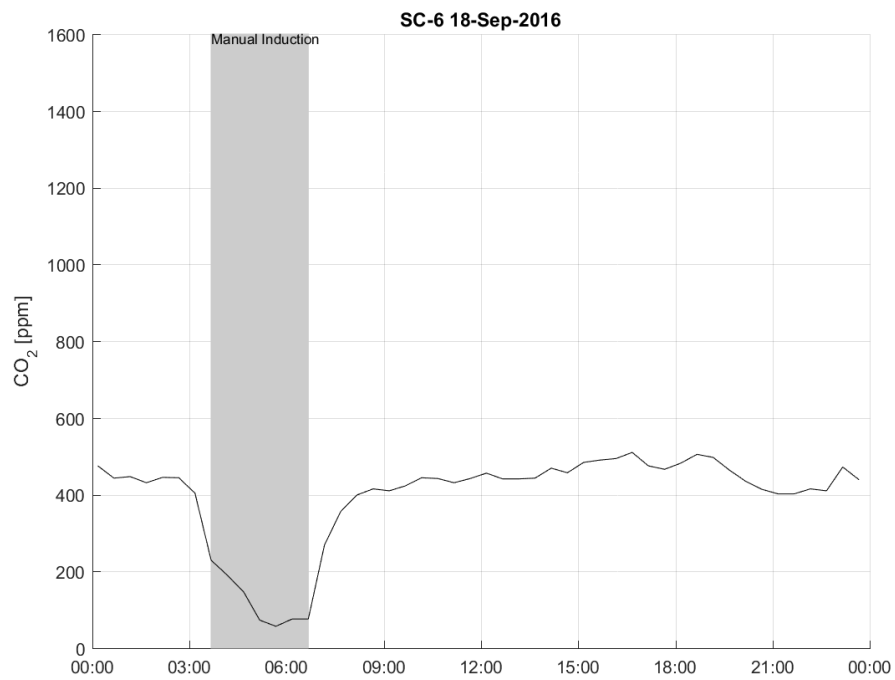


Figure 5.23: CO₂ levels - SunCooler 6, September 18th 2016

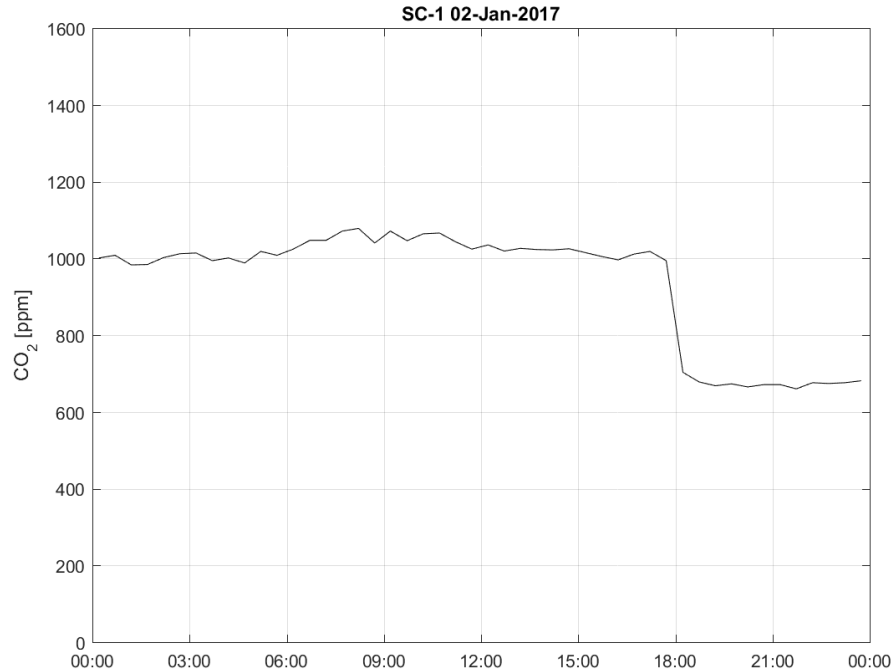
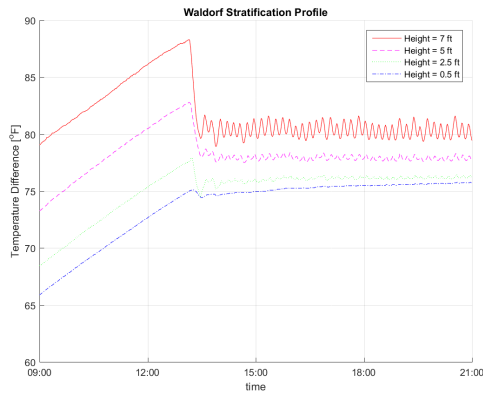


Figure 5.24: CO₂ levels - SunCooler 1, January 2nd 2017

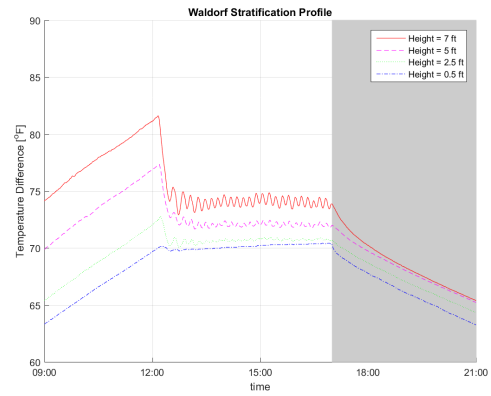
Figure 5.22 shows the CO₂ levels for a 24 hour period. During this time the SunCooler unit activates in induction mode, shown in gray, with seemingly no impact on CO₂ levels. Conversely, Figure 5.23 shows a decrease in CO₂ levels for the same mode of activation, followed by an increase in CO₂ after the SunCooler deactivates. Figure 5.24 shows a sudden drop in CO₂ levels with no contribution from the SunCooler units. Data follows this trend through the September 2016 - February 2017 period. This inconsistency makes it difficult to draw any conclusions about the SunCooler's impact on CO₂ levels from the available data.

5.2 Schoolhouse Results

Due to the limitations of the warehouse experimental setup, additional experiments were conducted in a smaller schoolhouse environment, as presented in Chapter XX. Here, the SunCooler unit was expected to exert a larger influence on the ambient environment. Temperature data for the school room was taken from the same setup with different conditions for each experiment. The control was established by obtaining data with the SunCooler unit deactivated for the full experiment window. The experiment was then collected on a separate weekend with the SunCooler unit turning on at 5pm and running until 9pm. The control, Figure 5.25a shows a very clear stratification profile developed by heating the room without the SunCooler active. This is the expected result of heating a room to a temperature greater than the external temperature. Figure 5.26b shows the temperature profile reaching a similar steady state, then rapidly cooling the room once induction cooling activates. With a new temperature difference being established within roughly one hour. Figure 5.25b suggests that the room would continue to cool if the SunCooler was left on, which fits with expectations, as the exterior temperature is notably lower than the interior in this case. It is difficult to draw firm conclusions from this data as the cooling of the room seems to follow a different behavior than simply mixing the internal air, due to the introduction of air at a much lower temperature than the rooms existing air.

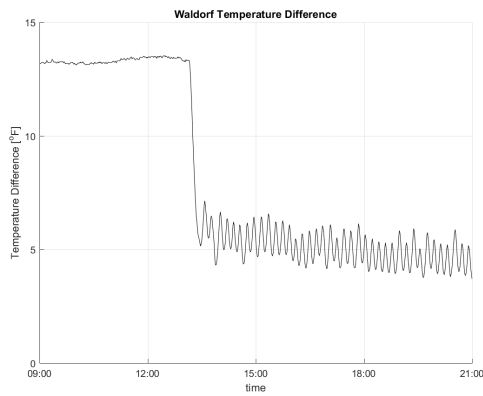


(a) Control

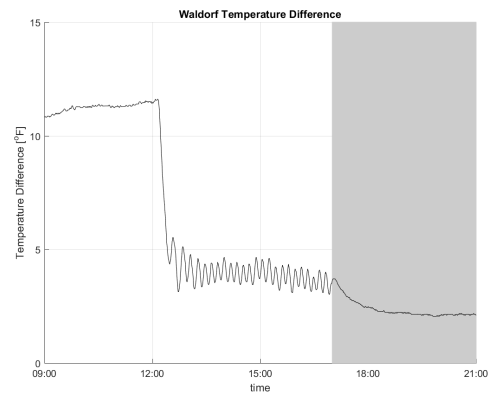


(b) Experimental

Figure 5.25: School room temperature at height - control and experimental



(a) Control



(b) Experimental

Figure 5.26: School room temperature difference - control and experimental

5.3 Discussion

When processing results from the warehouse, it became apparent that the heating performed by the warehouse was insufficient to develop the stratification pro-

files that heating normally creates. This renders data from the warehouse difficult to draw conclusions from as the accuracy reported by the sensors regularly has error greater than the difference between control and experimental zones. By comparison, the stratification profile from the school room had greater temperature differences from low elevation to peak than the warehouse offered, with the warehouse at roughly 3 times the ceiling height of the school. The warehouse profiles also showed a reaction to ambient temperature changes, with a notable increase of temperature at midday and returning to a lower temperature in the evening. Conversely, the school room showed a steady temperature profile, after development, in a 12-hour period. Finally, when comparing warehouse data from Figure 5.1 to the data from Porras-Amores et al. (2014), shown in Figure 1.1, the temperature profiles developed from the warehouse are akin to that of an unheated warehouse, thus indicating an under-heated environment. The under-heated status of the warehouse indicates that data collect for this experiment is not ideal for characterizing the capability of destratification. Which directed this study towards the school room data to validate modeling.

Chapter 6: Model Results

This chapter will cover the results of modeling for both the mixing and cooling models. It also provides the results of a model designed to show why the impacts of the SunCooler for destratification at the warehouse site were lower than anticipated.

6.1 Thermal Mixing Simulations

Destratification or thermal mixing was simulated for four different combinations of fan power, ceiling height, and fan spacing, as summarized in Table 6.1. The results are discussed in Sections 6.1.1 through 6.1.5.

Table 6.1 Mixing model results summary

Fan Power (CFM)	Ceiling Height (ft)	Fan Spacing (ft)	External Temp (°F)	HT Coeff ($\frac{W}{m^2K}$)	Time to Complete (s)
15000	40	90	5	0.3	162
15000	32	90	5	0.3	144
2500	32	15	5	0.3	48
2500	20	50	5	0.3	148

6.1.1 Thermal Mixing: 15k CFM SunCooler 40 ft Ceiling Height 90 ft Fan Spacing

The analysis was for a 40 ft ceiling height and a 90 ft spacing between each fan, with walls which were located 45 ft from the fans. Figure 6.1 shows a temperature slice at the mid-line of the model at time equal to 0 seconds. Initially, there is a gradual temperature profile from ground level to approximately 36 ft, the estimated heater height, after which a sharp temperature gradient exists to roughly 39 ft, representing the thermocline, followed by a gradual temperature increase to ceiling height. The temperature ranges from 60 °F to 70 °F to mimic values found in literature (Armstrong et al., 2009). Imposing this initial temperature condition mimics the warm pocket of air above the thermocline and the cooler air below. Figures 6.2 through 6.6 all represent the same slice through the model at different times, with all temperatures ranging from 60 °F to 70 °F.

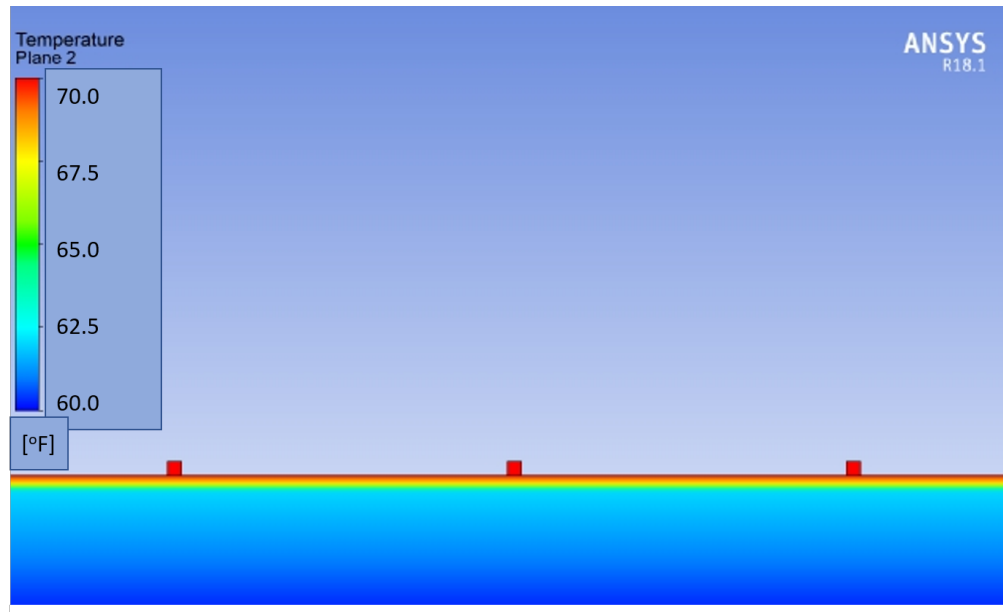


Figure 6.1: 5k CFM SunCooler 40 ft ceiling height 90 ft fan spacing: temperature, time = 0 seconds

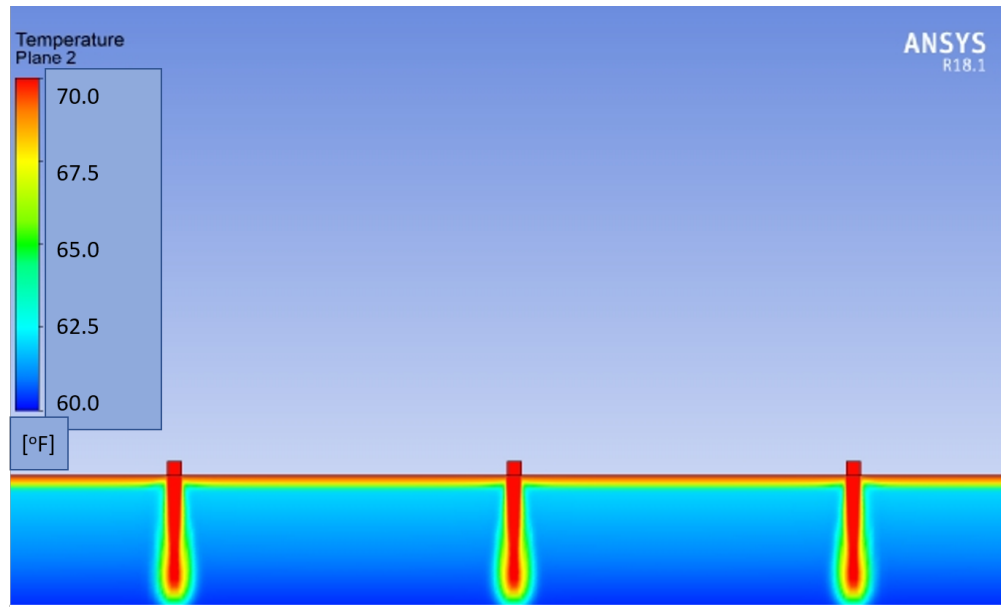


Figure 6.2: 15k CFM SunCooler 40 ft ceiling height 90 ft fan spacing: temperature, time = 4 seconds

Figure 6.2 shows the model 4 seconds into its run. This point in time shows the air from the inlets displacing the cooler air from the initial temperature profile. The velocity profile of the air is in a state of development as it will eventually interact with the air from neighboring inlets.

When time is equal to 36 seconds, shown in Figure 6.3, the deflected air from each of the columns has begun to interact with air from its neighboring columns and been deflected upwards towards the ceiling. It can be seen that the warmer air is beginning to mix into the system as the cooler air is displaced upward by the redirected inlet air. In Figure 6.4 full entrainment has begun to take effect and the warmer air that was initially trapped at the ceiling is mixing with the lower regions.

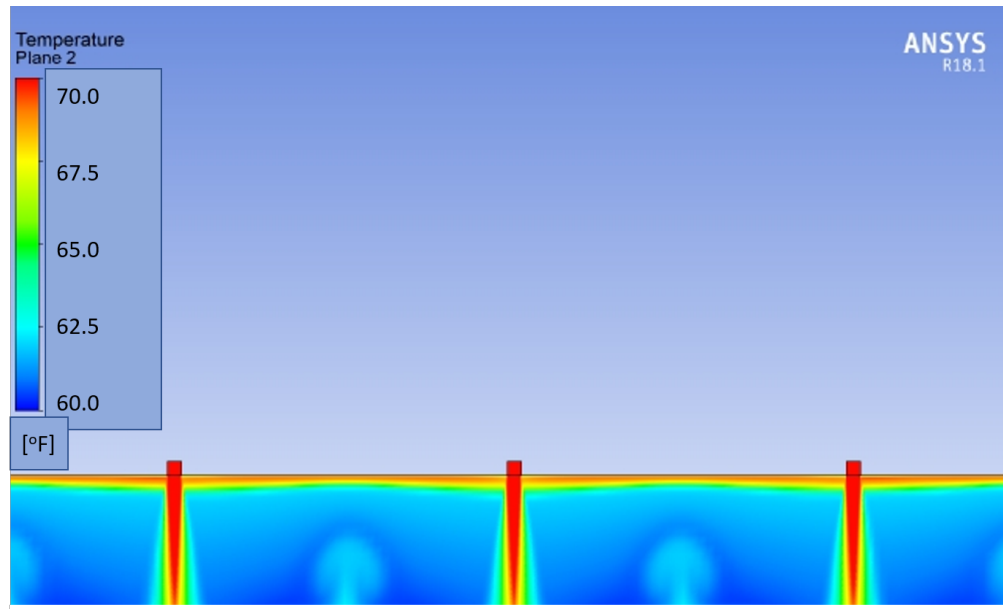


Figure 6.3: 15k CFM SunCooler 40 ft ceiling height 90 ft fan spacing: temperature, time = 36 seconds

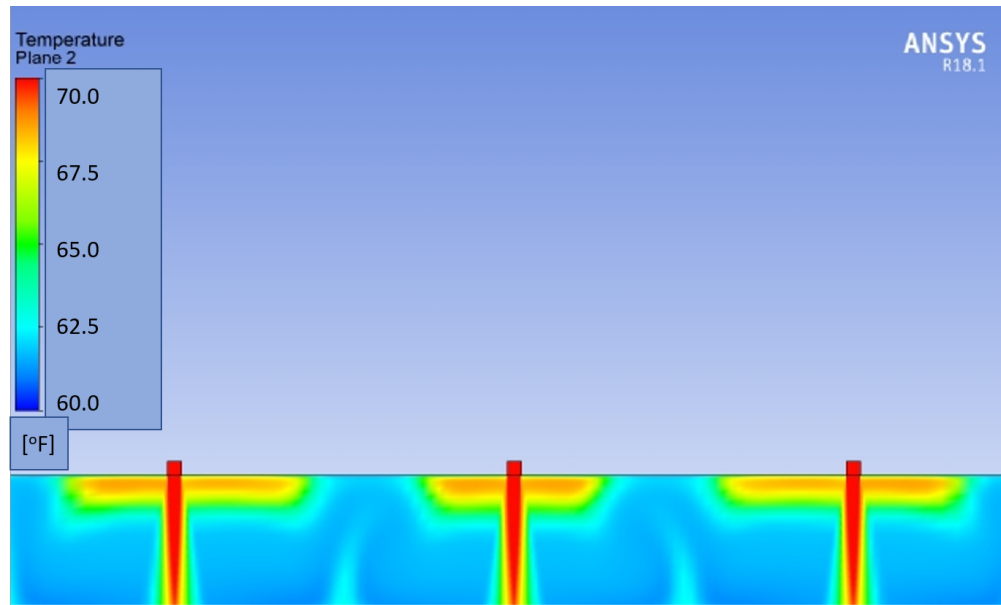


Figure 6.4: 15k CFM SunCooler 40 ft ceiling height 90 ft fan spacing: temperature, time = 84 seconds

Figure 6.5 shows the air being nearly completely mixed by 124 seconds, and by 162 seconds, Figure 6.6, the temperature between the inlets is effectively uniform. The inlet temperature continues to be 70 °F as that was the temperature the inlet was set to, but at all other locations the temperature has settled to approximately 63 °F. This final temperature matches data provided by Armstrong et al. (2009) which was presented in Figure 2.1.

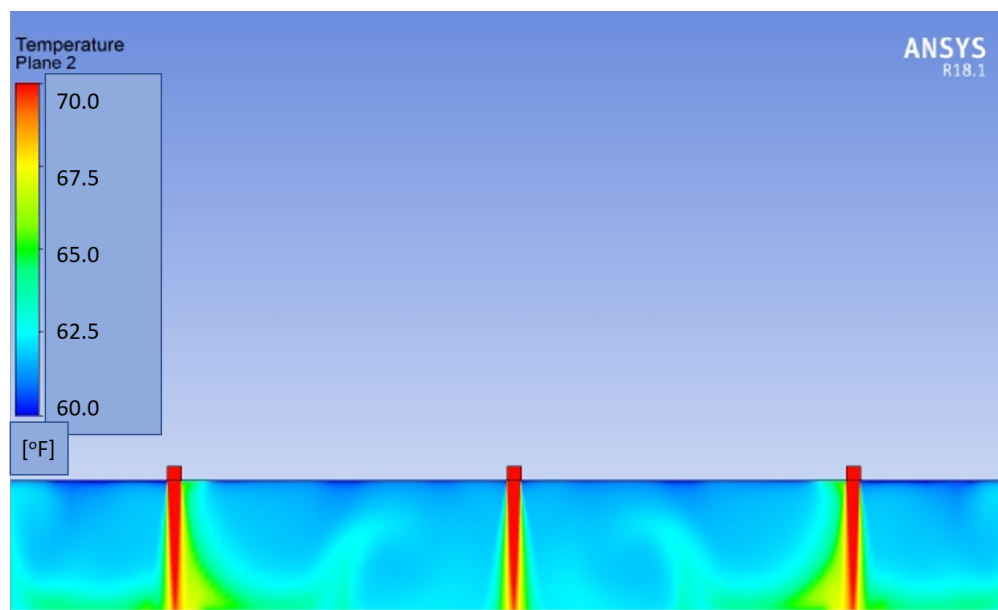


Figure 6.5: 15k CFM SunCooler 40 ft ceiling height 90 ft fan spacing: temperature, time = 124 seconds

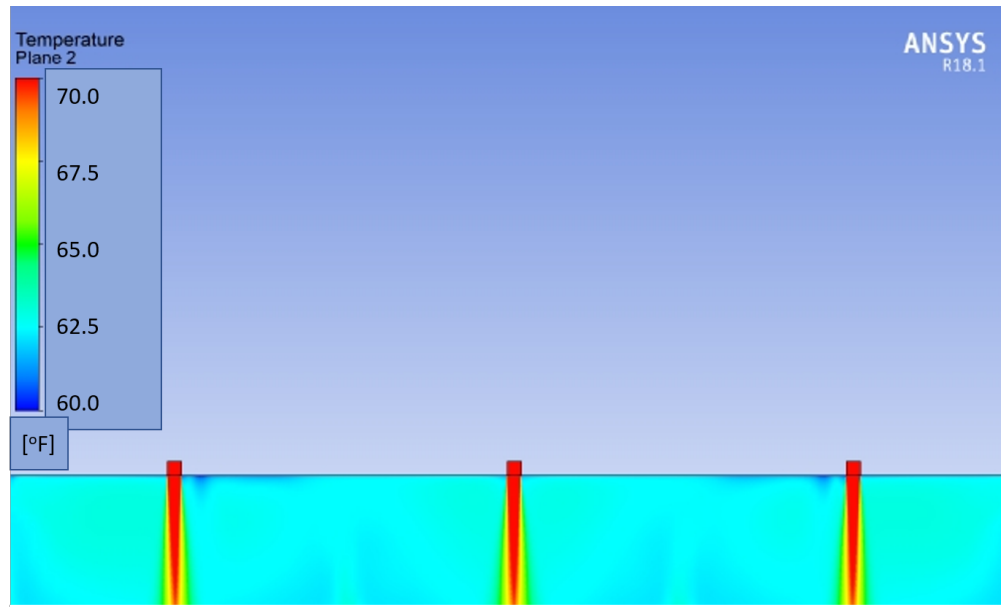


Figure 6.6: 15k CFM SunCooler 40 ft ceiling height 90 ft fan spacing: temperature, time = 162 seconds

To get a more precise time at which the temperature of the air everywhere is within the 0.5 °F convergence condition, points were placed in the model ranging from heights of 1 ft to 39 ft. These monitors were located at points mid-points between fans. The majority of the lines can be seen to converge at approximately 162 seconds, but two monitors show a continued increase in temperature, which puts them above the target delta. This is due to the heated nature of the inlet air continuing to warm the room after mixing has completed. The results can be seen in Figure 6.7

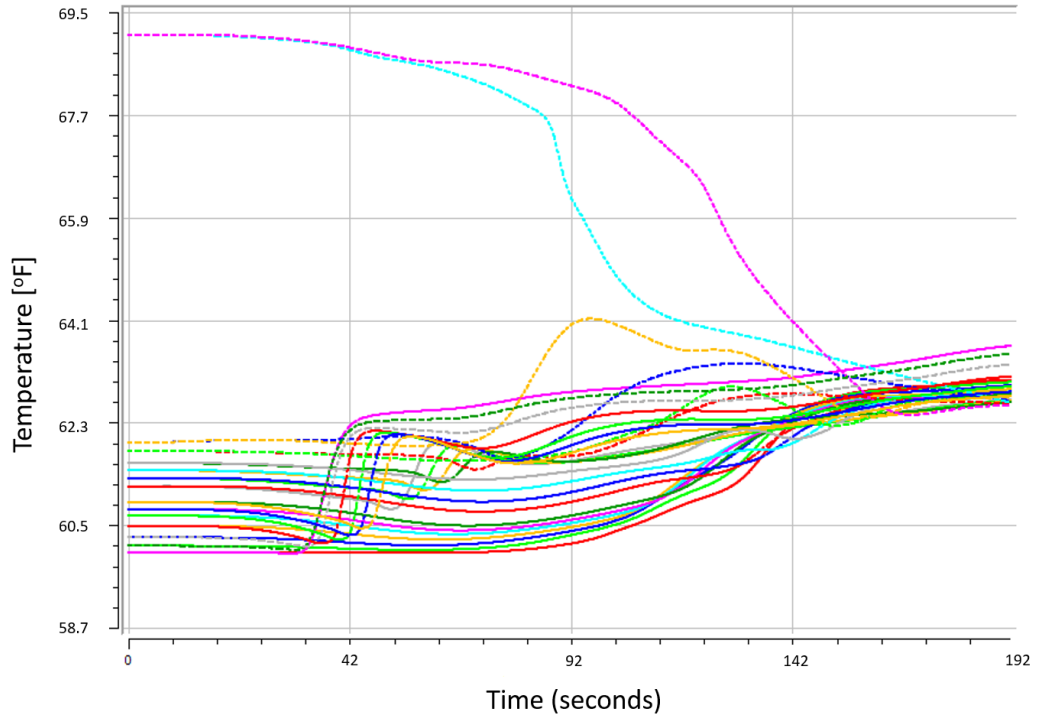


Figure 6.7: Temperature monitors for geometry with 40 ft ceiling height

6.1.2 Thermal Mixing: 15k CFM SunCooler 32 ft Ceiling Height 90 ft Fan Spacing

The second analysis considered a 32 ft ceiling height with 90 ft between each fan and a 45 ft spacing between fans at the edge of the model and the wall. As this model mostly closely represented the warehouse considered in the experimental effort, it was also used to investigate flow profiles created by the fans, which are shown later in this section.

As before, Figures 6.8 through 6.13 are colored by temperatures ranging from 60 °F to 70 °F. The initial time step, Figure 6.8, shows the same initial conditions as the 40 ft height model. When time is equal to 4 seconds, Figure 6.9, the column has reached floor level and diverged, whereas in the 40 ft height model the inlet air had not quite penetrated to floor level. The subsequent figures behavior is identical to that of the 15k CFM, 40 ft height, geometry. With a final mixing time of roughly 144 seconds, or 11% faster than the 40 ft ceiling case.

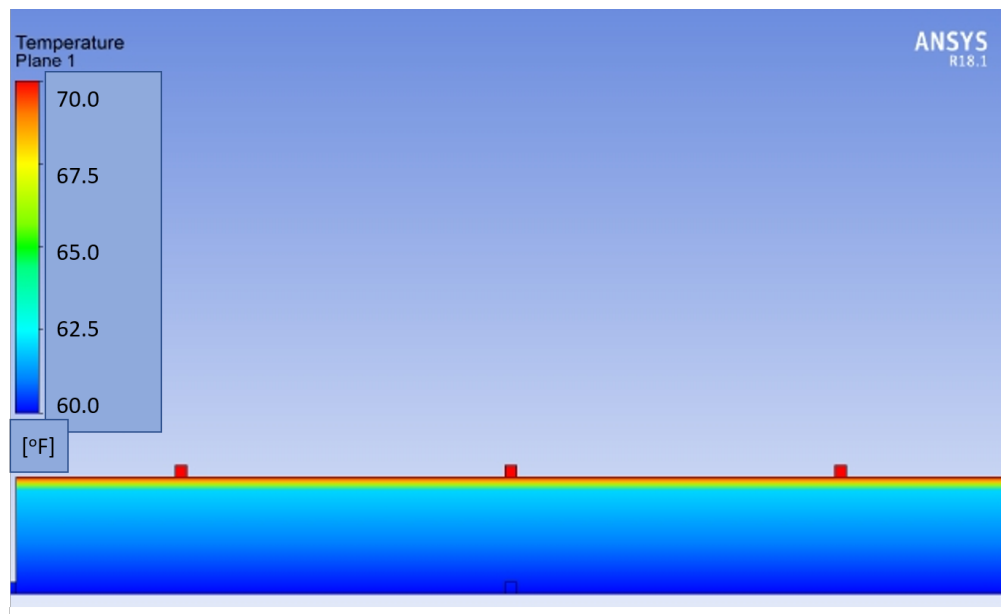


Figure 6.8: 15k CFM SunCooler 32 ft ceiling height 90 ft fan spacing: temperature, time = 0 seconds

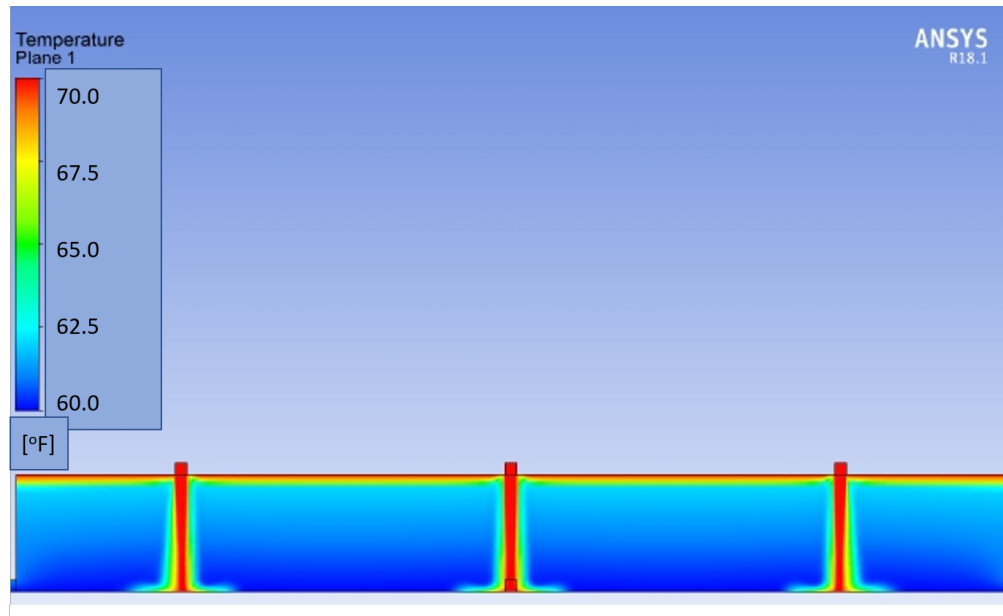


Figure 6.9: 15k CFM SunCooler 32 ft ceiling height 90 ft fan spacing: temperature, time = 4 seconds

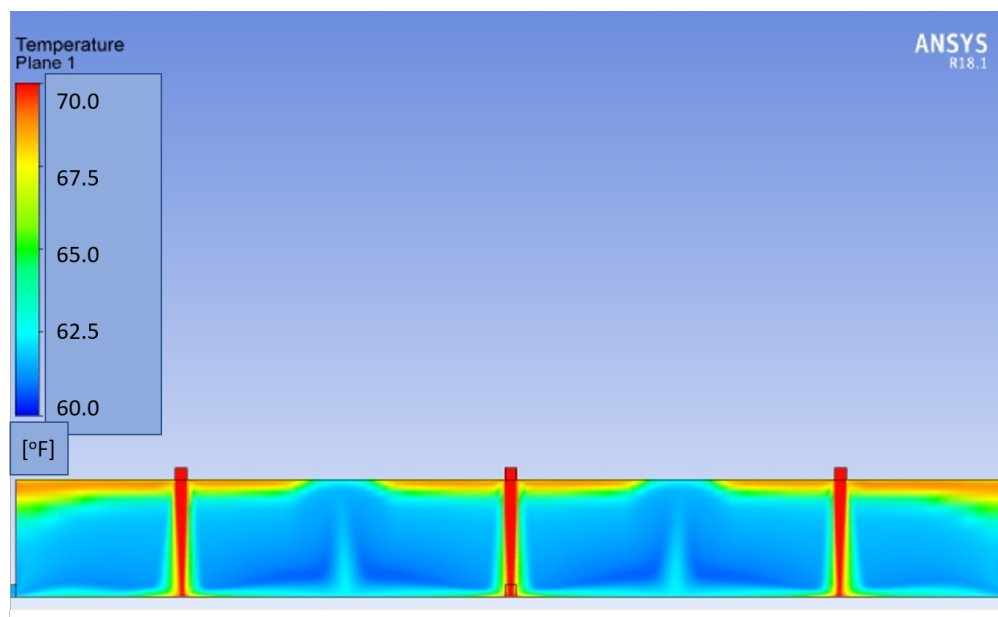


Figure 6.10: 15k CFM SunCooler 32 ft ceiling height 90 ft fan spacing: temperature, time = 36 seconds

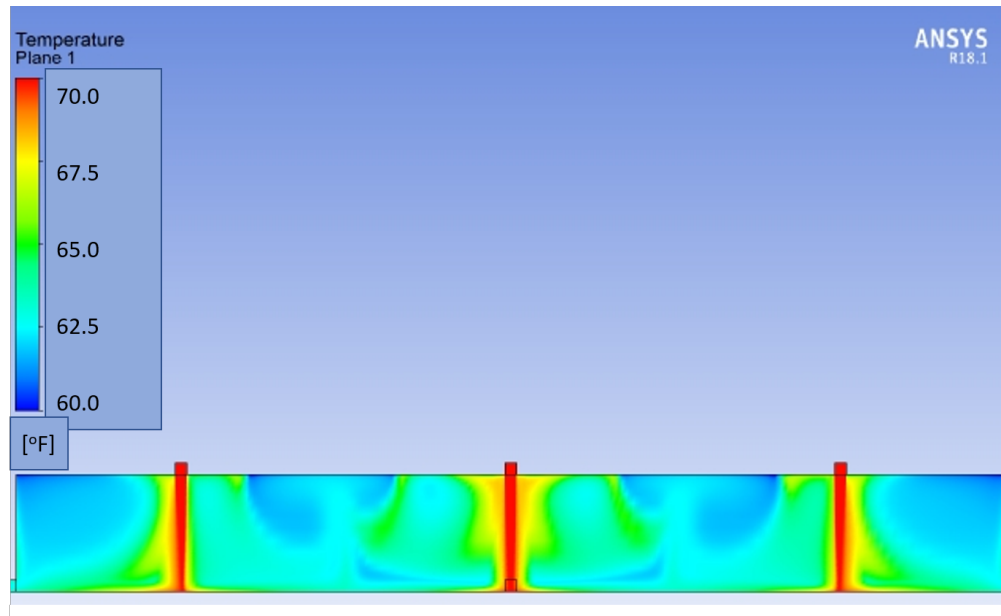


Figure 6.11: 15k CFM SunCooler 32 ft ceiling height 90 ft fan spacing: temperature, time = 72 seconds

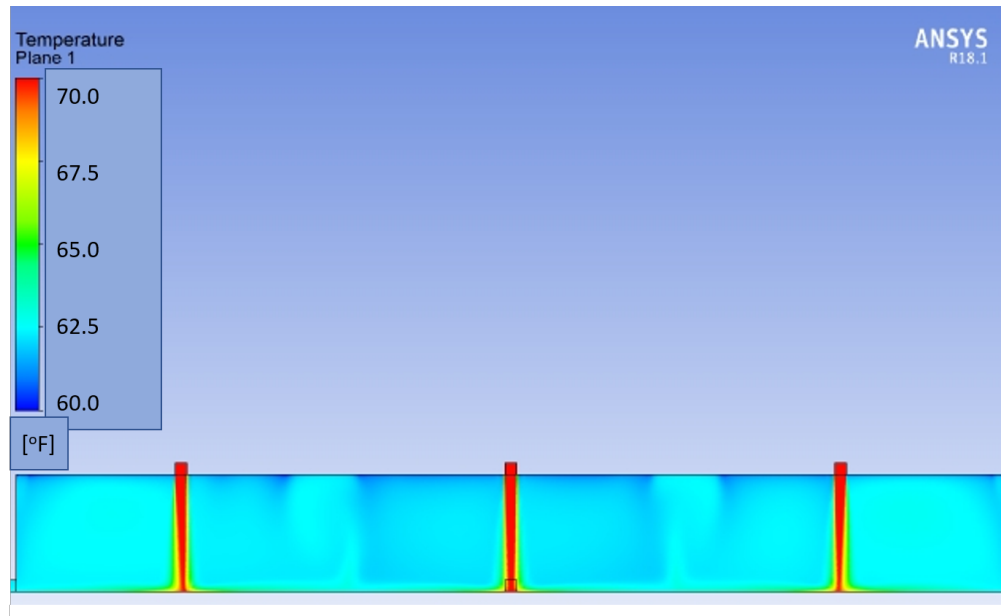


Figure 6.12: 15k CFM SunCooler 32 ft ceiling height 90 ft fan spacing: temperature, time = 108 seconds

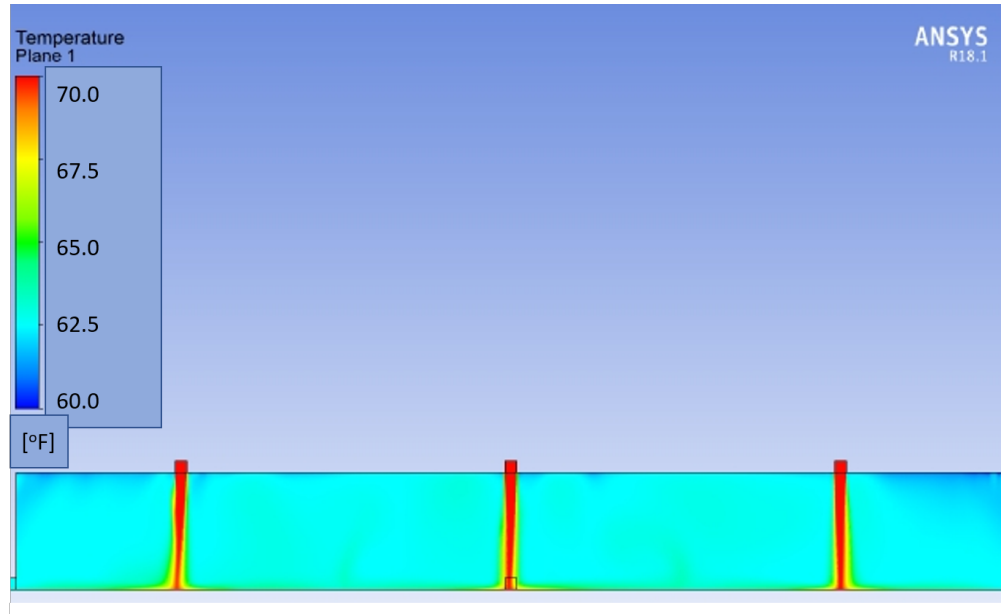


Figure 6.13: 15k CFM SunCooler 32 ft ceiling height 90 ft fan spacing: temperature, time = 144 seconds

Figures 6.14 through 6.16 provide flow information calculated for assuming steady state. Figure 6.14 shows the streamlines projected onto a plane slice through the model. From this we can see the effects of the interaction between air columns producing large vortices. Lines that do not appear to be part of a vortex are components of larger rotations which can be better seen in Figure 6.15. Figure 6.15 is a top view of the model with streamlines originating from the central inlet, marked by a red square. It can be seen that each inlet develops a region of influence, constrained by neighboring inlet regions. The central region, from which the streamlines are originating, shows a dense path of travel for local streamlines, thinning in density as they move to neighboring regions, further illustrating the mixing pattern.

Figure 6.16 is a plane slice through the model which is colored by velocity. Similar to Figure 6.14, it shows the interaction between the columns of air creating an upward mixing motion at a point between the columns of air. The color variation within the region between columns better demonstrates the mixing occurring throughout the geometry.

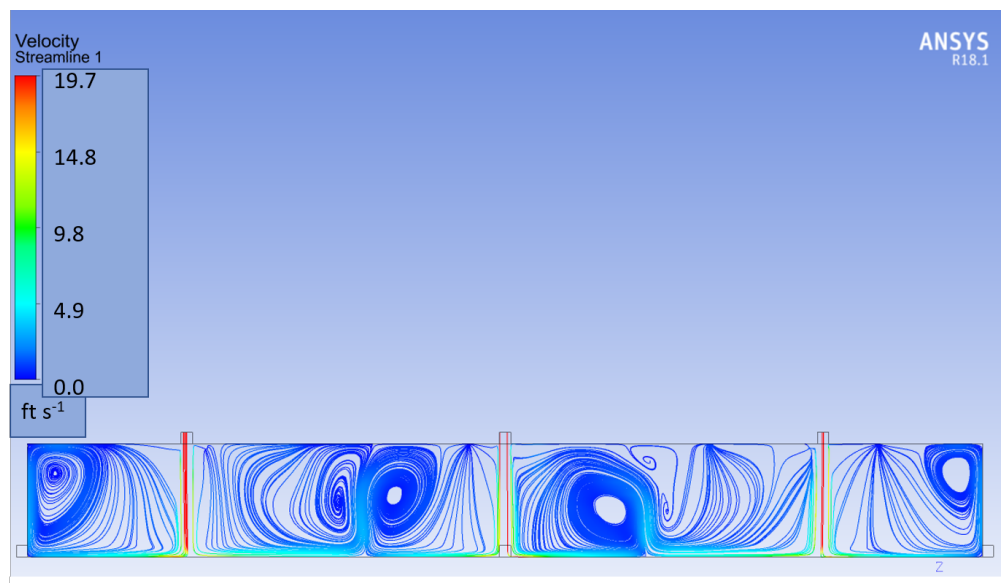


Figure 6.14: 15k CFM SunCooler 32 ft ceiling height 90 ft fan spacing: streamlines

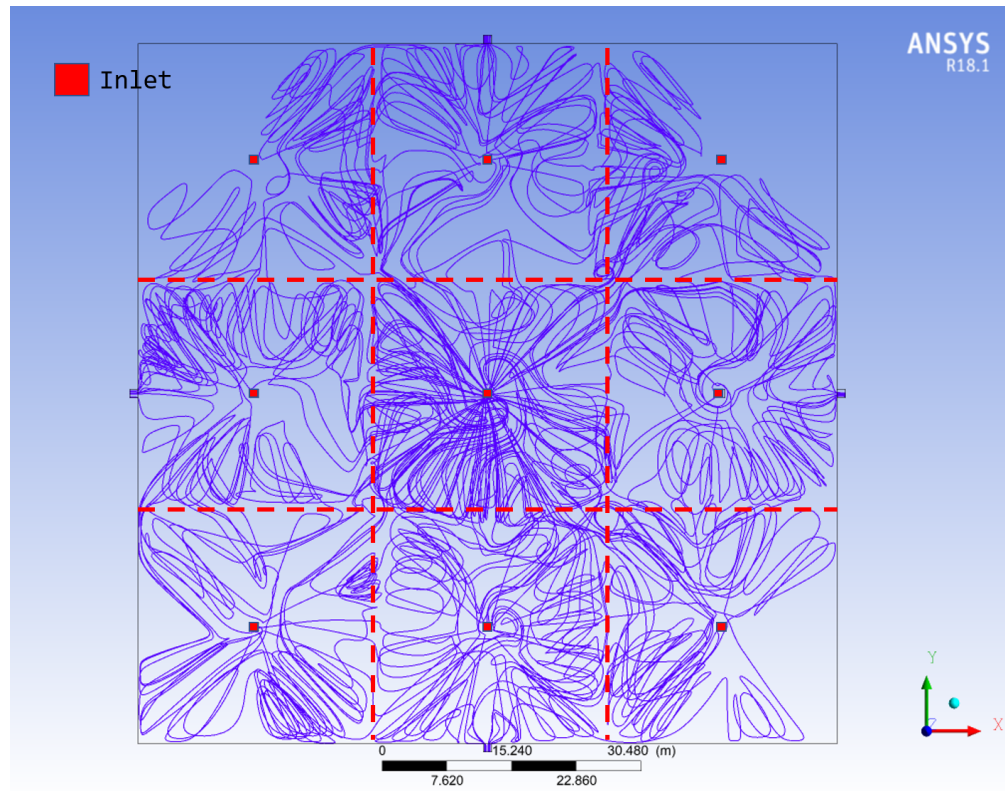


Figure 6.15: 15k CFM SunCooler 32 ft ceiling height 90 ft fan spacing: top view streamlines

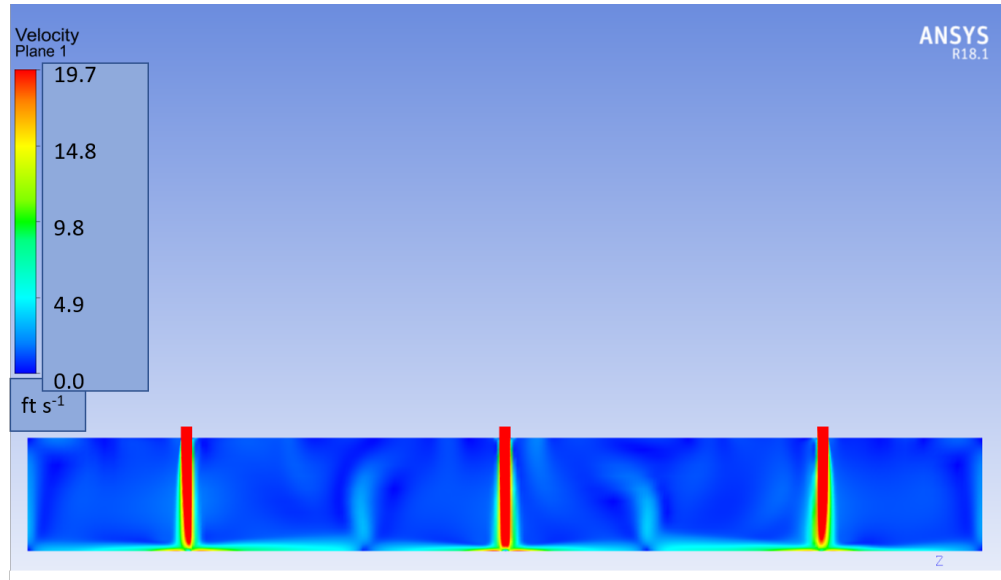


Figure 6.16: 15k CFM SunCooler 32 ft ceiling height 90 ft fan spacing: velocity

6.1.3 Thermal Mixing: 15k CFM SunCooler 32 ft Ceiling Height 90 ft Fan Spacing - Disabled Fans

To better understand the effects of attempting to mix a large room with only a single column of fans as in the experimental study, a simulation was conducted with six of the inlets disabled, leaving a single column of three enabled, and run to solve for steady state. Figure 6.17 shows a slice through the model with only the central inlet enabled. It can be seen that mixing is still occurring from this perspective due to the lines indicating the presence of the entrainment of air. Figure 6.18 shows the same model, but with a slice through the three enabled inlets. Interaction between the columns can be seen and the mixing profile is more apparent than in

Figure 6.17.

Figure 6.19 shows a top view of the model, with streamlines emanating from a plane wall through the center. When looking at these streamlines, columns of fluid motion, shown separated by dotted red lines, can be seen moving away from the interacting inlets. As these columns move further from the center line, the density of the line begins to dissipate, indicating less effective mixing. In this case, the wall boundary conditions allow for mixing despite the distance from the inlets, but it is reasonable to presume that given enough distance the mixing would dissipate entirely. For this study, the maximum region of influence is set to be 90 ft². This is based on a conversation with the CEO of NWREC (Wright, 2017). With the results shown in Figure 6.19, it seems likely that the fans could service a larger area and still provide mixing effects. It is uncertain the extent of the mixing range possible, especially as the current model assumes no obstructions within the warehouse. This is a factor that should be considered in any future studies performed on the subject of thermally mixed environments.

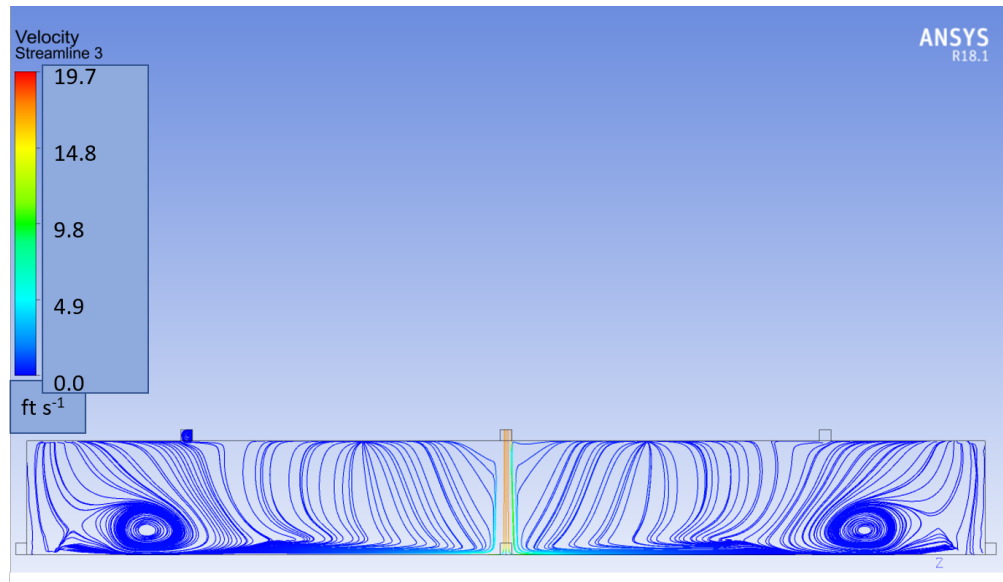


Figure 6.17: 15k CFM SunCooler 32 ft ceiling height 90 ft fan spacing: disabled fans

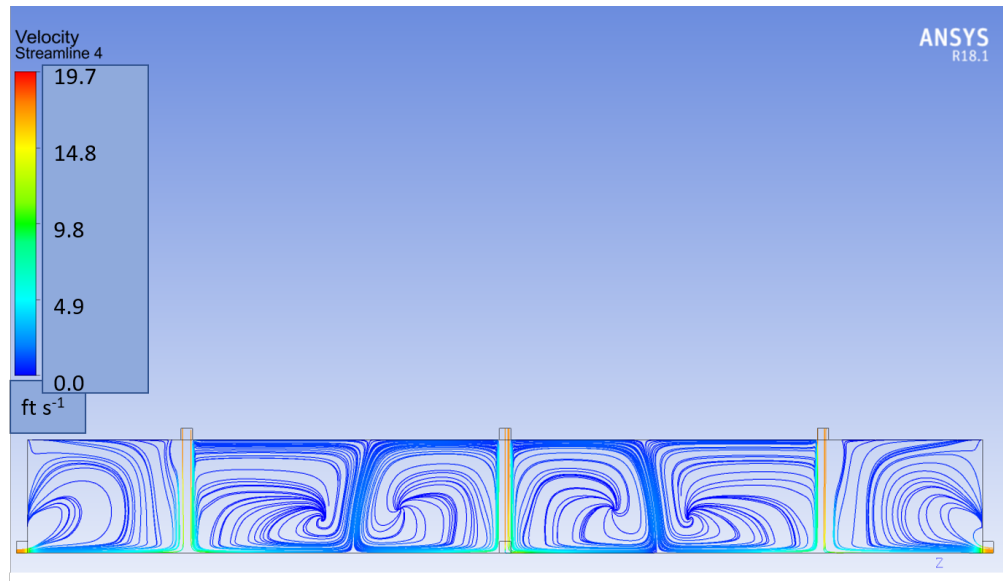


Figure 6.18: 15k CFM SunCooler 32 ft ceiling height 90 ft fan spacing: disabled fans - 90° rotation.

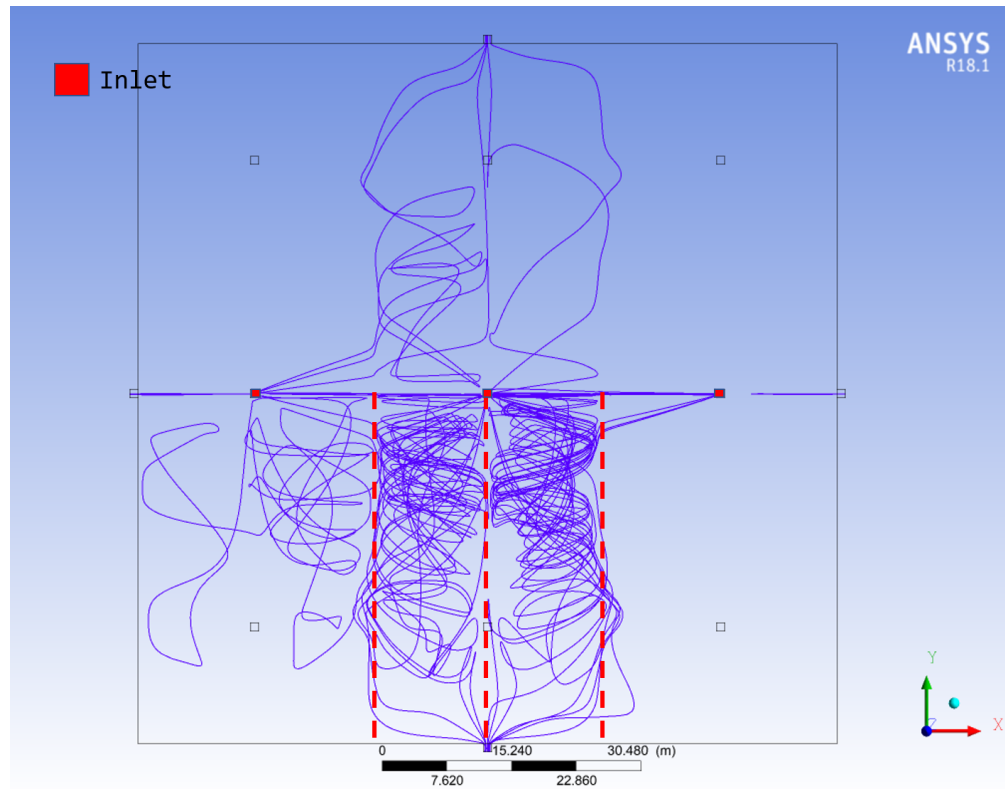


Figure 6.19: 15k CFM SunCooler 32 ft ceiling height 90 ft fan spacing: disabled fans - top view streamlines

6.1.4 Thermal Mixing: 2.5k CFM SunCooler 20 ft Ceiling Height 50 ft Fan Spacing

The final mixing model utilized the 2.5k CFM SunCooler unit and 50 ft fan spacing with a ceiling height of 20 ft. These values were again based on conversations with the NWREC CEO and his estimates for how he feels his equipment would be best utilized. With these adjustments, mixing occurred in approximately

148 seconds, which is when the temperatures converged to within 0.5 °F, according to monitor points shown in Figure 6.20. Figure 6.21 shows the streamlines for this geometry, which has larger more concentrated vortices, relative to the geometry. This is comparable to streamlines seen by other geometries which achieved mixing in short time frames. Indicating that mixing could potentially occur at a larger fan spacing, if no obstructions existed within the warehouse.

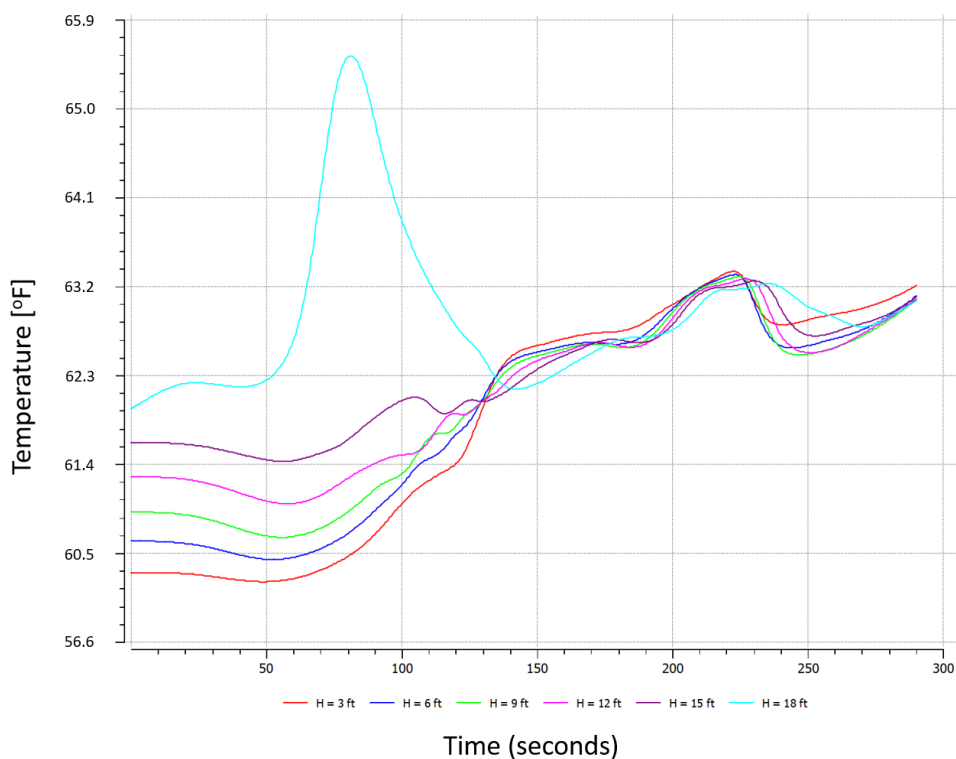


Figure 6.20: 2.5k CFM SunCooler 20 ft ceiling height 50 ft fan spacing: temperature monitors

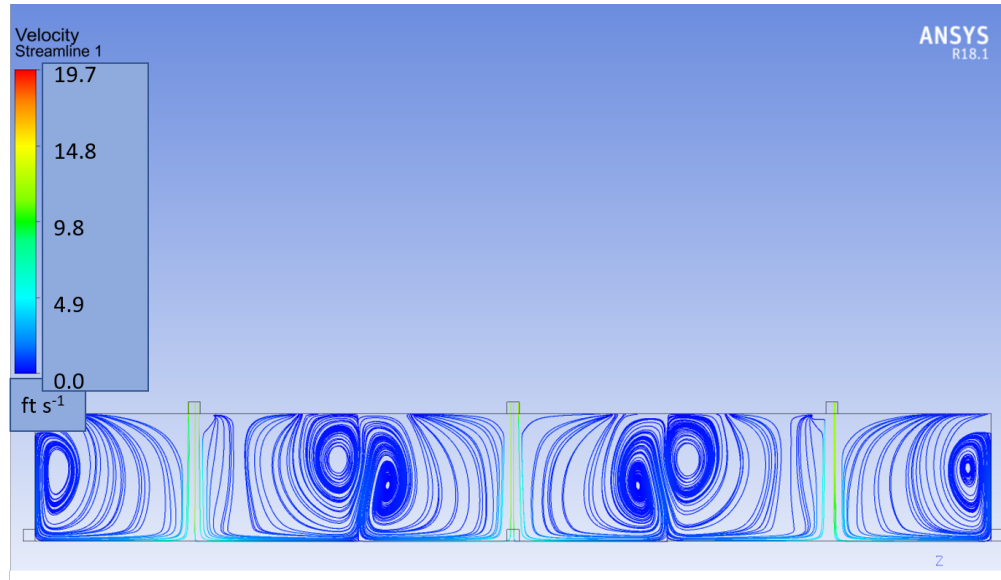


Figure 6.21: 2.5k CFM SunCooler 20 ft ceiling height 50 ft fan spacing: streamlines

6.2 Cooling

The cooling model was set to have a 20 ft ceiling height with a 150 x 150 ft floor space. The outdoor temperature was set to 5 °F and the wall and ceiling heat transfer coefficient of $0.3 \frac{W}{m^2K}$, the upper range of heat transfer coefficients recommended by the ASHRAE handbook (ASHRAE, 2017). The temperature was set to be uniformly 65 °F initially, as this is considered the temperature at which a commercial building would be maintained, and is used as the basis for calculating heating degree days. A heating degree day is defined as number of days the temperature is below 65 °F times the number of degrees below 65 °F (Investopedia, 2018). Each temperature figure is set from 60 °F to 65 °F. To track cooling temperature monitors were enabled within the geometry from 1 ft to 19 ft,

shown in Figure 6.22.

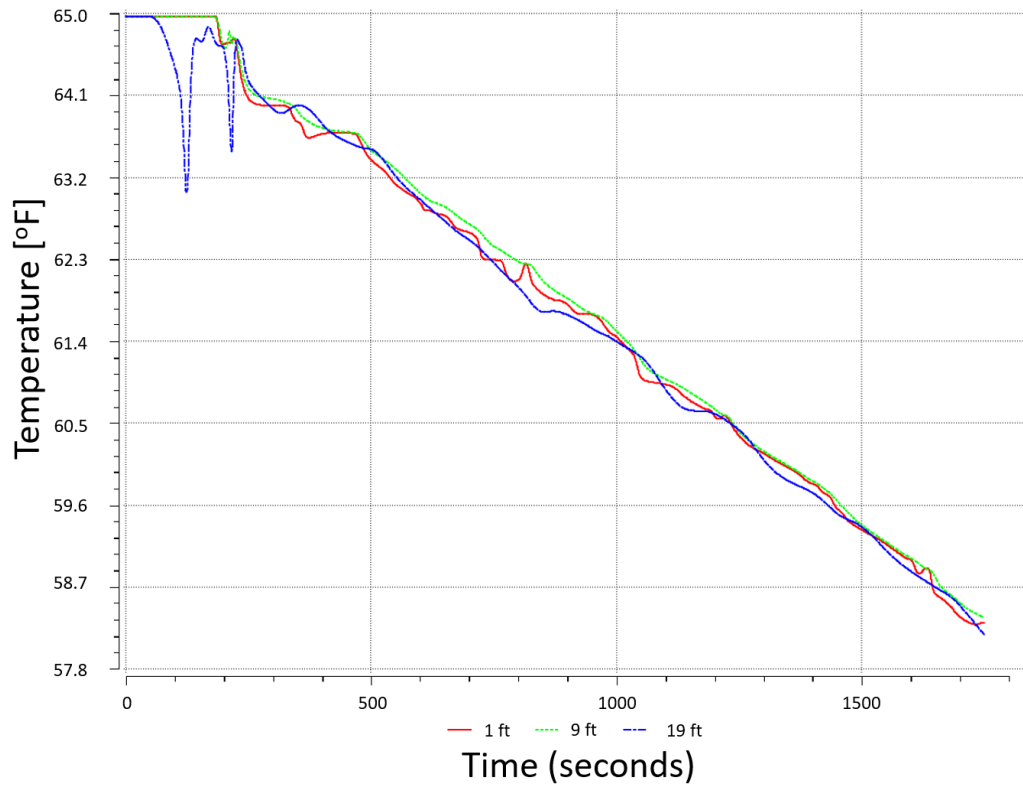


Figure 6.22: 20 ft ceiling height cooling: all time steps

As cooling behavior converges and decreases linearly after approximately 300 seconds, Figure 6.23 was created to provide a better look at the non-linear behavior occurring in the early stages of cooling.

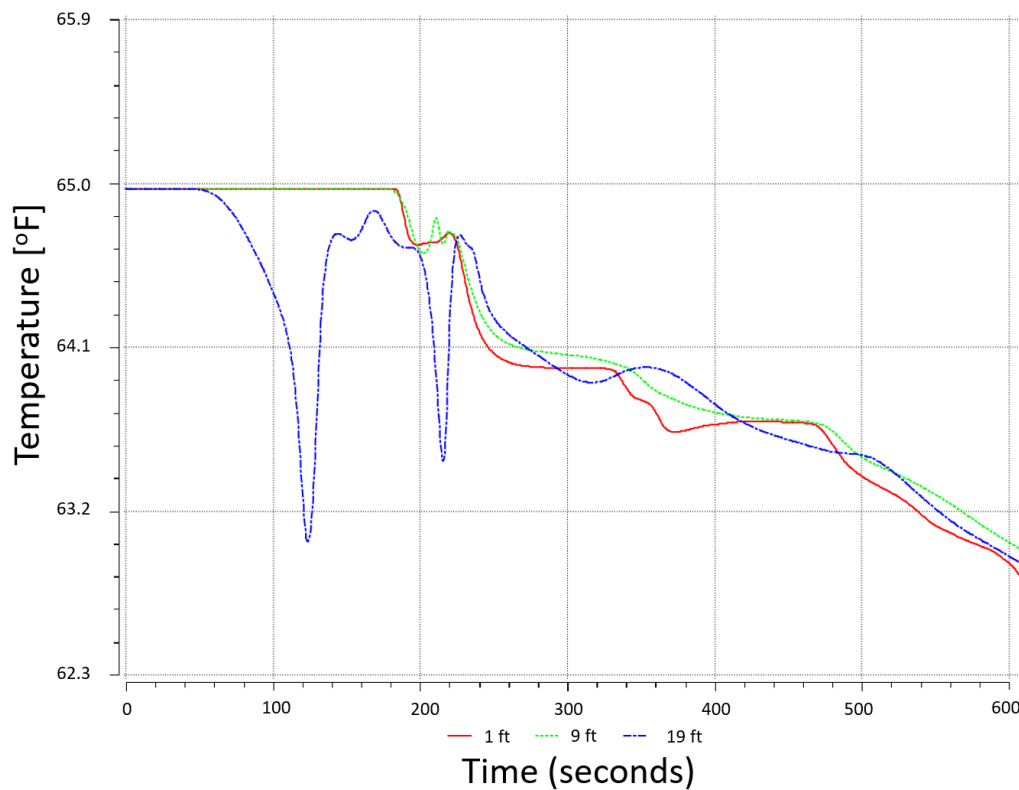


Figure 6.23: 20 ft ceiling height cooling: 0 - 600 seconds

Initially, the temperature is set everywhere to be 65 °F shown in Figure 6.24. Cooling is first observable on the walls as cool air travels downwards and forms a pocket along the floor of the room. Seem in Figure 6.25. While this is occurring, the air at the ceiling is beginning to cool, but has not yet begun to sink into the room, as seen in Figure 6.23.

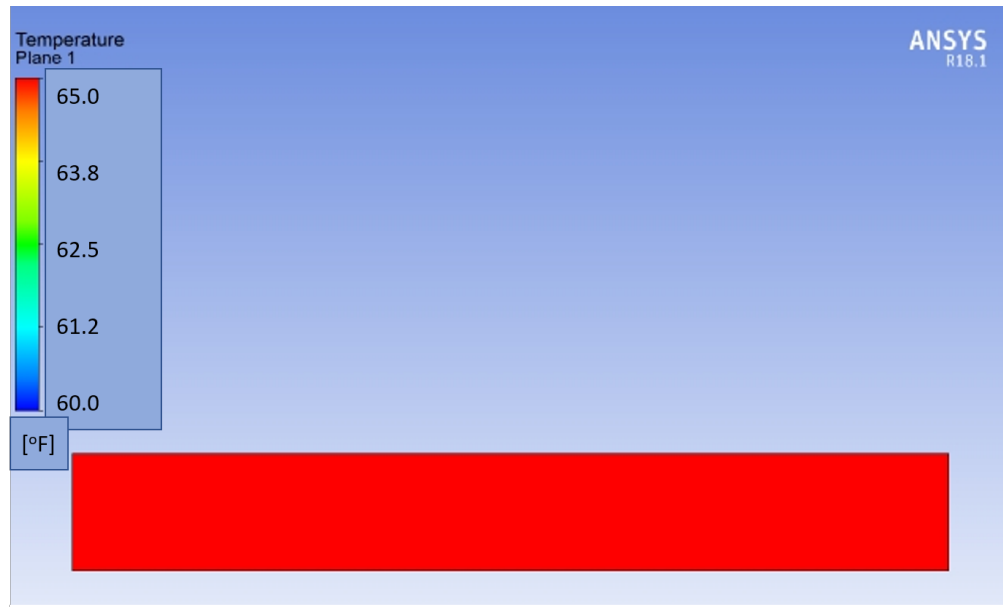


Figure 6.24: Cooling model, time = 0 seconds

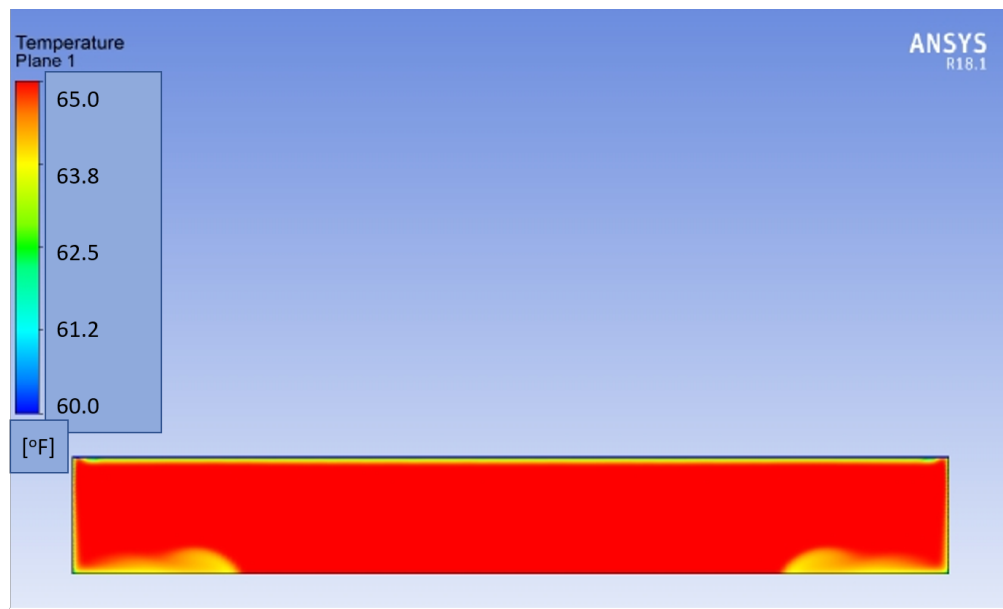


Figure 6.25: Cooling model, time = 96 seconds

At time equal to 132 seconds air begins to form downward traveling channels of cooler air, shown in Figure 6.26. As the cooler air descends into the warmer air it is warmed and mixes the air to a new temperature. shown in Figure 6.27. Figure 6.23 shows the initial large decrease in temperature at the ceiling, then an increase as warmer air moves upwards and the room is mixed to a new, lower, temperature. A second large dip then occurs as the process is repeated and a smaller scale.

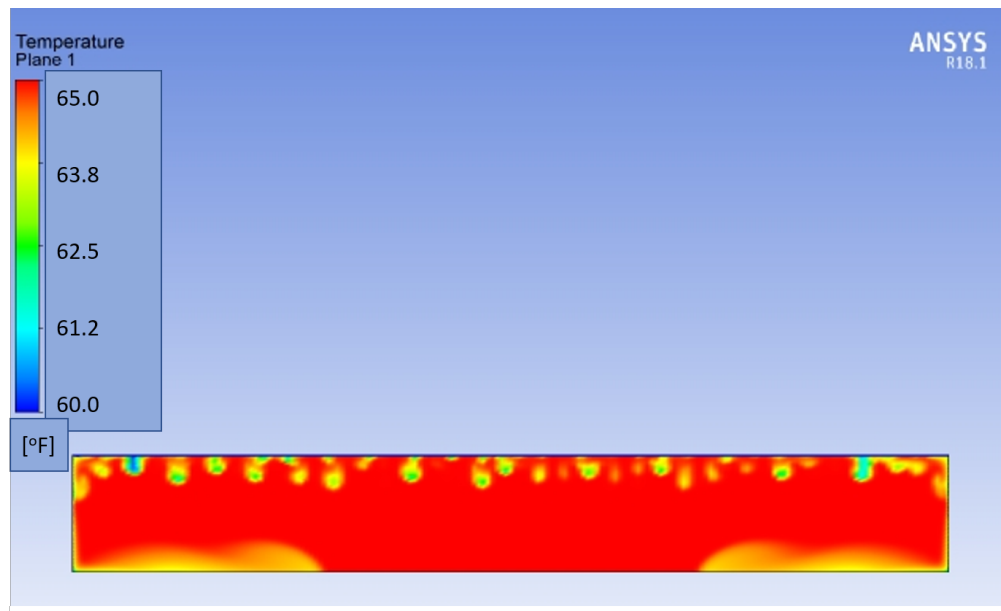


Figure 6.26: Cooling model, time = 132 seconds

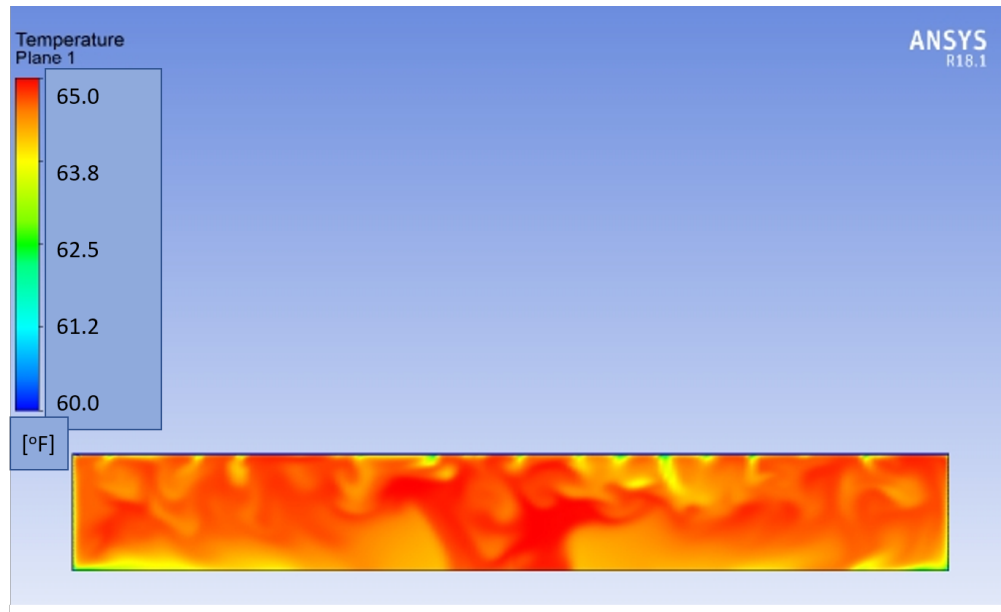


Figure 6.27: Cooling model, time = 200 seconds

At time equal to 380 seconds the cooling process has begun to settle into a more uniform process, starting to take on linear behavior. This is shown in Figure 6.28. As time proceeds forward cooling starts to happen more uniformly and there exists little to no temperature gradient while it occurs. This can be observed by the linear nature of temperature lines in Figure 6.23, and can be seen by the uniform coloring in Figures 6.29 and 6.30.

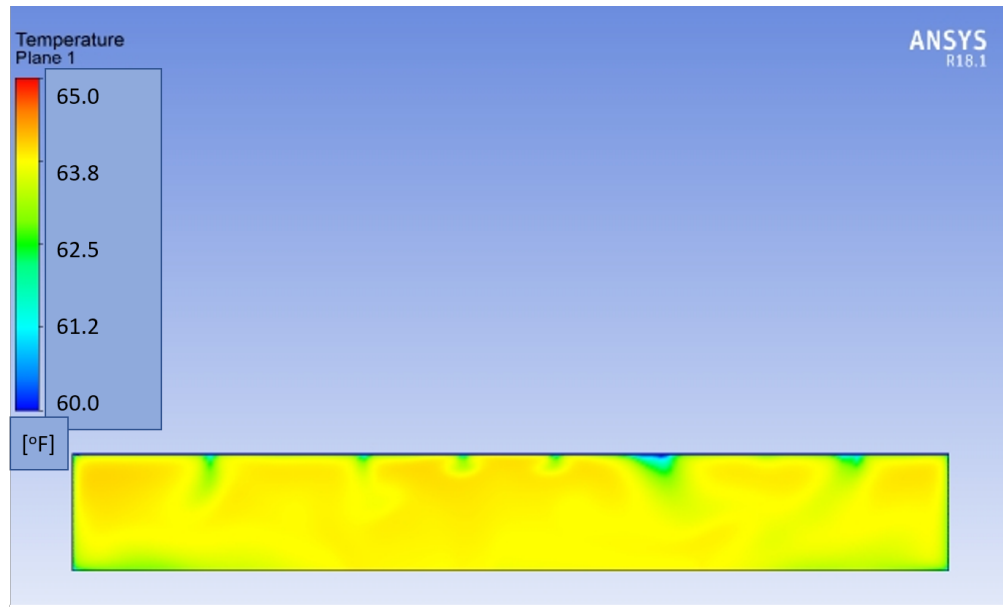


Figure 6.28: Cooling model, time = 380 seconds

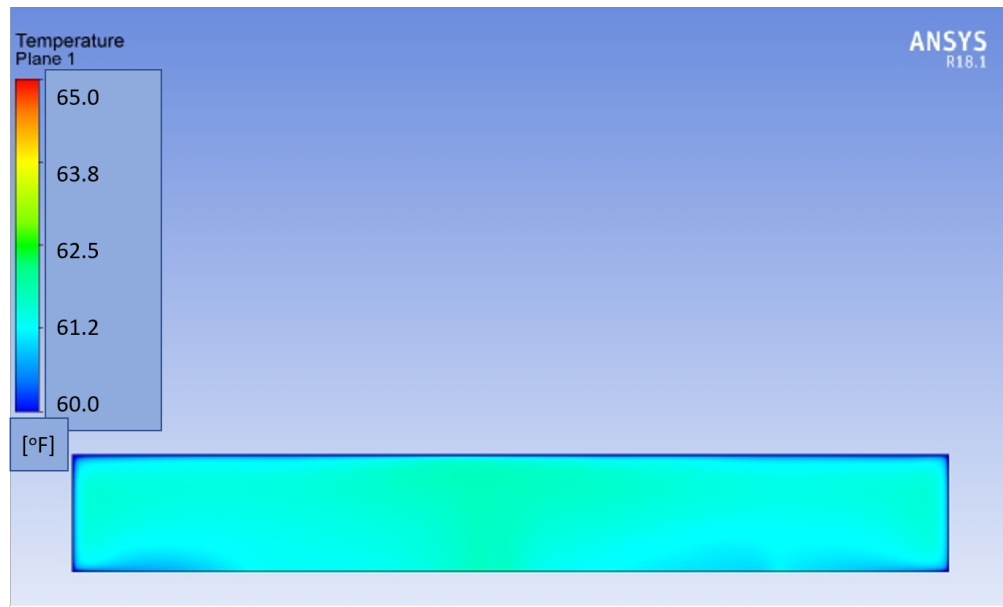


Figure 6.29: Cooling model, time = 968 seconds

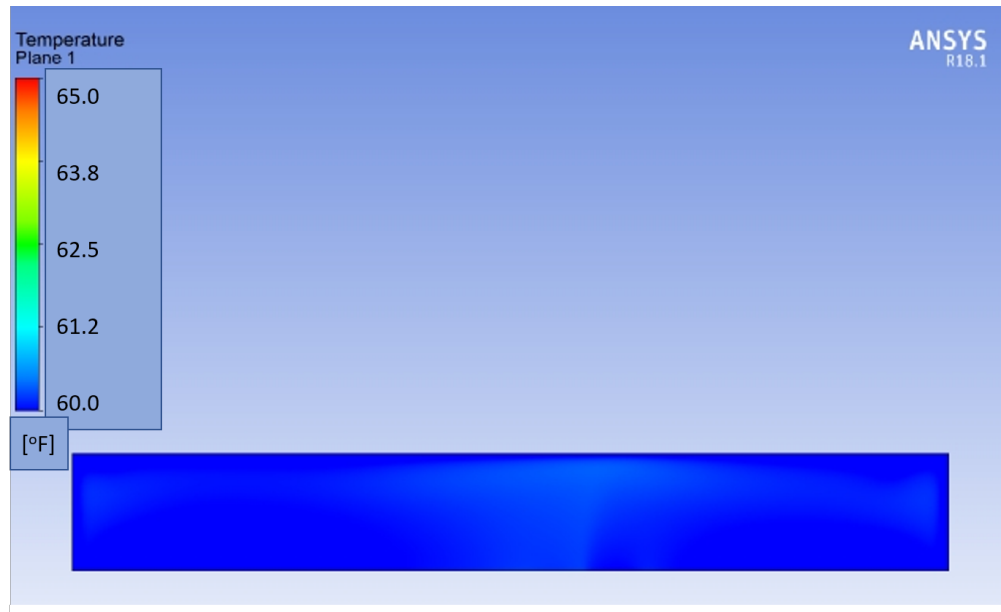


Figure 6.30: Cooling model, time = 1304 seconds

The time required to cool the room varies depending on how cool the end user is willing to let the room become. To this end, the time required to drop by 5 °F, broken into 5 steps, is shown in Table 6.2:

Table 6.2 Cooling model results

ΔT °F	Time (seconds)
1	280
2	560
3	800
4	1100
5	1350

6.3 Model Validation

To determine the quality of the simulations, a validation model was created of the school room, shown in Figure 6.31 and 6.32.

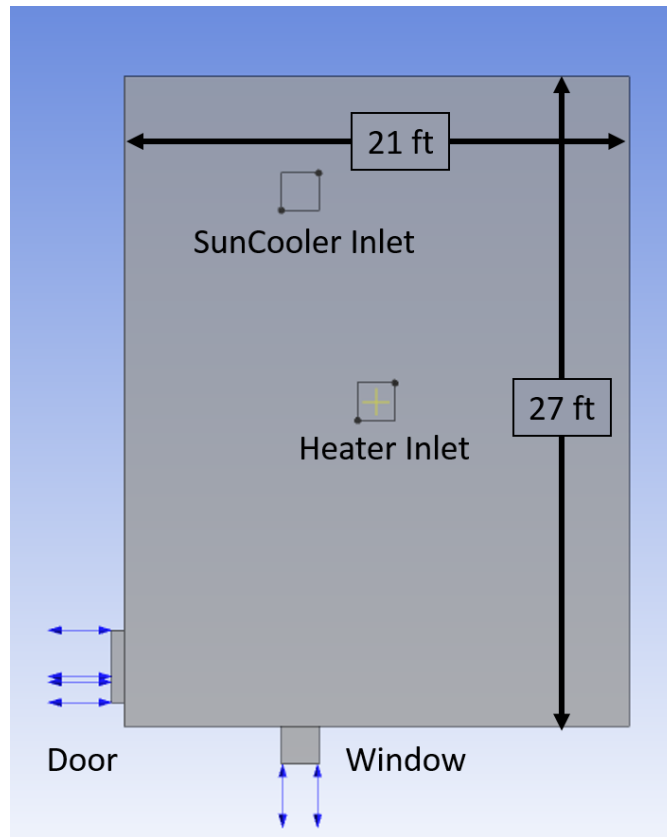


Figure 6.31: Top view of validation model

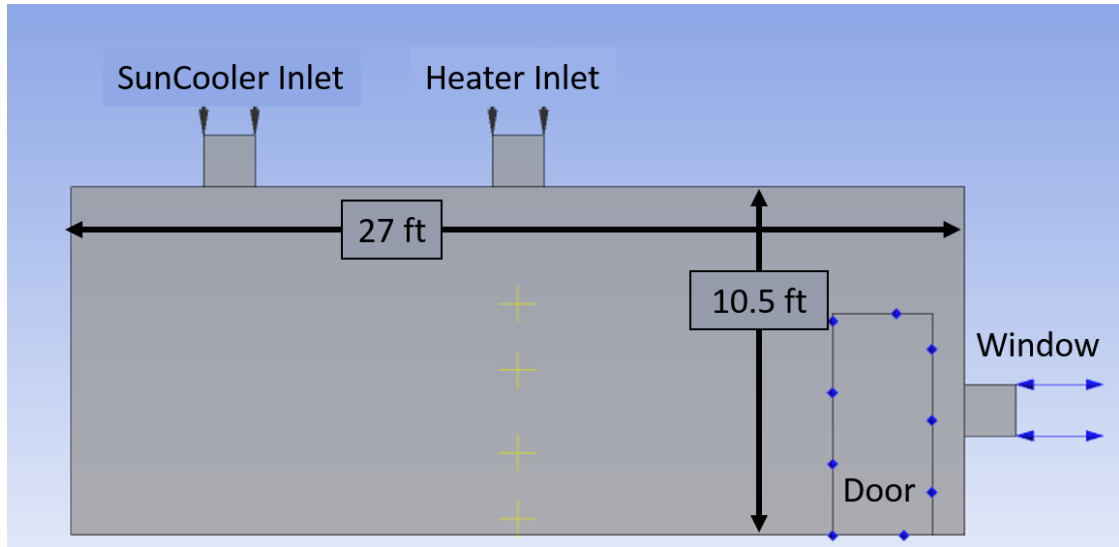


Figure 6.32: Side view of validation model

The model is designed to match the boundary conditions of the school room. However, it does not take into account any of the interior furniture or other features. The room is 21 ft by 27 ft and the roof height is approximated to be 10.5 ft, though in reality it slopes from 9 ft to 12 feet.

The SunCooler inlet is set to intake air at 1000 CFM at 40 °F, which was the average outdoor temperature on the day the experiment was performed. The heater inlet is set to be 100 CFM and operating at 90 °F. This is a third of the 300 CFM value given for the central heater which services the experiment room and the two neighboring classrooms. The room was set to maintain 80 °F, and the 90 °F inlet value is an approximation based on the expected heater outlet temperature.

Two openings are set to represent the window and the door which was opened to the neighboring classroom. The window opening is set at the outdoor temperature,

40 °F, and the door temperature is set to match the temperature gradient of the room. The temperature of the door opening does not change with time. The initial temperature of the room is set to match the temperature that the room was at when the SunCooler activates, ranging from approximately 70 °F to 74 °F.

All solver settings were kept identical to the mixing and cooling models. The model was run to an hour of simulation time and the results were compared to the data collected from the school room experiment, shown in Figure 6.33.

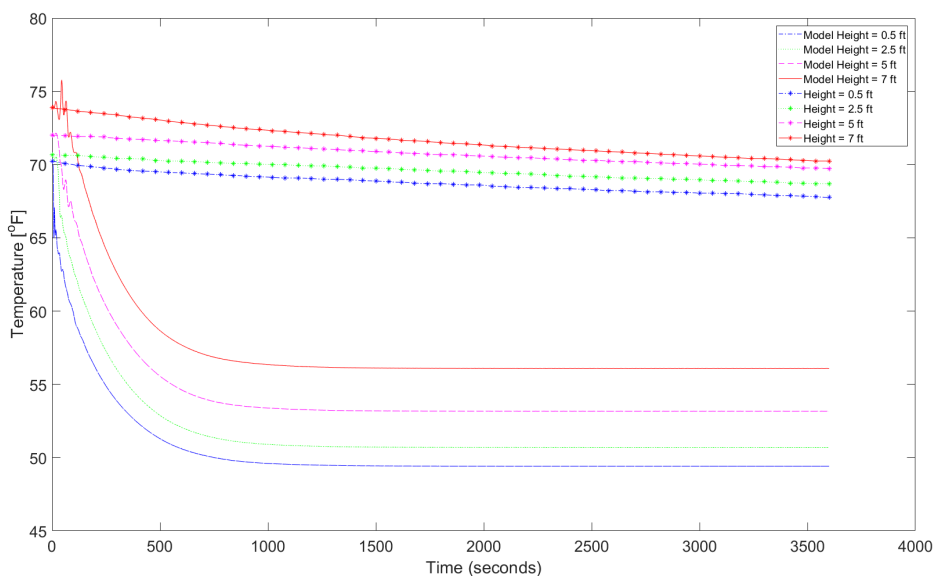


Figure 6.33: Model vs actual experimental temperature data points

The initial model results show that the model is cooling much more quickly than the experimentally observed. To get a better idea of why this might be occurring, the time axis of data collected from the school room was divided by a constant so that the temperature data concluded at the overlap point with the

model temperature data, shown in Figure 6.34.

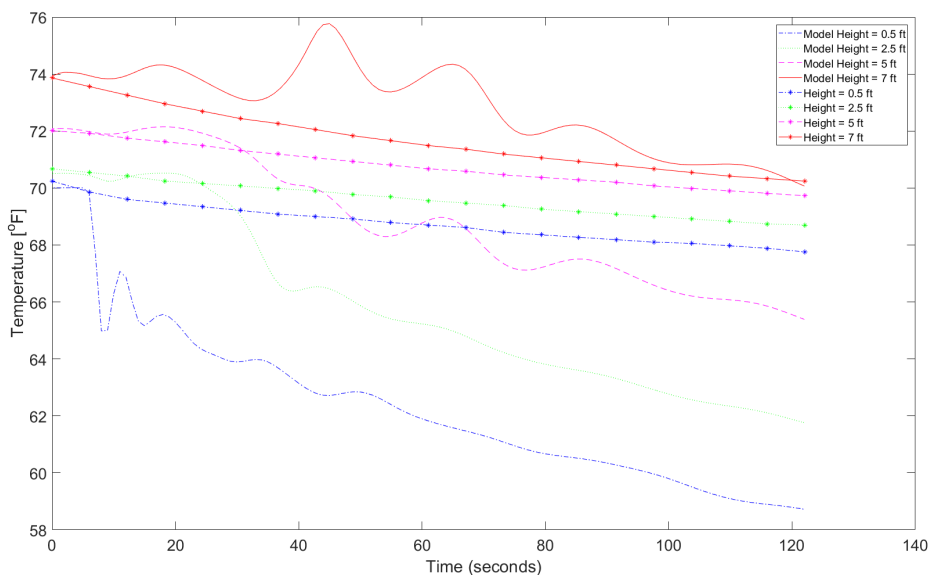


Figure 6.34: Model vs modified experimental temperature data points

With the current model setup, the model is cooling approximately 29 times faster than is reflected in reality at the highest measured point in the room. The 0.5 ft elevation cools significantly faster than that. The sharp drop at the initial time steps for the 0.5 ft height show that the air entering through the cooler inlet is having a much quicker impact than it should. This suggests that thermal mass has a very large part to play in the cooling profile shown by the collected data points. To verify this, another model was run with the floor temperature set at 80 °F. This value is artificially high to gauge the impact that changing it has on the models cooling profile. The new results were then compared to the previous model in Figure 6.35

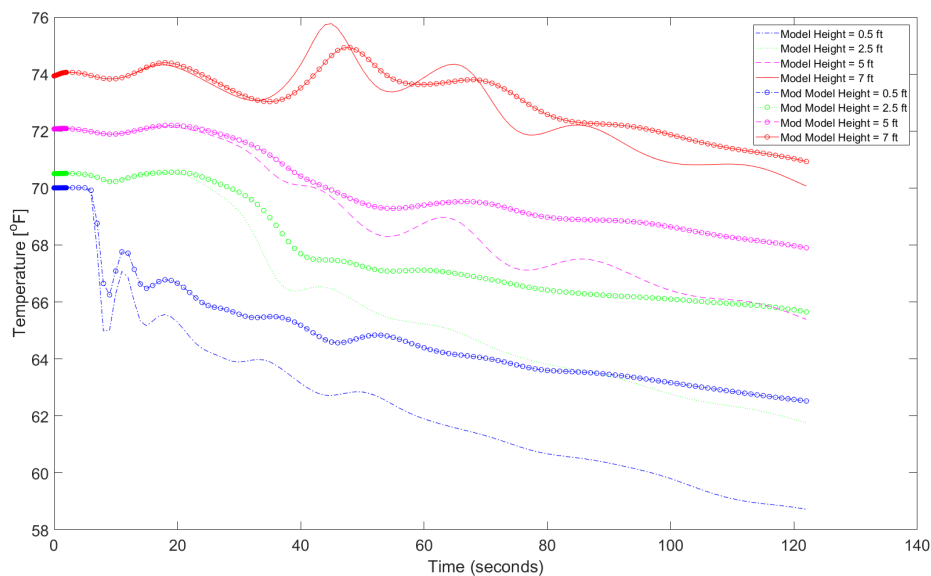


Figure 6.35: Comparison of model data, with and without a heated floor

The modified experimental data has a linear slope of 0.023 and an average temperature difference of 2.95 °F. The initial model data had a slope of 0.063 and an average temperature difference of 4.73 °F. By adding a floor temperature, the slope of the model data is decreased to 0.043. Indicating the model more closely resembles experimental data. Additionally, the average temperature difference is reduced to 3.9 °F, which also more closely resembles to modified experimental data. This supports the conclusion that thermal mass has a significant role to play in cooling behavior and time. The model itself still cools much more rapidly than reality, but the profile declines in an expected way.

6.3.1 Effect of Thermal Mass

To further verify the lack of thermal mass as the key cause of the rapid cooling seen in the model, a simple first law analysis was performed. In this analysis the density and specific heat of the contents of the room were lumped together to create an a single average value for both parameters. The first law analysis was applied to the room as a single entity with mass flow in and out of the room. The control volume is shown in Figure 6.36. The first law of thermodynamics is shown in Eq 6.1.

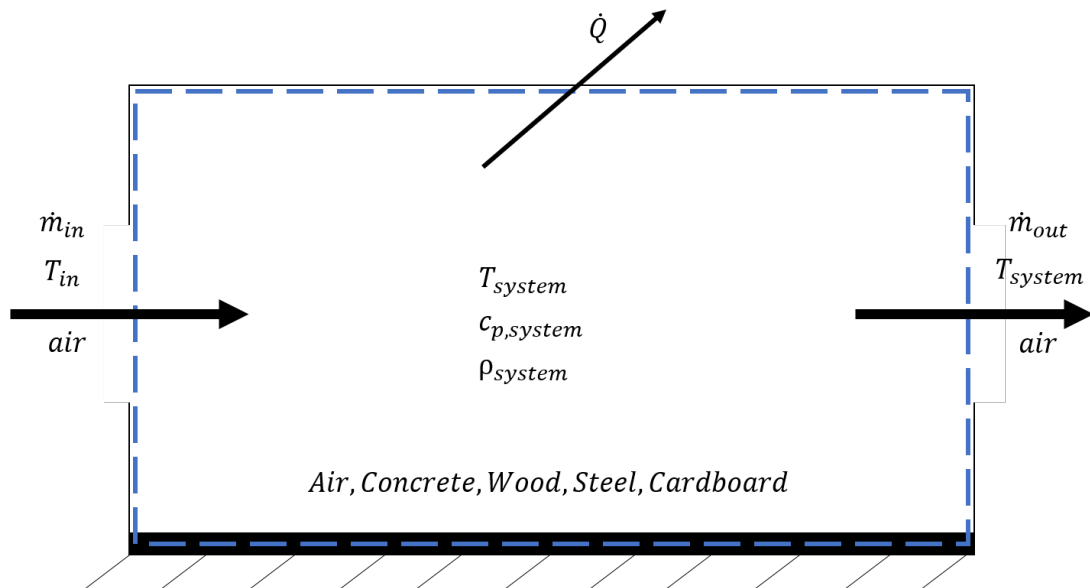


Figure 6.36: Control volume for thermal mass analysis

$$\frac{dE}{dt} = \dot{Q} - \dot{W} + \dot{m}_{in} \left(i + \frac{v^2}{2} + gz \right)_{in} - \dot{m}_{out} \left(i + \frac{v^2}{2} + gz \right)_{out} \quad (6.1)$$

Where $\frac{dE}{dt}$ is the change in energy, \dot{Q} is the rate of heat transfer, \dot{W} is the work

done, \dot{m} is the mass flow rate in and out of the system, v is the velocity at the inlet and outlet, z is the height of the inlet and outlet, and i is the enthalpy.

There is no work done on the system, so \dot{W} is equal to zero. The change in kinetic and potential energy is assumed to be zero, removing velocity and change in elevation terms from the left and right side of the equation. $\frac{dE}{dt}$ then is only represented by the energy storage term. \dot{Q} is represented by convective heat transfer with the system. Assuming air can be treated as an ideal gas with constant specific heat, the change in enthalpy is approximated by the specific heat times the temperature. The temperature of the air at the outlet is assumed to be equal to the temperature of the system, and the temperature at the inlet is equal to the surrounding temperature. Mass flow rate into the system is assumed to be identical to the mass flow rate out of the system, allowing for the combination of the \dot{m} terms. This simplification of the first law results in Eq 6.2:

$$\rho V c_p \frac{dT}{dt} = hA(T_\infty - T) + \dot{m}(c_{pa}T_\infty - c_{pa}T) \quad (6.2)$$

Where ρ is the average density of the system, V is the volume of the box, c_p is the average specific heat of the system, $\frac{dT}{dt}$ is the rate of change of temperature with respect to time, h is the convective heat transfer coefficient, A is the surface area of the system exposed to T_∞ , T_∞ is the surrounding temperature, T is the temperature of the system, and c_{pa} is the specific heat of air. $\frac{dT}{dt}$ can be converted to the difference between the room temperature, T , at some time in the future minus the current temperature over some change in time. The future temperature

can then be solved for so that the temperature change with time can be calculated using time steps, represented by dt . In this analysis the value of 0.1 seconds was used for dt . These changes result in Eq 6.3:

$$T_{i+1} = \frac{hA + \dot{m}c_{pa}}{V\rho c_p}(T_{\infty} - T_i) * dt + T_i \quad (6.3)$$

With the governing equation solve for, the variables in the equation need to be determined. First was the average of the specific heat and density for the system. Materials expected to make up the volume of the system included air, cardboard, wood, steel, and concrete. The values were looked up using the Engineering Toolbox website (EngineeringToolBox, 2018).

Table 6.3 Material Properties

	Air	Cardboard (Paper)	Wood (Pine)	Steel	Concrete
Density (kg/m ³)	1.225	800	530	7820	1500
Specific Heat (kJ/kg-K)	1.005	1.34	2.5	0.49	0.2

Other variables were approximated based on the school room experiment as follows:

- $h = 0.3 \text{ W/m}^2\text{-K}$
- $V = 1008 \text{ m}^3$
- $A = 161 \text{ m}^2$
- $\dot{m} = 0.58 \text{ kg/s}$

- $T_{\infty} = 279.9$ K
- Initial temperature = 298.2 K
- $dt = 0.1$ s

The time required for the room temperature to equal the surrounding temperature was then solved for with 5 different cases:

- Case 1: 100% Air ($c_p = 1.005$, $\rho = 1.225$)
- Case 2: 90% Air ; 5% Wood ; 5% Concrete ($c_p = 1.0395$, $\rho = 102.6$)
- Case 3: 80% Air ; 5% Wood ; 1% Steel ; 14% Concrete ($c_p = 0.9619$, $\rho = 315.9$)
- Case 4: 70% Air ; 10% Wood ; 5% Steel ; 15% Concrete ($c_p = 1.008$, $\rho = 669.9$)
- Case 5: 60% Air ; 40% Cardboard ($c_p = 1.139$, $\rho = 400.7$)

Figure 6.37 shows the results of the analysis.

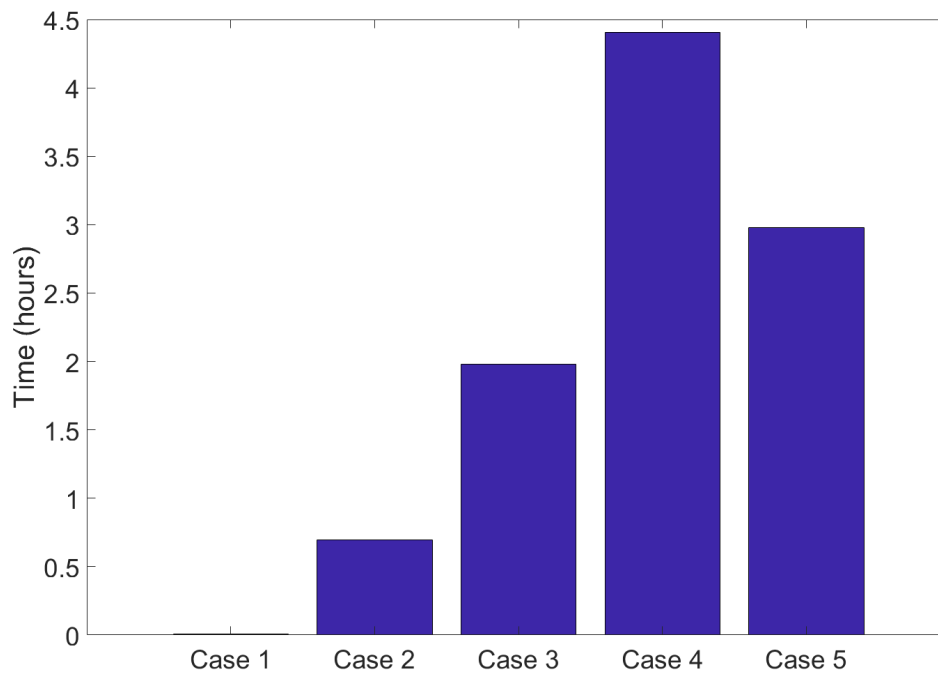


Figure 6.37: Results of thermal analysis

The first case with only air cools in 48 seconds, then when increasing the specific heat of the system by including other substances the cooling time increases dramatically, with a peak of 4.5 hours with case 4. When comparing the cases which include thermal mass to the case lacking thermal mass cooling times range from 88 times longer than air, to 550 times longer. This further demonstrates the importance of thermal mass when evaluating the cooling of a system. This analysis reinforces the conclusion that the validation model is representing a system other than what exists at the experimental site. In order to match experimental results the product of the average room density and specific heat needs to be equal to 2500

$kJ/m^3 - K$. This value is difficult to obtain with the specific heat and density values of the materials selected, with steel being the only value which exceeds the criteria, but is not outside of the realm of reality.

6.4 Model Limitations

From the validation, it becomes apparent that one of the largest shortcomings of existing models is the lack of thermal mass. The absence of the thermal mass results in much more rapid cooling behaviors than were observed in experimentation. There is also uncertainty in the models mixing time, as obstructions such as desks in the case of the school room and shelves for the warehouse would inhibit flow.

The model is narrow in the variables explored. It only investigates two possible flow rates when there is a broad range of possible flow rates that could be realistically investigated for grid powered fans. The model also stays within known regions of influence rather than exploring the extent of the capabilities for a given fan flow rate.

To improve on the validation model, representations for objects in the room would need to be incorporated into the model, both in volume and their material properties. Including the neighboring room would improve on the validation accuracy, as it currently is represented as an infinite reservoir. Additionally, an improved measuring of the school rooms features would aid in validation as many of the features in the current model were approximated. More accurate informa-

tion for the rooms heater could be attained by placing a sensor on the heater to get an accurate inlet temperature, and to determine when the heater was operational. Within the current validation model, heating was approximated as it was unknown when the neighboring rooms thermostat was activating the heater.

With an improved validation model, the importance of the different features in the building could be weighed. With the relative importance of different features evaluated, it would be more beneficial to return to the stock model, the 3 x 3 fan inlet geometry, and begin investigating the maximum areas of influence the fans could support for a range of fan strengths.

6.5 Discussion

When modeling mixing, it was found that the following geometries were able to achieve mixing within 3 minutes of activating inlets:

- 15000 CFM SunCooler
 - 90 ft Fan Spacing
 - 32 and 40 ft Ceiling Heights
- 2500 CFM SunCooler
 - 50 ft Fan Spacing
 - 20 ft Ceiling Height

Figure 5.19 shows a local impact of the SunCooler units, with a sharp drop in

temperature while the SunCooler is operating, and a rapid increase of temperature once the SunCooler is disabled. This is a result of insufficient SunCoolers to properly perform destratification on the warehouse. When modeled, the local effects of the SunCoolers on airflow can be seen. Figures 6.15 and 6.19 can be compared to see the region of influence supported by a single operating fan. For the case with all fans enabled, quadrants are formed which produce dense streamlines indicating thorough mixing of the area. When only a single column of fans is enabled, local mixing still occurs, as seen in Figure 5.19, but as the streamlines move away from the fan location they begin to dissipate, reducing the impacts of mixing. When looking at a very large warehouse, such as the one used for this study, the mixing effect will dissipate long before reaching a wall, which would support mixing. As a result, the SunCoolers do not have a long enough reach to dissipate the pocket of warmer air that collects at ceiling level. Once the SunCooler deactivates, the warmer air surrounding the semi mixed area quickly returns the area to the average ceiling temperature.

Cooling modeling showed that it requires 280 seconds to reduce the room temperature by 1 °F at floor level, and 1350 seconds to reduce it by 5 °F. It is felt that this is a conservative estimate, as the validation model indicates that thermal mass has a very large impact on cooling time. Another factor that would slow cooling is the models increased cooling by the modeled warehouse walls, which would account for a smaller percentage of cooling, relative to the roof size, in an actual warehouse.

This modeling is a preliminary study. It provides guidelines for the introduction

of duty cycles on fans intended for destratification. When applying the duty cycles discussed in this study, the warehouse for implementation should be investigated to determine its suitability for destratification. When implementing the duty cycles, the method of fan operation needs to be carefully considered. If the duty cycle is implemented simply as a binary on/off schedule, fans could reactivate before the heating system has enabled. This would result in the room being mixed to a lower temperature, which will only then activate the heating system. If the heat is poorly distributed, the fans may complete their duty cycle before the heaters have reintroduced the warmer air to the upper regions, leaving the room mixed at a lower temperature and increasing the likelihood of a stratification profile developing between fan duty cycles. This can be offset by longer fan run times, but these are factors that need to be considered when establishing a duty cycle, and some calibration may be required. It is also worth noting that after performing a validation study on the models, the mixing and cooling behaviors likely occur much more rapidly than in reality. However, by comparing the two models a reasonable percentage of operation time can still be estimated using the model results.

The finding of this study is that destratification fans nominally only need to operate for 35% of total operating time to maintain destratification. This assumes peak temperature is maintained at least 1 °F above the set point temperature. Percentage calculation is shown in Eq 8.1:

$$Operation\ Time = \frac{Fan\ Runtime}{Total\ Time} = \frac{148\ seconds}{280\ seconds + 148\ seconds} = 35\% \quad (8.1)$$

In order to properly mix and maintain the environment, fans need to be installed to service the entire enclosed area. Otherwise areas unaffected by the mixing will cause the mixed area to return to a stratified state more rapidly. As is observed in Figure 6.38.

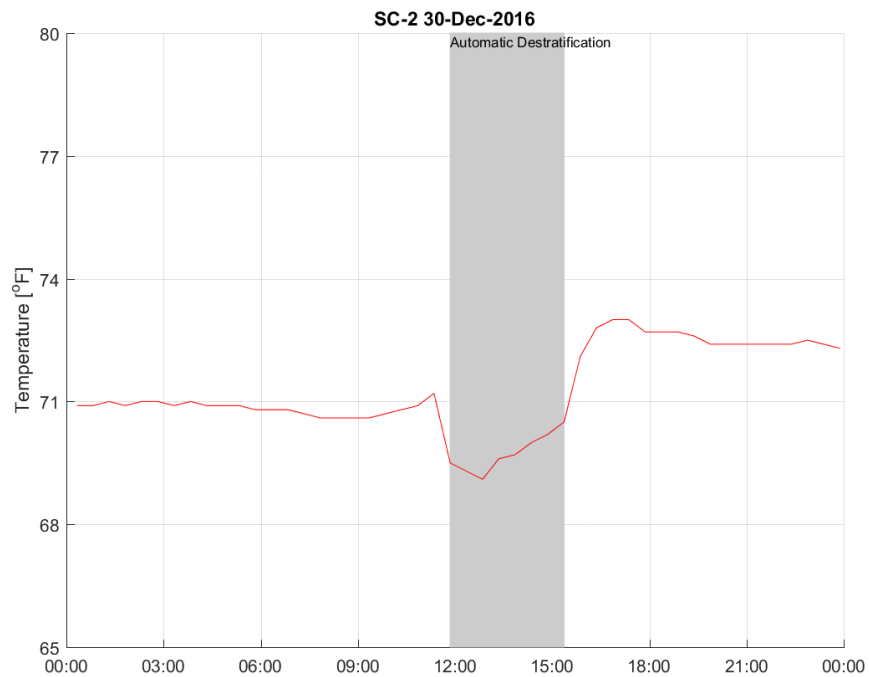


Figure 6.38: Ceiling height temperature - SunCooler 2, December 30th 2016

Chapter 7: Study Impact and Limitations

This chapter will discuss the cost of the SunCooler units and the potential savings they offer users. The analysis is based on the warehouse location described in Chapter 3. This chapter also discusses the requirements for maintaining a destratified environment without continuous fan operation, and improvements which can be made for future studies.

7.1 Estimated Simple Payback

This section discusses the simple payback expected from installing SunCooler units, as well as the supporting analysis used to determine the estimate.

7.1.1 Cooling Season Energy Costs and Savings Potential

This section discusses the cost of cooling the warehouse under the baseline condition, and potential energy savings by using the solar powered SunCooler units. To determine existing intake/exhaust fans operation time in the warehouse, sensors were placed on a single fan in each of 4 control zones. Zone fans are linked so that when one fan activates all of them will activate. Data collected showed on/off toggles for the fan the sensor was attached to. This was then multiplied by the number of fans in the given zone. Figure 7.1 shows the combined operation time

of all fans, in hours, for each month:

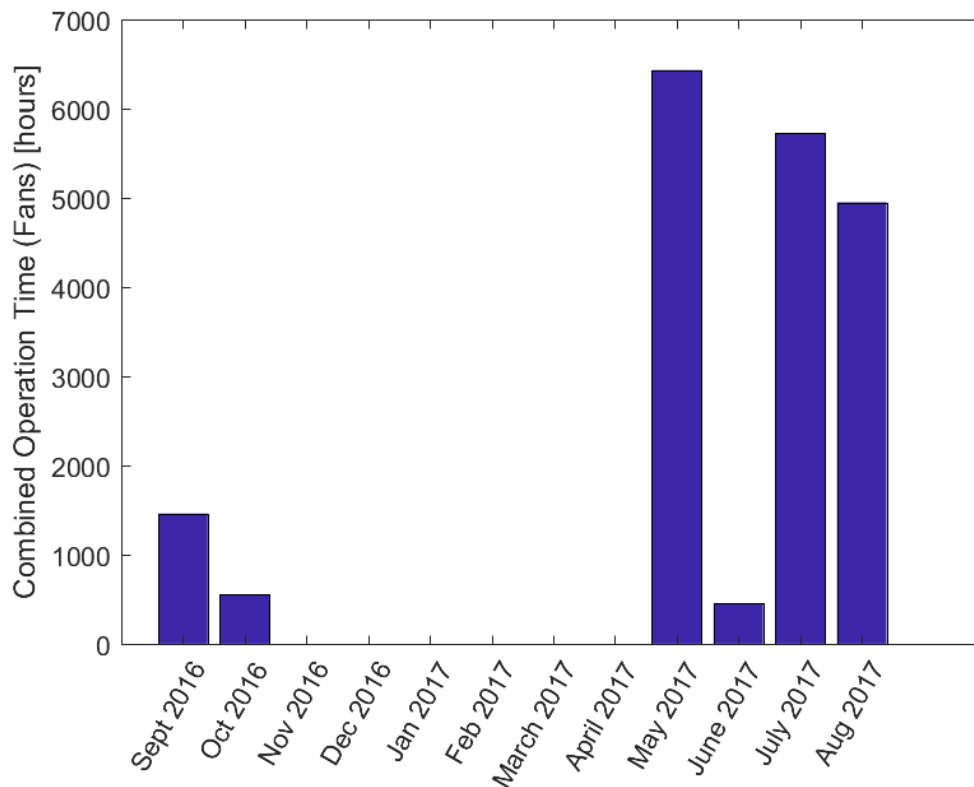


Figure 7.1: Combined run time for exhaust/intake fans

November 2016 through April 2017 shows no fan operation time as the facility was operating in winter mode, in which the fans are disabled and the heaters are enabled. June 2017 shows an unexpectedly low fan operation time. The exact cause of this is unknown. As the June 2017 operation time is much lower than the May 2017 and July 2017 operation times, two costs will be estimated from the available data. One set with the actual recorded run times, and one set with the June 2017 operation time as an average of the May 2017 and July 2017 operation

times.

To determine the cost of operation, the horsepower needs to be converted to watts by multiplying by the electric motor horsepower to kilowatt conversion constant, Eq 7.1. Then the fan motor wattage can be multiplied by the total hours of fan operation, 19573.6 hours, and the commercial cost of electricity per kilowatt hour in Albany, Oregon, $0.0843 \frac{\$}{kWH}$ (ElectricityLocal, 2018). This is shown in Eq 7.2. As an estimate, the fan motor is assumed to be fully loaded at the rated horsepower.

$$Conversion = 0.746(10) = 7.46 kW \quad (7.1)$$

$$Cost = 0.0843(7.46)(19573.6) = \$12309.41 \quad (7.2)$$

When adjusting the hours of operation in June 2017, an arithmetic mean of the operation hours from May 2017 and July 2017 is taken. Shown in Eq 7.3.

$$June\ Hours = \frac{6432.98 + 5728.52}{2} \quad (7.3)$$

This increases the June 2017 operational hours from 454.45 hours to 6080.75 hours. Bringing the new total number of hours from 19573.6 to 25199.9. Resulting in the final annual fan operation costs of:

- \$ 12309.41 without adjustment
- \$ 15847.66 with adjustment

7.1.2 Heating Season Energy Costs and Savings Potential

This section describes the baseline warehouse heating costs, and potential savings due to destratification. In Chapter 5, the experimental data showed that the warehouse was underheated. For an underheated or unheated warehouse, destratification is not expected to save significant energy during the heating season. Thus, estimates for potential savings are made assuming that the heating was upgraded such that the warehouse was properly heated.

7.1.2.1 Baseline Heating Cost Estimates

The cost of heating the experimental site was calculated using measured data from the MAU heaters. As there was not a direct way available to determine if a heater was operating, when the sensors located at the heater showed a temperature greater than 80 °F it was considered to be on. The measured data is from January 2017 - May 2017 as well as November and December 2017. These were the months indicated by the distribution center as operating in winter mode. The total operation time for all 7 MAU heaters was 9450.23 hours.

The MAU heaters are rated to operate at 1,300,000 BTU/hr with an efficiency of 0.92. To determine the number of dekatherms (1 dekatherm = 10 therms = MMBTU) consumed per hour by the heaters the BTU/hr value (assuming the heaters are operated at rated firing condition) is divided by the efficiency and the HHV of natural gas, 1,000,000 BTU/dekatherm. This results in 1.41 dekatherms/hr. This value is then multiplied by the cost of natural gas,

\$8.53/dekatherm, and the hours of operation. The result of which is the estimated cost of heating, \$113,906 for the area of the warehouse in which experiments were conducted.

7.1.2.2 Destratification Energy Savings Potential

To calculate the estimated heating savings, equations available in a study by Aynsley (2005) were utilized. These equations are shown in Eq 7.4 and 7.5.

$$\dot{Q} = UA\Delta T \quad (7.4)$$

$$FS = Hrs \frac{\dot{Q}_{bd} - \dot{Q}_{ad}}{(HHV)\eta} \quad (7.5)$$

Where \dot{Q} is the rate of heat loss through the roof before destratification (bd) and after destratification (ad). U is the average heat transfer coefficient for the roof. U is approximated as $0.13 \frac{BTU}{h \text{ ft}^2 \text{ } ^\circ F}$ as the actual value is not known. This value is identical to the one found in Aynsley (2005). A is the area of the roof for area in which the experiment was performed, $500,000 \text{ ft}^2$. ΔT is the temperature difference between the exterior and interior surfaces. The interior temperature will be hypothetical for this study, as the warehouse was under heated and destratification is not beneficial under this condition. However, destratification savings are related to the ratio between before and after destratification ceiling temperatures. Which means the savings are driven by the number of degrees the ceiling

temperature is able to be reduced, not the actual ceiling temperature. For the exterior temperature, weather data was collected from the National Oceanic and Atmospheric Administration (NOAA, 2018). The data can be seen in Table 7.1:

Table 7.1 Average temperature data - Albany, Oregon °F

	January	February	March	April	May	June	July	August	September	October	November	December
High	46	51	56	60	67	73	82	82	77	65	53	46
Low	34	35	37	39	44	49	52	51	48	42	38	34

Averaging the high and low temperatures for January through April, November, and December gives an average exterior temperature of 44.08 °F. These months were selected as those are the months in which the distribution center operated in winter mode. FS is the fuel saved for a given number of hours. Hrs is the hours in which destratification is being performed. Using the months in which winter mode was activated, this results in 4344 hours of operation. HHV is the higher heating value, or caloric value of the fuel being used. The MAU heaters utilize natural gas, which has an HHV of $1,000,000 \frac{BTU}{dekatherm}$ (EIA, 2018). η is the efficiency of the heaters, which is reported to be 92 % by the MAU specification sheet (Greenheck, 2018).

To calculate the savings from destratification, all values in equation 7.4 are held constant with the exception of the interior temperature. The interior ceiling temperature is estimated to be 86.5 °F. The value is assumed based on the warehouse set points of 62 °F and 63 °F and the 24 °F initial temperature difference found in the analysis performed by Aynsley (2005) for a heated warehouse. Then, to see a range of possible savings, the reduction in ceiling temperature due to destratifica-

tion is set to values of 1, 3, 5, and 7 °F. An example of the calculation is shown in Eq 7.6, and the results are shown in Table 7.2.

$$\dot{Q} = 0.13(500000)(T_{interior} - 44.08) \quad (7.6)$$

Table 7.2 Heat lost through ceiling at various temperatures.

No Reduction	$\Delta T = 1 \text{ }^\circ\text{F}$	$\Delta T = 3 \text{ }^\circ\text{F}$	$\Delta T = 5 \text{ }^\circ\text{F}$	$\Delta T = 7 \text{ }^\circ\text{F}$
2757083 $\frac{BTU}{hr}$	2692083 $\frac{BTU}{hr}$	2562083 $\frac{BTU}{hr}$	2432083 $\frac{BTU}{hr}$	2302083 $\frac{BTU}{hr}$

These values are then entered into equation 7.5 to determine the number of dekatherms saved by a reduction in temperature. Eq 7.7 shows a sample calculation and Table 7.3 shows the results.

$$FS = 4344 \frac{2757083 - \dot{Q}_{ad}}{(1000000)0.92} \quad (7.7)$$

Table 7.3 Fuel savings (dekatherms)

$\Delta T = 1 \text{ }^\circ\text{F}$	$\Delta T = 3 \text{ }^\circ\text{F}$	$\Delta T = 5 \text{ }^\circ\text{F}$	$\Delta T = 7 \text{ }^\circ\text{F}$
307 dekatherms	921 dekatherms	1535 dekatherms	2148 dekatherms

This value can be multiplied by the cost of natural gas in Oregon, \$8.53/dekatherm, to determine the dollar savings estimated from a ceiling temperature reduction (PPI, 2018). The results are shown in Table 7.4.

Table 7.4 Fuel savings (dollars)

$\Delta T = 1 \text{ } ^\circ\text{F}$	$\Delta T = 3 \text{ } ^\circ\text{F}$	$\Delta T = 5 \text{ } ^\circ\text{F}$	$\Delta T = 7 \text{ } ^\circ\text{F}$
\$ 2617.97	\$ 7853.90	\$ 10471.87	\$ 18325.78

7.1.3 Simple Payback

This section will evaluate the estimated simple payback for cases of a SunCooler unit with induction cooling only (no destratifier), with a destratifier for all possible temperature drops, and the previous cases with an increased exhaust fan run time in June.

In the case of no destratifiers, the number of SunCoolers required is determined by a 1:1 comparison of the rated CFM for existing fans to the SunCoolers 15000 CFM capability. The wall exhaust fans (WEF) are rated at 55000 CFM and the roof exhaust fans (REF) are rated at 37000 CFM. Within the experimental zones there are 8 WEFS and 2 REFS each of these values are multiplied by the fan CFM values and summed for a total CFM for the area, shown in Eq. 7.8.

$$Total\ CFM = 8(55000) + 2(37000) = 514000\ CFM \quad (7.8)$$

This value can then be divided by the SunCooler rated CFM value to determine the number of SunCoolers, rounded up, needed to replace the existing exhaust fans, shown in Eq 7.9.

$$\text{SunCooler's Needed} = \frac{514000}{15000} = 35 \text{ SunCoolers} \quad (7.9)$$

This is then multiplied by the cost of a SunCooler without a destratifier, \$4500. Shown in equation 7.10.

$$\text{SunCooler Cost} = \$4500(35) = \$157500 \quad (7.10)$$

With a destratifier included the number of SunCoolers needed is determined by the area being covered, 500000 ft^2 , and dividing by the area of coverage for a single SunCooler unit. The area of coverage for the SunCooler is currently considered to be 90 x 90 ft, this was demonstrated to be an acceptable spacing by modeling results, shown in Chapter 6, and is therefore the current design parameter used for SunCooler spacing. The calculation is shown in equation 7.11.

$$\text{SunCoolers Needed} = \frac{500000}{90^2} = 62 \text{ SunCoolers} \quad (7.11)$$

This is then multiplied by the cost of a SunCooler with a destratifier, \$5500. Shown in equation 7.12.

$$\text{SunCooler Cost} = \$5500(62) = \$341000 \quad (7.12)$$

The payback is then determined by dividing the SunCooler cost by the savings calculated in the previous sections. In the case of no destratifier the cost is divided only by the exhaust fan operation cost. In the cases with destratifiers, the cost is

divided by the fan operation cost and the estimated destratification savings for a given reduction in ceiling temperature. The calculated payback periods are listed in Table 7.5:

Table 7.5 Estimated simple payback (years)

	No Fan Adjustment	With Fan Adjustment
No Destratifier	12.80	9.94
$\Delta T = 1$ °F	22.84	18.47
$\Delta T = 3$ °F	16.91	14.39
$\Delta T = 5$ °F	13.43	11.78
$\Delta T = 7$ °F	11.13	9.98
AVG ΔT	14.97	12.96

The payback for replacing grid-powered fans is based on the relatively mild climate of Albany, OR. For climates such as Phoenix, more hours of operation in induction or exhaust mode would be expected. Figure 7.2 shows payback for replacing grid fans under different annual hours of operation and electricity cost scenarios. The plot assumes that it requires 3 SC15000 SunCoolers to replace a single, fully loaded, 10 HP, grid powered fan. The hours of annual fan operation range from 1000 hours to 8760 hours, the greater of which would be continuous annual operation. The three lines are for different power costs, ranging from 7 cents per kilowatt hour to 12 cents per kilowatt hour. The warehouse used in the

above example had 1910 hours of operation in 2017.

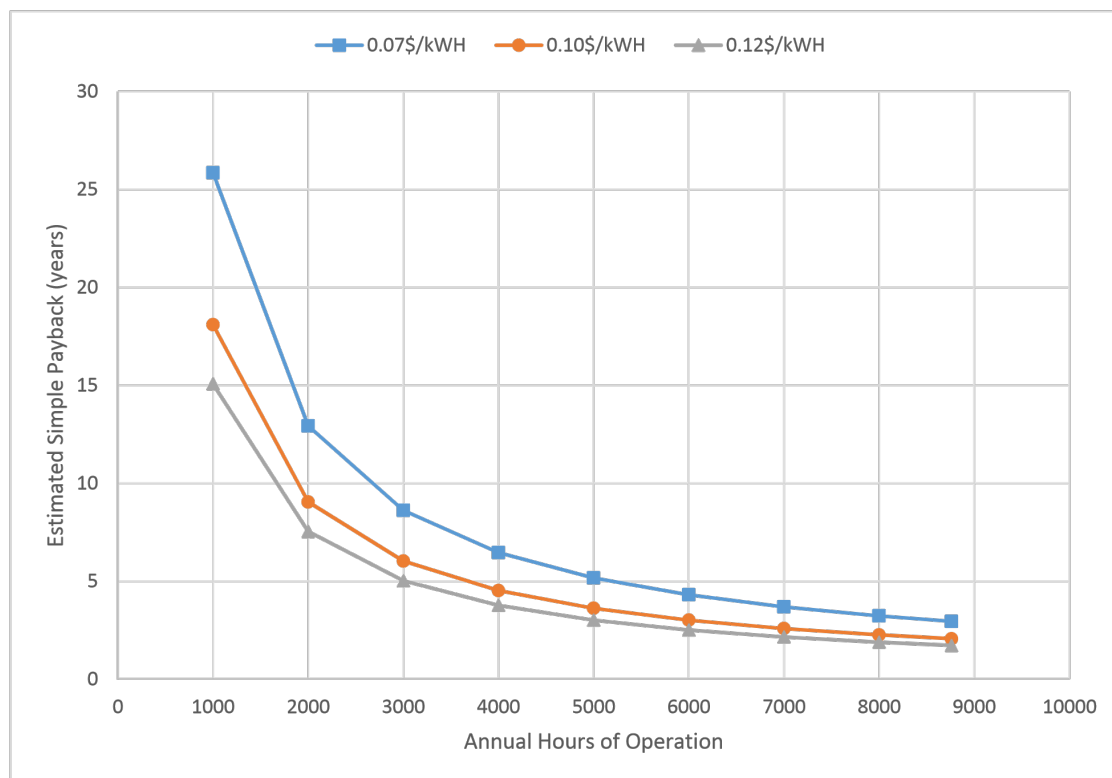


Figure 7.2: Estimated simple payback for varying hours of operation and power cost

For this particular warehouse section, replacing the grid powered exhaust fans with SunCooler units (matching the rated CFM) would result in an estimated annual electrical cost savings of between \$12,309 and \$15,847. Assuming that 35 SunCoolers are required at an estimated unit cost of \$3,000 to match the rated CFM, the simple payback period is 9.9 to 12.8 years for replacing the grid-powered fans only. If heating in the warehouse were increased, destratification can also be utilized for savings. The projected savings increases to somewhere between

\$22,781 and \$26,781 when assuming an average temperature reduction of 4 °F. Installing the SunCoolers for destratification would increase the number of SunCoolers needed to 62, and would adjust the payback period to require 13 to 15 years. In reality, it may be possible to utilize fewer SunCoolers to achieve the same cooling and mixing effects. Thus, this estimate is conservative.

7.2 General Impact on Destratification Control

A simple way to evaluate the effects of fans on a volume of air, is the time required to replace the existing volume using the fans rated flow rate. This is done by dividing the air volume by the flow rate to get a time required for air replacement. When investigating the two primary flow rates used in this study, 15000 and 2500 CFM, air replacement by the 15000 CFM flow rate occurs in under 1 hour for volumes of up to 180x180x40 ft. Whereas the 2500 CFM flow rate requires up to 5 hours for the same spacing, shown in Figure 7.3.



Figure 7.3: Time for air replacement at variable fan spacing

This information provides a useful guideline for the upper time limit that can be expected to achieve destratification. However, the results are limited as they do not inform the end user of how long the fan can then be disabled for. The following analysis can then be performed, using the results from modeling, to predict an operational percentage.

The geometries evaluated in this study primarily had an operational percentage of 35%, however there was some deviation between them. To expand upon the evaluated values and begin to predict operational requirements for other flow rates and geometries, the ratio of the fans flow rate to the volume of the area it is mixing

were compared to the expected operational percentage. These values were plotted and a trendline was created using Microsoft Excel. The resulting trendline can be seen in Figure 7.4.

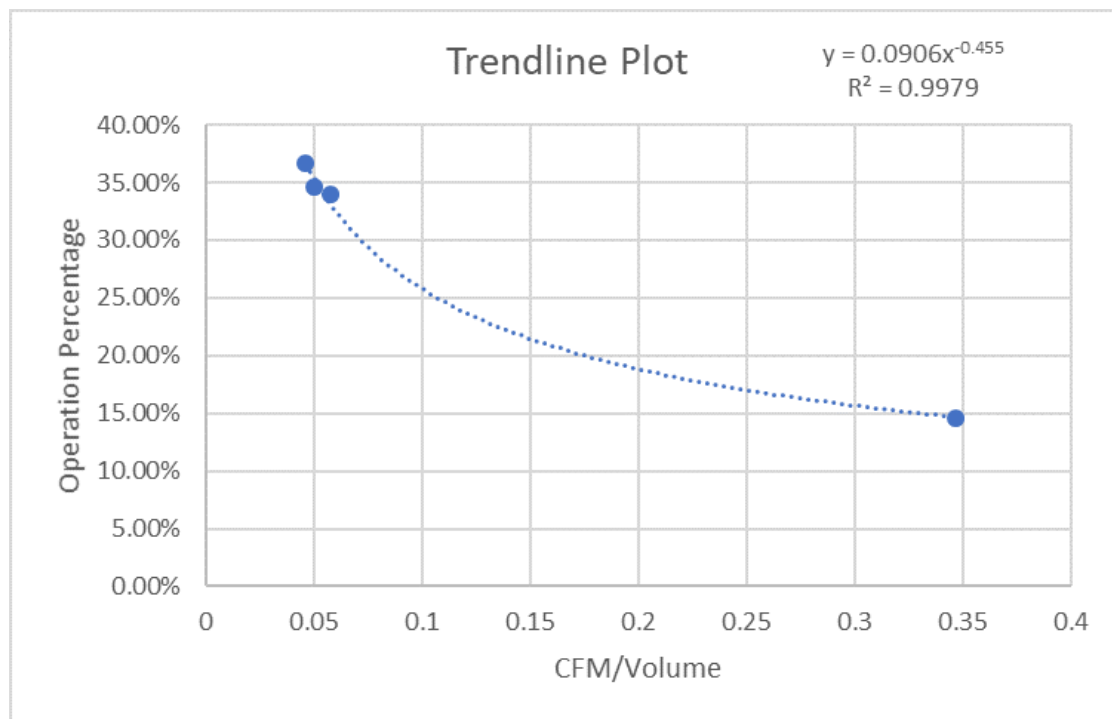


Figure 7.4: Trendline developed from model results

When creating the trendline, the power equation generated the highest R^2 value, resulting in an equation of:

$$\% = 0.0906R^{-0.455}$$

Where % is the fans required operational percentage, and R is the ratio between the volumetric flow rate and the volume being mixed. Using the equation created,

different scenarios were investigated, one holding the flow rate and the height constant while varying fan spacing, with the other holding the volume constant while varying the flow rate. Figures 7.5 and 7.6 show the results of these analyses.

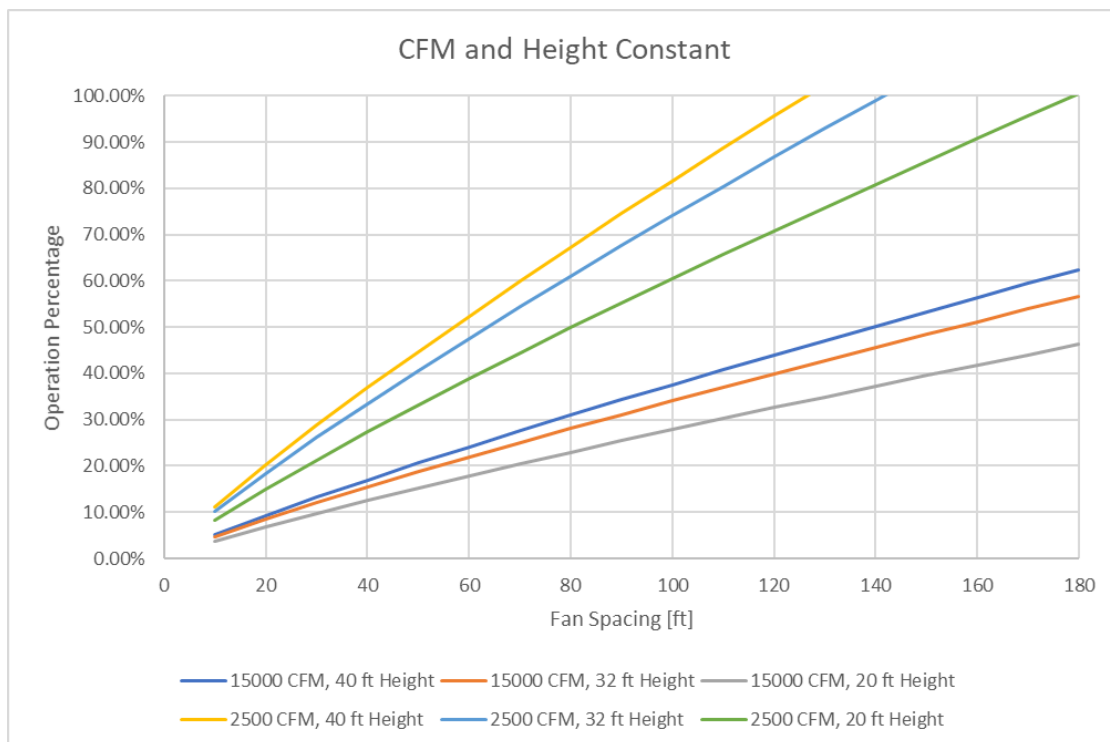


Figure 7.5: Variable fan spacing for constant flow rate and heights

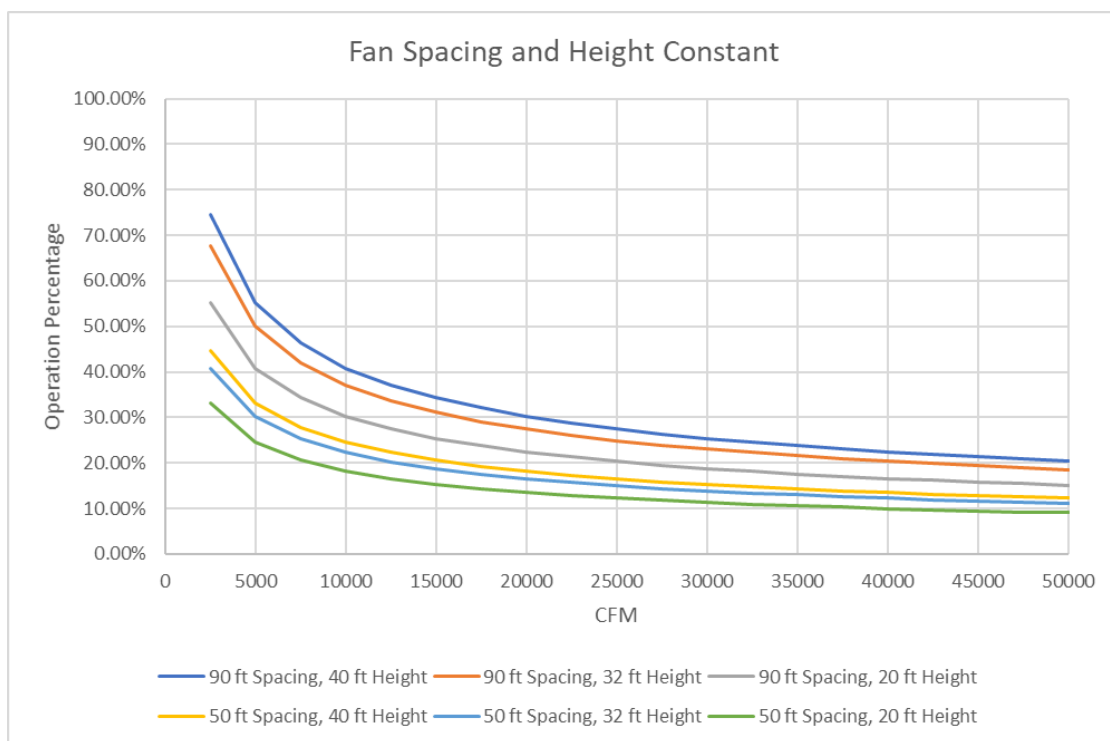


Figure 7.6: Variable flow rates for constant mixing volume

Figure 7.5 shows that for the 2500 CFM option, depending on height, continuous operation will be required to achieve mixing at or before a spacing of 180 ft. Whereas for the 15000 CFM options a fan spacing greater than 180 ft could conceivably be utilized before continuous operation was required. Though both of these cases assume an empty room without obstructions. Figure 7.6 shows that there are diminishing returns for increasing the flow rate at a locked fan spacing. With all volumes beginning to level off at 10000 CFM and having very little change after 30000 CFM.

In areas where there is more available solar power, fewer SunCoolers could be

employed to maintain destratification at higher operational percentages. This is beneficial as the higher available solar power also relates to decreased savings from destratification. In cases where grid powered fans are installed, the above figures can be used to determine how long the existing fans need to operate to maintain a destratified environment, yielding energy savings for the user.

7.3 Study Limitations

Over the course of this study, limitations were discovered with respect to the experimental setups. This section discusses those limitations and makes suggestions for future studies to avoid similar challenges.

For the warehouse setup, three regions of sensors were setup to provide data for a control, the experiment where the fans were operating, and a buffer zone to provide confirmation that the control and experimental regions were isolated from each other. One of the effects of creating three regions was spreading the available sensors thinly. This created a shortage of sensors in any single location, resulting in lower resolution data. To improve on this limitation, the additional regions away from the destratification units can be removed. The data from those locations, especially in such a large warehouse, may not be directly comparable to the data collected from the experimental zone due to activity within the warehouse. Instead, the sensors made available by the removal of the additional regions can be used to provide increased accuracy in the experimental zone. To create a control, a data set can be generated while the destratification units are inactive. This is especially

true of this study, as the goal of the study is to have the destratification units operate periodically. With regard to the sensors, it is also beneficial to acquire sensors with a higher accuracy. The reduction in the number of zones created can also lead to a lower number of sensors needed to collect data. This allows for the purchase of fewer, higher accuracy sensors.

Another significant limitation was the warehouse location. The warehouse available for this study was located in a relatively mild climate. This meant that the benefits of destratification would be less significant as there is a smaller temperature difference between the indoor setpoint temperature and the outdoor ambient temperature. This also contributes to less energy needed for heaters to maintain the indoor temperature, and therefore a lower stratified ceiling temperature. The warehouse utilized also had the issue, as discussed in chapter 5, of being underheated, which can also be viewed as a symptom of the more mild climate. Future studies should seek to locate a warehouse which is located in a colder, northern, climate where winter temperatures more frequently fall below freezing. A warehouse in a colder climate would require a more robust heating system to offset the cold temperatures, and cause a more significant stratification profile to be present. Thus providing more distinct data for analysis. On the other end of the study is the investigation of the cooling benefits for exhaust and intake ventilation. If this topic was the subject of interest for a study, a warehouse located in warmer, southern, climates would be preferable. To perform a comprehensive summer a location such as southern Utah, which has cold winters and warm summers, would be ideal.

For this study, the timeline of the project was compressed to accommodate deadlines. This resulted in the overlap of several key components of the study, experimental setup, literature review, and model development. By overlapping these key components within the study, the project had very little flexibility and information revealed through one of the components, such as the literature review, was not able to be applied to the experiment setup. This meant that errors had to be worked around rather than being able to be corrected directly. When preparing study such as this one, at least two years should be allotted for completion. This allows for a literature review to be performed comprehensively prior to setting up the experiment, ensuring that the experiment will be optimized for the studies needs. Then with an experimental setup in place, sufficient time will be allowed for modeling to be performed and the modification of models to reflect data collected through experimentation.

The compression of this study also resulted in the hasty addition of a second experiment, to be used for the collection of data to compare against model results. While the data collected from the second experimental site was superior for comparison to that from the warehouse, it still presented challenges. The building continued to be in used during experimentation, resulting in limited data collection options. Due to its use, there were also several parameters that were not able to be controlled, such as human activity within the building, uncertain heating schedules, and the room being reorganized between data collection events. As the creation of a validation model is of high importance to future work on this subject, the creation of an idealized experiment is also of interest to any future

investigations. One possibility is the acquisition of an enclosed room, such as a trailer, and having complete control of the environment in which the experiment is being performed. However, this could be prohibitively expensive, in which case a scaling method could be utilized to create a smaller, less expensive, experiment which could be used for model validation.

To determine the dimensionless variable groups which would be utilized for the scaling method, the Buckingham Pi method can be utilized. There are 12 variables which impact the stratification of a room and its mixing time. They are:

- The height of the room (H)
- The width of the room (W)
- The length of the room (L)
- The velocity of the inlet fluid (v)
- The area of the inlet (A)
- The initial temperature difference in the room (ΔT)
- The final temperature of the thermally mixed room (T)
- The total mass in the room (m)
- The average density of the room (ρ)
- The average specific heat of the room (c)
- The time to mix the room to a uniform temperature (t)

- The viscosity of the inlet fluid (μ)

For these 12 variables there are four unique dimensions: distance, time, mass, and temperature. This means that there will be eight pi groups created using the Buckingham Pi method. The four repeating variables used are: height (H), velocity (v), density (ρ), and final temperature (T). Multiplying the 4 repeating variables with each of the remaining 8 variables, and solving for the power of each variable such that the group is dimensionless, results in the following Pi groups:

$$\pi_1 = \frac{W}{H} ; \pi_2 = \frac{L}{H} ; \pi_3 = \frac{a}{H^2} ; \pi_4 = \frac{\Delta T}{T}$$

$$\pi_5 = \frac{mH^3}{\rho} ; \pi_6 = \frac{cT}{Hv} ; \pi_7 = \frac{tv}{H} ; \pi_8 = \frac{\mu}{Hv\rho}$$

These 8 dimensionless groups can be used to create a scaled experiment which could be more easily assembled and controlled. This allows for the creation of a validation model which could then be used to quantify the importance of each parameter which affects mixing time. With a better understanding of the importance of these parameters, generalized mixing model could be developed to draw broader conclusions about the relationship between mixing, cooling, and geometric properties.

Chapter 8: Conclusions

8.1 Summary

An experimental and computational study of the performance of SunCooler solar powered ventilator/destratification units was conducted. Experiments were conducted for more than 12 months in a large warehouse, and a smaller experiment in a single school room. In the warehouse, the SunCoolers operated reliably for the entire project period. SunCoolers were able to operate at night and during short, cloudy winter days without operational issues. During the cooling season, the SunCoolers were shown to function adequately during night-flush cooling operations. The area of influence of the SunCooler were maintained at comparable temperatures to the rest of the warehouse. For this particular warehouse section, replacing the grid powered exhaust fans with SunCooler units (matching the rated CFM) would result in an estimated annual electrical cost savings of between \$12,309 and \$15,847. Assuming that 35 SunCoolers are required at an estimated unit cost of \$4,500 match the rated CFM, the simple payback period is 9.9 to 12.8 years for replacing the grid-powered fans only. In reality, it may be possible to utilize fewer SunCoolers to achieve the same cooling effect. Thus, this estimate is conservative.

Modeling of a large warehouse with no obstructions or thermal mass provides a comparison between heating and cooling under similar conditions. While each

model does not exactly predict the time required to mix or cool the building independently, the relationship between the two can be used as a baseline for estimating the daily number of hours fans need to run to maintain destratification. Modeling results indicate that destratification fans nominally only need to operate for 35% of total operating time to maintain destratification. This assumes peak temperature is maintained at least 1 °F above the set point temperature and that the room has full fan coverage. Making the destratification application of SunCoolers theoretically viable anywhere that can provide enough power for the fans to operate 8.4 hours of a 24-hour period. This is dependent on implementation of the operation regime. A binary on/off cycle is unlikely to be successful, whereas setting destratifiers to operate in tandem with heaters is more likely to bring about the desired results.

During the heating season, the SunCoolers were run in destratification mode. The SunCoolers showed a local effect, decreasing the ceiling temperature several degrees Fahrenheit. However, a more significant observable impact on the building environment was limited by (1) the large square footage compared to destratification effect, and (2) the fact that the warehouse was under-heated, preventing the formation of a significant thermal stratification profile. Thus, a separate smaller experiment was conducted and detailed computational model was developed to understand destratification behavior, including the required time to destratify a given environment. The results indicated that for the warehouse under investigation, SunCoolers should be arranged in a grid pattern with units separated by approximately 90 feet to produce a meaningful destratification effect. Using de-

stratification energy savings models from the literature, it was estimated that the warehouse could reduce heating costs by between \$2,617 to \$18,325 for a ceiling temperature reduction from 1°F to 7°F, respectively, assuming the warehouse was sufficiently heated. For a 90 spacing in the 500,000 square foot section of the warehouse, this suggests 62 SunCoolers at a cost of \$5,500 are required to achieve the desired destratification effect. At a cost of \$5,500 per unit, the simple payback (inclusive of cooling season savings) ranged from 9 to 13 years for ceiling temperature reductions from 3°F to 7°F. If the number of SunCooler is specified primarily to achieve the cooling effect, the payback period would be less than 6.6 years for cooling and heating season, even if destratification was not optimal.

8.2 Contribution

This study has demonstrated that there is the potential to achieve greater savings by modifying existing destratification methods. These savings are achieved by reduction of fan operation times, or replacement of grid powered fans with solar powered destratification units. The study provides a foundation of work from which to investigate the further refinement of destratification strategies such as regions of influence for destratification and the possibility of more intricate fan duty cycles.

8.3 Recommended Future Work

A further study into the impacts of objects on the development of velocity profiles and the subsequent impacts on mixing time and the significance of thermal mass within the mixing environment is critical to the further development of this body of work. To achieve a greater understanding of these impacts, a small control environment should be set up for experimentation with mixing and cooling techniques, either with traditional grid powered fans or with the SunCooler technology utilized in this study. Then extensive time could be devoted to developing a model which is able to match the experimental data collected. Once the model has been validated, the various parameters of the room, such as material properties or physical obstructions, could be adjusted and evaluated for their relative importance to the models accuracy. This would allow for the development of a more accurate generalized model which could be utilized to investigate the range of influence for different fan powers within a warehouse or other enclosures. With more detailed information on fan capabilities, mixing times, and cooling times a suitable warehouse could be selected to study and verify computational findings.

Bibliography

- ANSYS. Ansys help manual, 2017. Accessed: 2018-02-05.
- Mark Armstrong, Bill Chihata, and Ron MacDonald. Cold weather destratification energy savings of a warehousing facility. *ASHRAE Transactions*, 115(2):513–518, 2009.
- ASHRAE. *ASHRAE Handbook - Fundamentals*. ASHRAE, 2017.
- Richard Aynsley. Saving heating costs in warehouses. *ASHRAE Journal*, 47(12): 46–51, December 2005.
- Fred Bauman, Tom Webster, and Corinne Benedek. Cooling airflow design calculations for ufad. *ASHRAE Journal*, 49:36–44, 2007.
- Abdelhakim Bouzinaoui, Paul Vallette, Fabrice Lemoine, Jean Raymond Fontaine, and Ren Devienne. Experimental study of thermal stratification in ventilated confined spaces. *International Journal of Heat and Mass Transfer*, 48(19):4121–4131, 2005.
- EIA. Heat content of natural gas consumed, 2018. URL https://www.eia.gov/dnav/ng/ng_cons_heat_at_aE_PG0_VGTH_btucf_a.htm.
- ElectricityLocal. Albany, oregon electricity statistic, 2018. URL <https://www.electricitylocal.com/states/oregon/albany/>.
- EngineeringToolBox. Densities of solids, 2018. URL https://www.engineeringtoolbox.com/density-solids-d_1265.html.
- Greenheck. Direct gas-fired make-up air models dg and dgx, 2018. URL http://www.greenheck.com/media/pdf/catalogs/DGDGX_catalog.pdf.
- Son H. Ho, Luis Rosario, and Muhammad M. Rahman. Numerical simulation of temperature and velocity in a refrigerated warehouse. *International Journal of Refrigeration*, 33:1015–1025, March 2010.

Joel C. Hughes. Technology evaluation of thermal destratifiers and other ventilation technologies. In *American Industrial Hygiene Conference & Exposition (AIHce EXP)*. <https://www.aiha.org/aihce06/handouts/d1hughes.pdf>, Chicago, Illinois, 2006.

Investopedia. Heating degree day - hdd, 2018. URL <https://www.investopedia.com/terms/h/heatingdegreeday.asp>.

Kisup Lee, Guangqing Xue, Zheng Jiang, and Qingyan Chen. Thermal environment in indoor spaces with under-floor air distribution systems: Part 1. impact of design parameters. *HVAC&R Research*, 18(6):1182–1191, 2012.

Zhang Lin, T.T. Chow, K.F. Fong, Qiuwang Wang, and Ying Li. Comparison of performances of displacement and mixing ventilations. part i: thermal comfort. *International Journal of Refrigeration*, 28:276–287, 2005.

NOAA. National weather service forecast office, 2018. URL <http://w2.weather.gov/climate/index.php?wfo=pqr>.

NWREC. Northwest renewable energy corp. Available at http://www.nwrec.us/application/files/8015/0256/8559/Complete_specs_v29.pdf (2017/1

Porrás-Amores, Mazarrón F.R., and Canas I. Study of the vertical distribution of air temperature in warehouses. *energies*, 7:1193–1206, February 2014.

PPI. Average price of natural gas (per 1,000 cubic feet), 2018. URL <http://www.ppiny.org/reports/jtft2004/naturalgas.htm>.

P. Rohdin and B. Moshfegh. Numerical modelling of industrial indoor environments: A comparison between different turbulence models and supply systems supported by field measurements. *Building and Environment*, 46:2365–2374, 2011.

H K Versteeg and W Malalasekera. *An Introduction to Computational Fluid Dynamics: The Finite Volume Method*. Addison Wesley Longman Limited, Edinburgh Gate, Harlow, Essex CM20 2JE, England, 1995.

Jason Wright. personal communication, 2017.

Zhao Zhang, Wai Zhang, Zhiqiang (John) Zhai, and Qingyan (Yan) Chen. Evaluation of various turbulence models in predicting airflow and turbulence in enclosed environments by cfd: Part 2 - comparison with experimental data from literature. *HVAC&R Research*, 13(6):871–886, November 2007.

